AD_____

Award Number: W81XWH-08-1-0455

TITLE: Isolation and Characterization of Prostate Cancer Stem Cells

PRINCIPAL INVESTIGATOR: Isla Garraway, MD-PhD

CONTRACTING ORGANIZATION: University of California, Los Angeles
Los Angeles, CA 90095

REPORT DATE: August 2012

TYPE OF REPORT: Annual Summary

PREPARED FOR: U.S. Army Medical Research and Materiel Command
Fort Detrick, Maryland 21702-5012

DISTRIBUTION STATEMENT: (Check one)

X Approved for public release; distribution unlimited

REPORT DOCUMENTATION PAGE

Form Approved
OMB No. 0704-0188

1. REPORT DATE	2. REPORT TYPE	3. DATES COVERED
1 Aug 2012	Annual Summary	1 AUG 2011 - 31 JUL 2012

4. TITLE AND SUBTITLE

Isolation and Characterization of Prostate Cancer Stem Cells

5a. CONTRACT NUMBER

5b. GRANT NUMBER
W81XWH-08-1-0455

5c. PROGRAM ELEMENT NUMBER

6. AUTHOR(S)

Isla P. Garraway, M.D., Ph.D.

E-Mail: igarraway@mednet.ucla.edu

5d. PROJECT NUMBER

5e. TASK NUMBER

5f. WORK UNIT NUMBER

7. PERFORMING ORGANIZATION NAME(S) AND ADDRESS

University of California, Los Angeles
Los Angeles, CA 90095

8. PERFORMING ORGANIZATION REPORT NUMBER

9. SPONSORING / MONITORING AGENCY
U.S. Army Medical Research and Materiel Command
Fort Detrick, Maryland 21702-5012

10. SPONSOR/MONITOR'S ACRONYM(S)

11. SPONSOR/MONITOR'S REPORT NUMBER(S)

12. DISTRIBUTION / AVAILABILITY STATEMENT
Approved for Public Release; Distribution Unlimited

13. SUPPLEMENTARY NOTES

14. ABSTRACT

Human prostate epithelial cells that can develop into "prostaspheres" display characteristics of stem/progenitor cells, including self-renewal and ability to induce prostate tubule formation in vivo. FISH analysis of prostaspheres derived from patient specimens containing the TMPRSS-ERG translocation, however, are not preserved in sphere-forming cells. In order to evaluate whether prostate cancer stem cells containing the TMPRSS-ERG translocation can be isolated, we have proposed a series of experiments to isolate tumor cells for characterization and in vivo expansion. Previously, we have found that although cancer cells can be isolated from tumor tissue, preservation of these cells in vitro and generation of xenografts is rare. In order to optimize retrieval of tumor cells and support tumor regeneration in vivo, we have implemented multiple strategies, including optimization of tissue processing to single cells, cell fractionation, and refinement of the microenvironment. This has enabled successful enrichment of TMPRSS-ERG+ tumor fractions and may lead to further identification of tumor-initiating cells present in primary prostate tumors.

15. SUBJECT TERMS
Prostate Cancer, prostate stem cells, TMPRSS-ERG, prostate tissue regeneration

16. SECURITY CLASSIFICATION OF:			17. LIMITATION OF ABSTRACT	18. NUMBER OF PAGES	19a. NAME OF RESPONSIBLE PERSON
a. REPORT	b. ABSTRACT	c. THIS PAGE			USAMRMC
U	U	U	UU	63	19b. TELEPHONE NUMBER *(include area code)*

Table of Contents

I - INTRODUCTION:

The aims of this proposal are based on the observations from initial studies with human prostate cancer surgical specimens. We discovered that prostate stem/early progenitor cells recovered from tumor specimens lack the TMPRSS-ERG translocation found in the original tumor, when examined by fluorescence in situ hybridization (FISH). Our findings suggest either ETS rearrangements are not present at the stem/progenitor cell level, or that genetically deranged prostate stem/progenitor cells are particularly vulnerable to apoptosis or senescence in vitro, resulting in selective advantage of benign cells. We have subsequently evaluated a variety of growth conditions that may enable survival and expansion of cancer cells, using TMPRSS-ERG fusion status as an indictor, since the ability to generate an extensive collection of human prostate cancer cells would provide valuable biological tools for understanding characterizing prostate cancer stem/progenitor cells, the mechanisms of tumorigenesis, and identifying new therapeutic targets.

We have identified a variety of factors that may effect successful isolation/expansion of primary tumors, including low tumor grade/volume present in many surgical samples, increased sensitivity of tumor cells to apoptosis after tissue dissociation, semi-competent immune systems in many SCID mouse strains that inhibit tumor take, and a microenvironment that lacks critical growth factors and cellular interactions. Our laboratory has evaluated many of the issues above, as evident in the published and unpublished data presented over the course of this grant. We have optimized conditions that enable isolation of TMPRSS-ERG+ cancer cells, by reducing tissue ischemia time, modifying tissue digestion conditions, and incorporating tumor dissection and FACS sorting. We have identified culture conditions that enable expansion of these cells in vitro, although only transiently. We are evaluating approached that enable recapitulation of the tumor microenvironment in vivo, by recombining freshly isolated tumor cells with a variety of human stromal sources. We have isolated primary stromal cells from human fetal prostate specimens and found that they support normal prostate tubule formation, induced by benign (adult) human prostate epithelial cells, eliminating the need for murine additives (i.e., urogenital sinus mesenchyme). Human fetal stroma is also capable of supporting xenografts from rare primary tumors, resulting in the recapitulation of the patient's original cancer specimen. Efficient and reproducible tumor regeneration will likely require additional support via development of microenvironmental cues.

II - BODY:

Background and Specific Aims:

Expansion of Prostate Stem/Progenitor Cells: The study of prostate stem cells (SCs) is facilitated by culturing dissociated primary cells as spheres[1, 2]. Spheres are multicellular globes that form in anchorage-independent conditions, and these cultures have been commonly used to study mammary and nervous system development[3, 4]. In our human prostate studies, spheres can be dissociated and passaged for multiple generations (self-renew), as well as be induced to form fully differentiated glands in vivo[5].

The TMPRSS-ERG Fusion is Not Identified in Prostaspheres: Since prostaspheres were generated from primary tumors, we presumed that in vitro cultures would include clonally derived benign and cancerous prostaspheres, reflective of the heterogeneity of glands found in tissue specimens. We were not able, however, to distinguish prostaspheres based on phenotype, marker expression, or growth rate. With the discovery of prevalent gene rearrangements involving ETS family members in prostate cancer, we anticipated that cytogenetic tools may enable identification of cancerous prostaspheres[6]. Gene fusions involving ERG, ETV1, and ETV4 involve a variety of 5' partners that direct aberrant expression of these transcription factors and possibly initiate a cascade of events leading to tumorigenesis [6]. The most common rearrangement involves juxtaposition of the androgen-regulated TMPRSS2 gene with ERG. TMPRSS-ERG gene fusions have been detected in primary prostate tumor specimens, metastases, and xenografts by fluorescence in situ hybridization (FISH)[6]. Analysis of prostate tumor surgical cohorts have found 36-78% of prostate cancers possess the TMPRSS-ERG fusion[6]. We wondered whether we could use TMPRSS-ERG

to distinguish normal and malignant prostaspheres. The presence of this fusion in individual prostaspheres may suggest that cancer stem/early progenitor cells can be expanded in our cultures.

To test the feasibility of this approach, FISH analysis was performed on select prostate tissue specimens and coordinating prostaspheres. The TMPRSS-ERG fusion was found in approximately 60% of cancer cases tested. Surprisingly, the fusion was conspicuously absent from prostasphere cultures derived from TMPRSS-ERG+ tissues, even when the specimens contained >90% tumor. Analysis of monolayer cultures concomitantly derived from prostate tumor specimens also failed to demonstrate the presence of the gene fusion, indicating that both spheroid and adherent cultures select for fusion-negative cells[5].

Review of ETS Rearrangements in Cultured Prostate Epithelial Cells: The TMPRSS-ERG fusion has previously been identified in only one prostate cancer cell line, NCI-H660, derived from an androgen-independent small cell carcinoma of the prostate[7, 8]. None of the common prostate cancer cell lines including LnCaP, DU-145, PC-3, and CWR22 contain this fusion[6]. LnCaP and MDA-PCa2b were recently reported to contain rearrangement of the ETV1 gene to a prostate specific region resulting in aberrant expression with increased invasive activity[6]. The general inability to culture primary prostate cells that contain TMRPSS-ERG, and the under-representation of ETS rearrangements in prostate cancer cell lines is intriguing and suggests critical elements are absent in vitro, preventing the growth of these cells.

We have formulated three distinct possibilities why TMPRSS-ERG is not preserved in human prostate cells in vitro 1) prostate cancer stem cells responsible for propagating primary cells do not contain the TMPRSS-ERG fusion, rather it is a genetic event that occurs later in tumorigenesis as a result of genomic instability 2) Fusion-positive prostate cells undergo anoikis, apoptosis, or senescence unless additional growth/survival factors or stromal interaction is provided, or 3) genetically normal cells have a dramatic growth advantage over TMPRSS-ERG cancer cells, resulting in their rapid overgrowth.

Since the TMPRSS-ERG fusion is so prevalent in prostate cancer regardless of grade or stage, analyses of the genetic impact of these rearrangements is critical. Deciphering the fundamental survival factors necessary for culturing these cells will yield biological tools for the study of ETS rearrangements in addition to valuable insight into the vulnerabilities of these cells. Consequently, we proposed to define what factors are critical for survival and expansion of TMPRSS-ERG fusion-positive prostate cancer cells via the following aims:

Aim 1: Generate a collection of tumor specimens that contain the TMPRSS-ERG translocation, as demonstrated by FISH of the primary tumor.

a. Generate xenografts from TMPRSS-ERG tissue specimens
b. Generate prostasphere and monolayer (adherent) cultures from TMPRSS-ERG specimens in a variety of culture conditions, including altering media and additives (i.e., androgen, stroma)
c. Generate stocks of cryopreserved dissociated prostate cells from TMPRSS-ERG specimens

Aim 2: Assess for the retention of the TMPRSS-ERG mutation in xenografts, expanded in vitro monolayer (adherent) cultures, and prostasphere cultures.

Aim 3: Assess the effect of inhibiting anoikis and/or apoptosis pathways in dissociated prostate epithelial cells derived from TMPRSS-ERG+ tissues on prostasphere formation via viral mediated gene transfer of genes that are known to disrupt these processes (i.e., Bcl-2, Ras, dominant negative p53).

III -KEY RESEARCH ACCOMPLISHMENTS:

The tasks of the training program include:

1) Regularly meet with mentor to discuss career goals and progress
2) Attend group meetings, journal clubs, and seminars related to research topics
3) Direct research project outlined in the proposal according to the specific aims:
    a. Generate xenografts from (TMPRSS-ERG+) cancer specimens
    b. Evaluate the ability to preserve the TMPRSS-ERG fusion in vitro by varying culture conditions.
    c. Perform viral mediated gene transfer of genes that block anoikis and apoptosis pathways in dissociated human prostate cells in an effort to maintain TMPRSS-ERG+ cells in vitro.

Progress on Tasks/Specific Aims:

Training/Mentoring (Tasks 1 and 2): During the transition towards an independent research focus in human prostate stem cells and their role in tumor-initiation, my mentor interactions continue in the form of meetings and interactions with members of his research team to share data and discuss new strategies in prostate stem cell research. Members of my laboratory have become active members of the prostate cancer research community at our Institution. We are invited to present at journal clubs and seminars throughout the year and have formed collaborations with numerous intramural and extramural laboratories.

Collecting Primary Human Prostate Cancer Samples: We have continued to expand our collection of human prostate tissue samples, adding about 60 samples/year. In addition to working with the Tissue Procurement Core Laboratory (TPCL) at UCLA for tumor isolation from prostate specimens, we have expanded out procurement to the Greater Los Angeles VA Medical Center. This has enabled collection of significantly more high-risk tumors (Gleason score >8, PSA >10, advanced clinical stage). At both institutions, we have standardized procurement procedures in order to minimize ischemia time. Upon en bloc removal of the prostate surgical specimen, an GU pathologist or experienced technician prepares 5 or 6 prostatic sections ranging in thickness from 3-4mm. A sleeve of fresh tissue is obtained from the posterior (peripheral zone) of selected sections. Frozen slides are prepared and stained by H&E staining. The GU pathologist examines the slides and cancerous areas are marked and mapped to the remaining fresh tissue. Tumor nodules are then dissected and isolated from benign tissue for further study.

Epcam/CD44 Fractionation Enables Enrichment of TMPRSS-ERG+ Cancer Cells: In an effort to improve the retrieval of TMPRSS-ERG+ prostate cancer cells that are required for our studies, we utilized Epcam/CD44 fractionation to isolate luminal cells from tumors. In initial experiments with tumor tissues, however, it was noted that only a minor population of $Epcam^{+}CD44^{-}$ luminal cells remained after standard 12-hour digestion with Collagenase (Figure 1A). This result was surprising, since the majority of cells present in tumor nodules should display $Epcam^{+}CD44^{-}$ (luminal) profiles. In order to evaluate whether or not standard enzymatic digestion procedures resulted in over digestion and loss of tumor cells, a series of experiments evaluating a variety of digestion times and collagenase concentrations was performed (data not shown). When digestion time was reduced to 4 hours in 0.25% collagenase, a marked shift in $Epcam^{+}CD44^{-}$ cells was noted, enabling optimization of luminal cells recovery (Figure 1B). FACS and RT-PCR of fractionated cells confirmed enrichment of basal $Epcam^{+}CD44^{-}$ and luminal $Epcam^{+}CD44^{+}$ fractions (Figure 1C and E). In order to confirm enrichment of tumor cells, PCR for TMPRSS-ERG fusion was performed on RNA isolated from cell fractions. Significant TMPRSS-ERG message was detected exclusively in the $Epcam^{+}CD44^{-}$ cell fraction (Figure 1E). This confirms that the luminal cell optimization procedure for enzymatic digestion of prostate tumor specimens enables robust recovery of tumor cells containing TMPRSS-ERG.

Recreating the Tumor Microenvironment May Enable Expansion of Primary Prostate Tumor Cells: In addition to enrichment of the TMPRSS-ERG+ cells, we have continued to focus on recreating the microenvironment that is conducive to prostate tumor growth. One factor that may enable cancer cell growth is the incorporation of human support cells in place of murine urogenital

sinus mesenchyme for use in tissue regeneration assays with tumor cells. It is possible that murine growth factors secreted by these cells may not be optimal stimulants of human tumor growth. As a result, we have isolated stromal cells from fetal tissue, which demonstrate abundant growth in vitro and supports benign human prostate tissue regeneration when combined with adult prostate cells or prostaspheres (published in attached paper by Guo et al., 2012). The use of fetal prostate stroma for tissue regeneration assays of primary prostate tumor cells has enabled retrieval of rare tumor grafts. Tumor nodules were dissected from high-grade surgical specimens and combined with human fetal prostate stroma and Matrigel prior to subcutaneous injection into NOD-SCID mice. Approximately 12-weeks following implantation, grafts were harvested and evaluated by immunohistochemistry (Figure 2). High-grade tumor foci were observed as well as areas of benign growth. Tumor foci demonstrated similar expression pattern of prostate markers as the original tumor (data not shown).

The ability to regenerate primary tumors would represent a significant leap forward in our ability to identify and characterize human prostate stem cells. We have subsequently isolated Epcam+CD44- tumor cells from several dissected high-grade tumor nodules and recombined with fetal stroma in tissue regeneration assays, however, the results are somewhat equivocal (Figure 3). The majority of the regenerated grafts that we have evaluated appear to contain mostly benign tubular structures containing basal cells. We are currently in the process of performing FISH on the regenerated tissue samples in order to evaluate TMPRSS-ERG status. If the regenerated structures contain TMPRSS-ERG, then it is possible that the microenvironment does not support the tumor phenotype, even when cells share similar genetics to the original tumor. We are in the process of further exploring other human support cells, including isolating cancer-associated fibroblasts (CAFs) for in vitro expansion and in vivo validation. Bona fide CAFs are capable of the malignant transformation of the benign cell line, BPH-1, demonstrated by tumor formation in vivo. In collaboration with Dr. Neil Bhowmick, an expert in the tumor microenvironment, we are in the process of validating 20 CAFs that have been generated from primary tumors procured by our laboratory. So far, 1/5 putative CAFs demonstrate transforming capability of BPH-1 (data not shown). Upon determination of bona fide CAFs, we will assess their ability to support TMPRSS-ERG outgrowth in vitro and in vivo.

IV - REPORTABLE OUTCOMES:

We published the following original articles since our last progress report was submitted (please see appendix for copies):

1. Guo, C, Liu, H., Zhang, B, Cadaneanu, RM, Mayle, AM, and **Garraway, IP***. Epcam, CD44, and CD49f Distinguish Sphere-Forming Human Prostate Basal Cells From a Subpopulation With Increased Tubule Initiation Capability. PLOS One, April 13, 2012. PMID: 22514625; PMC3326009

2. **Garraway, IP***. Will identification of a prostate cancer stem cell lead to its cure? Urologic Oncology: Seminars and Investigations, 2012.

3. Jing, J, Hindoyan, A, Goldstein, A, Lawson, D, Chen, D, Li, Y, Wang, S, Guo, C, Zhang, B, Gleave, M, Witte, O, **Garraway, IP**, and Wu, H. Identification of CD166 as a marker for enriching prostate tumor initiating cells. PLOS One, August 3, 2012. PMID: 22880034; PMCID: PMC3411798

4. Hance, MW, Dole, K, Fopal, U, Bohonowych, JE, Jerzierska-Drutel, A, Neumann, CA, Liu, H, **Garraway, IP**, and Isaacs, JS. Secreted Hsp90 is a novel regulator of the epithelial to mesenchymal transition (EMT) in prostate cancer. Journal of Biological Chemistry, September 18, 2012. PMID: 22989880

The following manuscripts are in preparation:

1. Zhang, B, Guo, C, An, D, and **Garraway, IP***. Human fetal prostate stroma supports prostate tissue regeneration. In Preparation.

2. Liu, H., Lai, K., Cadaneanu, R., Mayle, AM, **Garraway, IP*.** Keratin 13 is a marker of human prostate stem/progenitor cells and is expressed on a rare subpopulation in benign prostate tissue. In Preparation

3. Liu, H. Lai, K., and **Garraway,IP*.** Genetic profiles distinguish subpopulations of prostate epithelial cells with different functional capabilities. In Preparation.

Our data was presented at the Prostate Cancer Foundation Annual Retreat in Lake Tahoe, in September, 2012.

V - CONCLUSIONS:

Timeline for completion of research tasks documented in the original statement of work is listed below:

Months 0-6: Initiate cloning of viral vectors; obtain regulatory approval for human and animal research protocols.

Months 7-18: Collect prostate tissue specimens, attempt to establish new xenografts and monolayer cultures, and begin to evaluate TMPRSS-ERG fusion status in collected tissue specimens via FISH.

Months 19-30: Continue to collect tissue and evaluate for TMPRSS-ERG status. Begin altering growth conditions of dissociated cells that contain the translocation in attempt to preserve cells containing the fusion in vitro. Begin viral-mediated gene transfer of anti-anoikis and anti-apoptosis genes

Months 31-60:Continue characterization of prostaspheres generated in altered growth environments and upon gene transfer of anti-anoikis/apoptosis genes. Evaluated ability to generate prostaspheres from newly established xenografts.

Major Findings:

1)TMPRSS-ERG+ cells can be isolated using the combination of tumor macrodissection and cell sorting for Epcam+CD44-CD49fLo antigenic profile (Figure 1). These cells can be expanded in vitro, but only transiently, prior to undergoing senescence (data not shown, see 2011 report).
2) TMPRSS-ERG+ tumors fail to routinely expand in vivo as xenografts or reconstituted tumors, even with the addition of support cells of human origin (Figure 3).
3) Human tubule-initiating cells are predominantly Epcam+CD44-CD49fHi. The mechanisms that these cells utilize in order to interact with the niche and initiate new tubules may be exploited by tumor cells (See published report, Guo et al., 2012).
4) Cancer-associated fibroblasts can be isolated from dissected primary tumor nodules and expanded in vitro (data not shown). These cells may be important for sustaining the growth of tumor cells in vitro and in reconstitution assays.

VI - REFERENCES:

1. Al-Hajj, M. and M.F. Clarke, *Self-renewal and solid tumor stem cells.* Oncogene, 2004. **23**(43): p. 7274-82.

2. Singh, S.K., et al., *Cancer stem cells in nervous system tumors.* Oncogene, 2004. **23**(43): p. 7267-73.
3. Dontu, G., et al., *In vitro propagation and transcriptional profiling of human mammary stem/progenitor cells.* Genes Dev, 2003. **17**(10): p. 1253-70.
4. Bez, A., et al., *Neurosphere and neurosphere-forming cells: morphological and ultrastructural characterization.* Brain Res, 2003. **993**(1-2): p. 18-29.
5. Garraway, I.P., et al., *Human prostate sphere-forming cells represent a subset of basal epithelial cells capable of glandular regeneration in vivo.* Prostate, 2010. **70**(5): p. 491-501.
6. Tomlins, S.A., et al., *Recurrent fusion of TMPRSS2 and ETS transcription factor genes in prostate cancer.* Science, 2005. **310**(5748): p. 644-8.
7. van Bokhoven, A., et al., *Widely used prostate carcinoma cell lines share common origins.* Prostate, 2001. **47**(1): p. 36-51.
8. Mertz, K.D., et al., *Molecular characterization of TMPRSS2-ERG gene fusion in the NCI-H660 prostate cancer cell line: a new perspective for an old model.* Neoplasia, 2007. **9**(3): p. 200-6.
9. Litvinov, I.V., et al., *Low-calcium serum-free defined medium selects for growth of normal prostatic epithelial stem cells.* Cancer Res, 2006. **66**(17): p. 8598-607.
10. Goldstein, A.S., et al., *Trop2 identifies a subpopulation of murine and human prostate basal cells with stem cell characteristics.* Proc Natl Acad Sci U S A, 2008. **105**(52): p. 20882-7.
11. Lunacek, A., et al., *Growth curves of the fetal prostate based on three-dimensional reconstructions: a correlation with gestational age and maternal testosterone levels.* BJU Int, 2007. **99**(1): p. 151-6.

APPENDIX:

FIGURE LEGENDS:

Figure 1: TMPRSS-ERG fusion expression in fractionated prostate epithelial cells. The combination of Epcam and CD44 was used to isolate Epcam+CD44+ basal-enriched (A) and Epcam+CD44- luminal-enriched cell fractions (B) for quantitative RT-PCR. Fractionated cells were compared to total (unfractionated) cells. Relative increased expression of luminal markers (AR, PSA, CK8) in Epcam+CD44^{-} fractions confirms enrichment in this population (D). Expression of TMPRRS-ERG is detected exclusively in the Epcam+CD44- fraction (E).

Figure 2: Prostate Cancer Regeneration. A slice of tissue from a radical prostatectomy specimen from a patient with high-grade (Gleason 5+4, pStage T3bN1M0) prostate cancer was procured with preparation of an adjacent frozen section. Tumor and benign tissue were separated and tissues were dissociated into single cells. $5x10^4$ epithelial cells were combined with $1x10^6$ fetal prostate stroma and injected subQ into NOD-SCID mice. After 5 months, grafts were harvested for histological analysis.

Figure 3: Tumor Regeneration of High-Grade, Macrodissected Tumor Nodules (Gleason 8-10). With the exception of patient 1, benign-appearing tubule outgrowth is observed on histology.

ATTACHED FIGURES:

Figure 1
Figure 2
Figure 3

Original manuscripts attached.

Figure 1

Luminal Enrichment Enables TMPRSS-ERG+ Cell Isolation

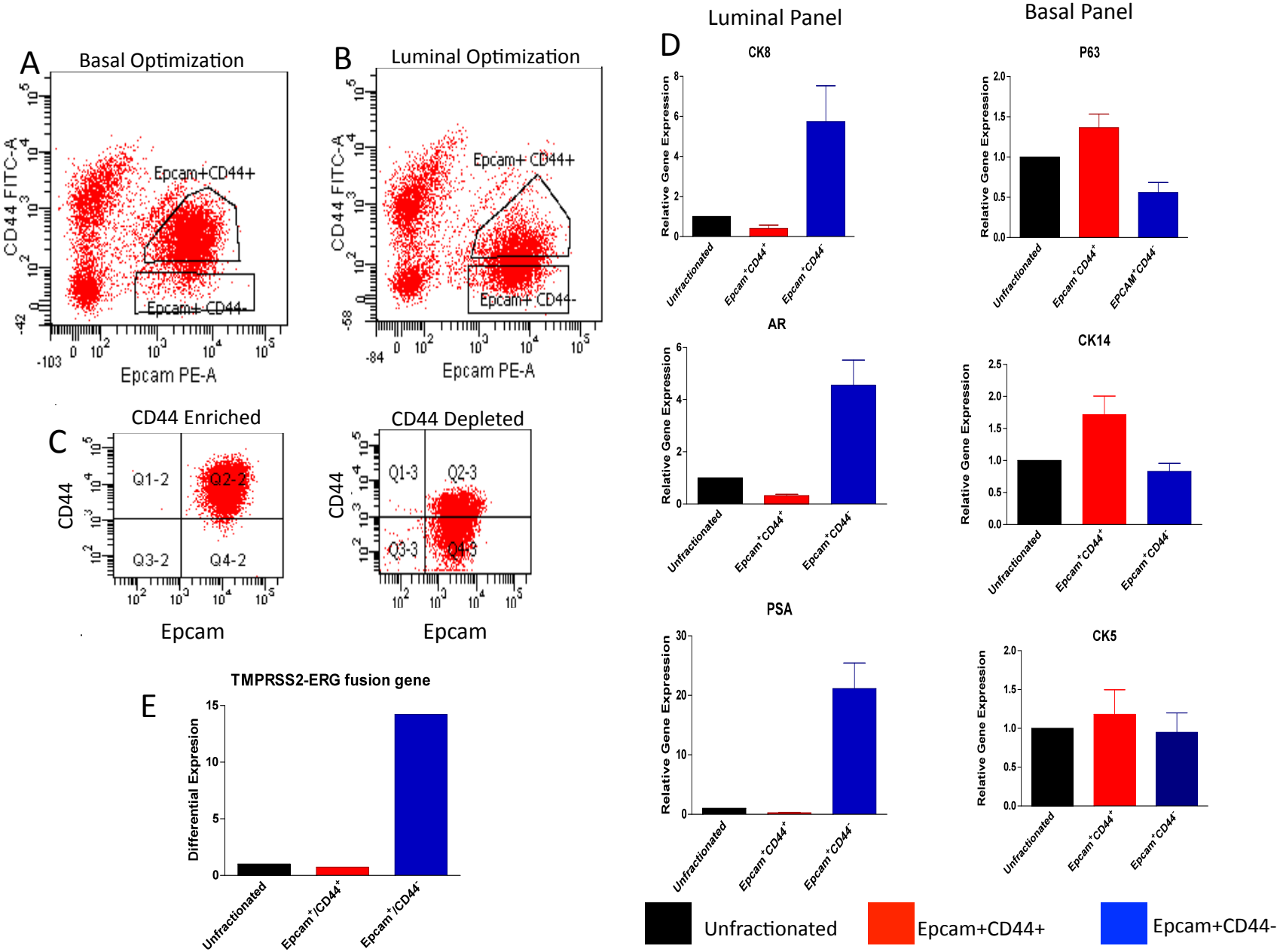

Figure 2

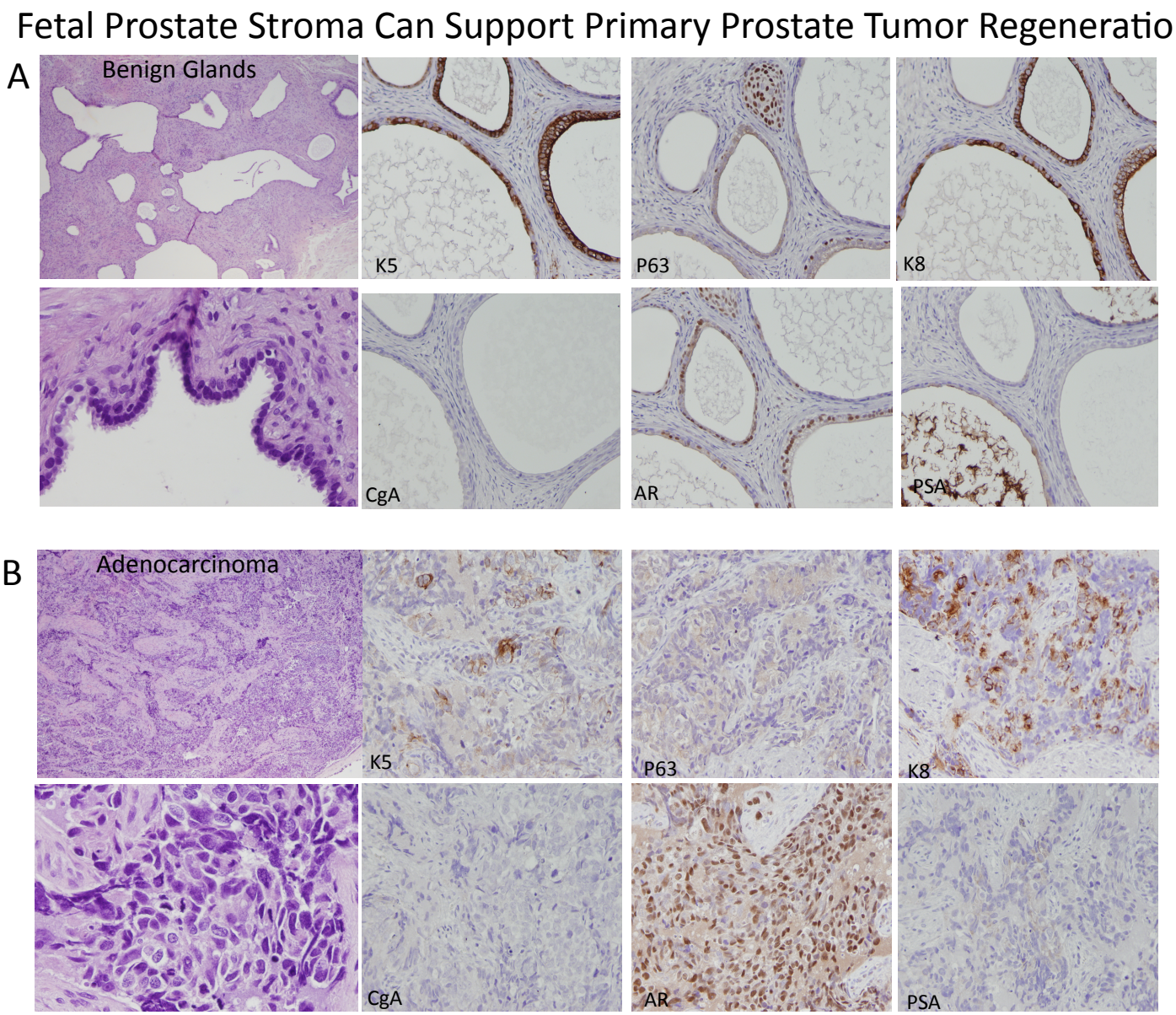
Fetal Prostate Stroma Can Support Primary Prostate Tumor Regeneration
A
Benign Glands
K5
P63
K8
CgA
AR
PSA
B
Adenocarcinoma
K5
P63
K8
CgA
AR
PSA

Figure 3

Fetal Prostate Stroma Is Not Routinely Sufficient to Support Primary Human Prostate Tumor Regeneration

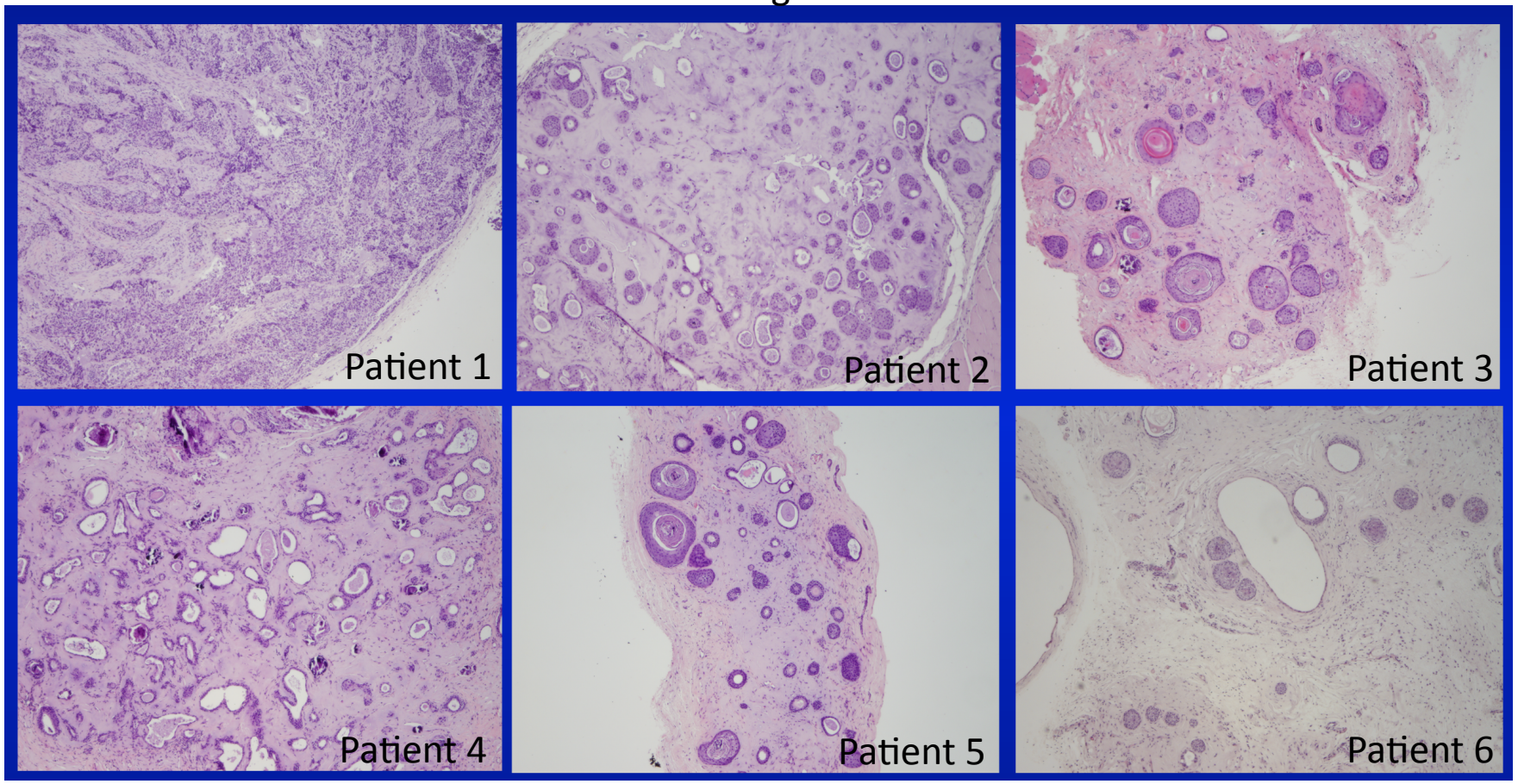

OPEN ACCESS Freely available online

PLoS one

Epcam, CD44, and CD49f Distinguish Sphere-Forming Human Prostate Basal Cells from a Subpopulation with Predominant Tubule Initiation Capability

Changyong Guo[1,2], Haibo Liu[1,2], Bao-Hui Zhang[1,2], Radu M. Cadaneanu[1,2], Aqila M. Mayle[1,2,3], Isla P. Garraway[1,2,3]*

1 Department of Urology, David Geffen School of Medicine at University of California Los Angeles, Los Angeles, California, United States of America, **2** Jonsson Comprehensive Cancer Center, David Geffen School of Medicine at University of California Los Angeles, Los Angeles, California, United States of America, **3** Greater Los Angeles Veterans Affairs Medical Center, Los Angeles, California, United States of America

Abstract

Background: Human prostate basal cells expressing alpha-6 integrin ($CD49f^{Hi}$) and/or CD44 form prostaspheres in vitro. This functional trait is often correlated with stem/progenitor (S/P) activity, including the ability to self-renew and induce differentiated tubules in vivo. Antigenic profiles that distinguish tubule-initiating prostate stem cells (SCs) from progenitor cells (PCs) and mature luminal cells (LCs) with less regenerative potential are unknown.

Methodology/Principle Findings: Prostasphere assays and RT-PCR analysis was performed following FACS separation of total benign prostate cells based upon combinations of Epcam, CD44, and/or CD49f expression. Epithelial cell fractions were isolated, including $Epcam^{+}CD44^{+}$ and Epcam+CD44+$CD49f^{Hi}$ basal cells that formed abundant spheres. When non-sphere-forming $Epcam^{+}CD44^{-}$ cells were fractionated based upon CD49f expression, a distinct subpopulation ($Epcam^{+}CD44^{-}CD49f^{Hi}$) was identified that possessed a basal profile similar to $Epcam^{+}CD44^{+}CD49f^{Hi}$ sphere-forming cells ($p63^{+}AR^{Lo}PSA^{-}$). Evaluation of tubule induction capability of fractionated cells was performed, in vivo, via a fully humanized prostate tissue regeneration assay. Non-sphere-forming $Epcam^{+}CD44^{-}$ cells induced significantly more prostate tubular structures than $Epcam^{+}CD44^{+}$ sphere-forming cells. Further fractionation based upon CD49f co-expression identified $Epcam^{+}CD44^{-}CD49f^{Hi}$ (non-sphere-forming) basal cells with significantly increased tubule induction activity compared to $Epcam^{+}CD44^{-}CD49f^{Lo}$ (true) luminal cells.

Conclusions/Significance: Our data delineates antigenic profiles that functionally distinguish human prostate epithelial subpopulations, including putative SCs that display superior tubule initiation capability and induce differentiated ductal/acini structures, sphere-forming PCs with relatively decreased tubule initiation activity, and terminally differentiated LCs that lack both sphere–forming and tubule-initiation activity. The results clearly demonstrate that sphere-forming ability is not predictive of tubule-initiation activity. The subpopulations identified are of interest because they may play distinct roles as cells of origin in the development of prostatic diseases, including cancer.

Citation: Guo C, Liu H, Zhang B-H, Cadaneanu RM, Mayle AM, et al. (2012) Epcam, CD44, and CD49f Distinguish Sphere-Forming Human Prostate Basal Cells from a Subpopulation with Predominant Tubule Initiation Capability. PLoS ONE 7(4): e34219. doi:10.1371/journal.pone.0034219

Editor: Andreas Androutsellis-Theotokis, Universitätsklinikum Carl Gustav Carus an der Technischen Universität Dresden, Germany

Received November 17, 2011; **Accepted** February 27, 2012; **Published** April 13, 2012

Funding: Support for these studies was provided by the Prostate Cancer Foundation (Challenge Award, PI: Dr. Owen Witte), the Jean Perkins Foundation, the Department of Defense (PC061068 and PC07373), and the National Institutes of Health CA-16042 and AI-28697. The funders had no role in study design, data collection and analysis, decision to publish, or preparation of the manuscript.

Competing Interests: The authors have declared that no competing interests exist.

* E-mail: igarraway@mednet.ucla.edu

Introduction

Human adult prostate S/Ps are characterized by surface marker expression, as well as functional traits, including the ability to self-renewal and differentiate into multiple lineages [1,2,3,4,5]. Markers that have been utilized to isolate human prostate S/Ps include Trop2, CD44, $alpha_2beta_1$-$integrin^{Hi}$, $alpha_6$-$integrin^{Hi}$ (CD49f), and CD133 [1,2,4,6]. However, a consensus does not exist regarding the antigenic profile of a functionally pure human prostate SC population and how to distinguish multipotent tubule-initiating SCs from progenitors with more limited potential. Making such a distinction may have important implications in understanding the etiology of prostatic disease, including benign prostatic hypertrophy and cancer.

Sphere-forming cells isolated from dissociated primary tissues are enriched in S/P cells in multiple organ systems [7,8,9,10]. In the human prostate, sphere-forming capability enables the selection of a subpopulation of epithelial cells with SC-like traits, including self-renewal and the ability to differentiate into tubular structures when implanted into immunocompromised mice [1,4]. Previous studies evaluating the antigenic profile of cells capable of forming prostaspheres indicate that they reside within the basal layer of normal prostatic ducts [1,4,11,12]. onsequently, the combination of Trop2 and $CD49f^{Hi}$ expression enables isolation of the basal cell fraction ($Trop2^{+}CD49f^{Hi}$), which exclusively forms

spheres, regenerates benign tubules, and demonstrates malignant transformation after genetic manipulations [1,4,6]. Sphere-forming cells are rare in prostate subpopulations that display luminal profiles ($Trop2^{+}CD49f^{Lo}$ or $Trop2^{+}CD44^{-}$)[1,4].

Subdivision of the basal population and enrichment of a sphere-forming and/or tubule-regenerating SC population has yet to be accomplished. However, a functional delineation of the human prostate cellular hierarchy, in addition to basal/luminal profile, could provide more specific insight about the cells of origin for prostate cancer and the pathways utilized by normal SCs that may become corrupted in prostate disease. The aim of this work is to employ in vitro sphere culture and in vivo tissue regeneration assays to interrogate combinations of surface antigens that may further subdivide human prostate epithelial cells and enable functional separation of tubule-initiating SCs from progenitors with more limited capabilities. In this report, we accomplish these goals by incorporating a refined tissue regeneration assay, in which human fetal prostate stroma (hFPS) is utilized to induce tubule formation/differentiation in a fully humanized system. Our results demonstrate that the combination of Epithelial Cell Adhesion Molecule (Epcam), CD44, and CD49f can be used to isolate three distinct populations: (i) a putative prostate SC population that does not form spheres, but induces relatively robust tubule regeneration, (ii) PCs possessing maximal sphere-forming ability, but decreased tubule-initiation capability, and (iii) terminally differentiated LCs that lack both sphere-forming and tissue regenerating potential. The uncoupling of sphere-forming and tubule-initiating functions indicates that human prostate cells with the most potential for niche interaction and tubule development appear to be quiescent in sphere-forming culture conditions.

Results

Epcam and CD44 enable separation of prostate cell lineages.

Epcam/Trop1 is a pan-epithelial antigen that is also expressed on most carcinomas, including prostate cancer [13]. In benign human prostate, immunohistochemical (IHC) staining demonstrates confinement of Epcam expression to epithelial cells that compose prostate ducts and acini (Figure 1A). CD44 is a single pass transmembrane glycoprotein involved in cell-cell matrix adhesion, cell signaling, inflammation, and cell migration ([14]). In the benign human prostate, CD44 marks basal cells and rare neuroendocrine cells [15]. Based on the expression pattern of Epcam and CD44 observed in IHC analysis of benign prostate tubules, it appears that $Epcam^{+}CD44^{+}$ cells compose the basal layer, while $Epcam^{+}CD44^{-}$ cells appear predominantly luminal (Figure 1A). We hypothesized that fractionating total prostate cells based upon the combination of Epcam and CD44 expression profiles could be a first step in determining antigenic profiles that delineate human prostate cellular hierarchy, by enabling basal and luminal separation. An advantage of both Epcam and CD44 is that conjugated magnetic beads are readily available that enable rapid fractionation of prostate cells without the need for a cell sorter. This may increase the accessibility and feasibility of fractionating surgical specimens. FACS analysis of total prostate epithelial cells using fluorescent antibodies to detect Epcam and CD44 expression demonstrate clear separation of ($Epcam^{+}$) epithelial cells from ($Epcam^{-}$) stromal/blood cells (Figure 1B). Although FACS analysis demonstrates that separation based on CD44 expression is not as distinct as Epcam, both $CD44^{+}$ and $CD44^{-}$ fractions were obtained via cell sorting or magnetic beads separation (Figure 1B).

Expression of basal- and luminal-specific genes correlates with Epcam/CD44 status.

Prostate basal and luminal cells can be distinguished based on marker profile, in addition to architectural organization. The tumor protein p63 is a hallmark indicator of basal cells, which also express relatively low levels of AR and PSA [16,17]. On the other hand, luminal cells lack p63, but express strong levels of AR, PSA, and cytokeratin 8 (CK8) [18,19]. In order to confirm enrichment of basal and luminal cells after fractionation based on Epcam/CD44 expression, quantitative RT-PCR analysis was performed on total RNA isolated from fractionated cells with primers targeting basal-specific and luminal-specific genes (Figure 1C). Compared to unfractionated cells and the $Epcam^{+}CD44^{+}$ fraction, $Epcam^{+}CD44^{-}$ cells demonstrated significantly increased expression of AR, PSA, and CK8 with low relatively low expression of the basal marker, p63. On the other hand, $Epcam^{+}CD44^{+}$ cells demonstrated virtually undetectable AR, PSA, and CK8 and enhanced expression of p63. These results are compatible with the known expression profiles of basal and luminal cells and indicate that the combination of Epcam and CD44 can effectively enrich for these lineages [19,20].

We have previously shown that prostate S/P cells are capable of prostasphere formation in vitro [4]. Additionally, we have found that basal cells are exclusively capable of forming spheres [1]. Therefore sphere-forming capability of $Epcam^{+}CD44^{+}$ and $Epcam^{+}CD44^{-}$ cell fractions was evaluated in comparison to unfractionated (U) cells. Consistent with previous studies, virtually all of the sphere-forming cells were confined to the basal-enriched $Epcam^{+}CD44^{+}$ cell fraction (Figure 1D), and this fraction demonstrated a 3-fold increase in sphere-forming cells compared to unfractionated total prostate cells. This data suggests that Epcam/CD44 fractionation enables a functional segregation of epithelial cell populations, in addition to basal and luminal separation.

HFPS Supports Prostate Tissue Regeneration Induced by Adult Human Prostate Cells In Vivo.

We have previously described regeneration of human prostate tissue following implantation of adult prostate cells (or prostaspheres) combined with rat urogenital sinus mesenchyme (rUGSM) and Matrigel® into Non-Obese Diabetic Severely Combined Immunodeficient mice that are Interluekin-2 Receptor Null (SCID-$NOD^{IL2grNULL}$) [4,6]. In an effort to employ a fully humanized prostate tissue regeneration system, rUGSM was replaced with human prostate stromal cells cultured from dissociated fetal prostate tissue (Figure 2). Histological evaluation of fetal prostate specimens demonstrates abundant stroma surrounding the prostatic urethra with developing epithelial buds/tubules (Figure 2A). FBS-supplemented culture media supported the outgrowth of a nearly pure (Epcam-negative) human fetal stromal cell population (hFPS) that could be passaged continuously for more than 10 generations (Figure 2B and data not shown). Cryopreservation of hFPS, followed by thaw and re-culture enabled further expansion of these cells prior to use in vivo. When hFPS was combined with freshly isolated adult prostate epithelial cells (Figure 2C) or sphere-forming cells (data not shown) and Matrigel®, followed by subcutaneous implantation into SCID-$NOD^{IL2grNULL}$ mice, epithelial cord-like structures formed as early as 6 weeks (data not shown). Fully differentiated ductal/acinar structures with PSA-expressing luminal cells were prominent by 6 months (Figure 2C). Epithelial cords and/or tubular structures failed to form if Matrigel® and hFPS were recombined in the absence of prostate epithelial cells (Figure S1). No differences in tubule development were noted in grafts induced by rUGSM or hFPS (Figure S1). All structures typically identified in benign

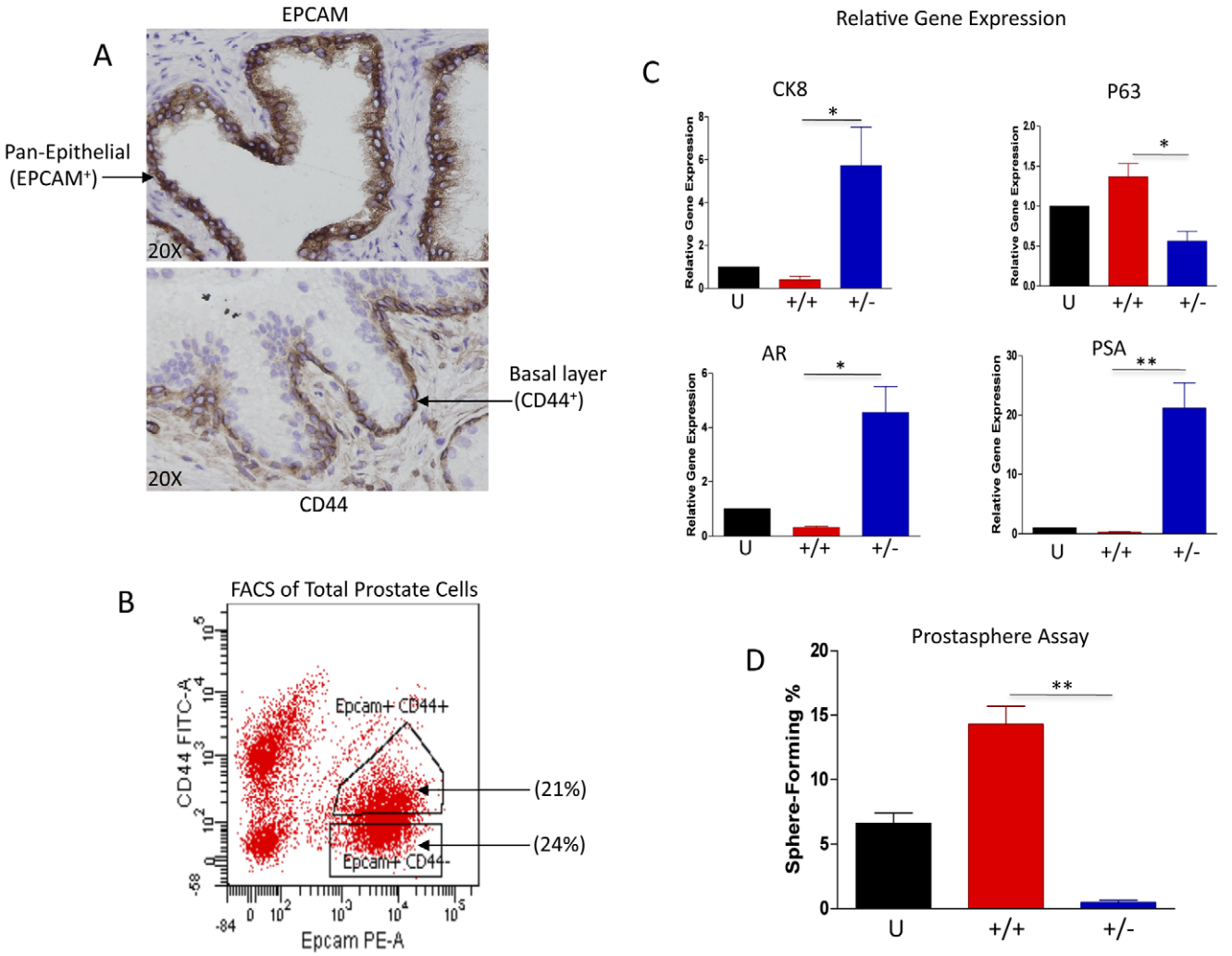

Figure 1. Variation in expression of Epcam and CD44 enables separation of distinct populations of prostate cells from dissociated surgical specimens. A. Immunohistochemical analysis of Epcam and CD44 expression in benign human prostate tissue specimens (20× magnification). B. FACS analysis of Epcam and CD44 expression in total prostate cells isolated from dissociated benign human prostate tissue. Total prostate cells stained with Epcam-PE and CD44-FITC conjugated antibodies prior to FACS analysis. C. Epcam^{+}CD44^{+} and Epcam^{+}CD44^{-} fractions display basal (P63+) and luminal (CK8+, AR+, PSA+) profiles, respectively. Quantitative RT-PCR reactions were performed in triplicate with a minimum of 3 individual patient specimens. Black columns represent Unfractionated (U) cells, red columns represent Epcam^{+}CD44^{+} cells (+/+), and blue columns represent Epcam^{+}CD44^{-} cells (+/−). D. Unfractionated prostate epithelial cells isolated from benign prostate tissue specimens or cells fractionated based on Epcam/CD44 expression were evaluated for sphere-forming capability in vitro. 1×10^{4} cells were plated in semi-solid (Matrigel®) cultures. Approximately 14 days after seeding, prostaspheres were quantitated in all wells and the percentage of sphere-forming cells was calculated in each fraction. All experiments were performed in triplicate, using a minimum of three individual patient samples. Statistical analysis was performed using standard one-way ANOVA analysis; $P<0.05$(*), $P<0.01$(**).
doi:10.1371/journal.pone.0034219.g001

prostate surgical specimens were present in hFPS regenerated grafts, including epithelial cords, corporal amylacea, and secretion-filled ducts/acini. Layers of epithelial cells expressing basal markers (K5, P63), luminal markers (K8, AR, PSA), or a combination of both were also identified (Figure 2C). HFPS was generated from 6 different fetal specimens and all demonstrated similar growth in culture, FACS profile, and ability to support tubular outgrowth when combined with adult prostate epithelial cells (data not shown).

Tubule initiating capability is prevalent in the non-sphere-forming Epcam^{+}CD44^{-} luminal-enriched cell fraction.

Although sphere formation is a common feature of S/Ps, one critical characteristic that prostate SCs must demonstrate is the ability to induce new tubule formation inclusive of ducts/acini composed of both basal and luminal cells. Prostate tissue regeneration assays have been utilized to interrogate the tubule initiation capability of putative S/P populations in mouse and human [4,21,22]. In these assays, total or fractionated cells obtained from fetal or adult prostate tissues are combined with supportive stroma (i.e., UGSM) followed by sub-renal implantation as a collagen graft or subcutaneous implantation with Matrigel® into immunocompromised mice. Cell fractions that possess S/P activity induce multi-layered tubular outgrowths with secretions surrounded by stroma. We have previously shown that sphere-forming cells as well as basal cells isolated based on co-expression of Trop2 and high levels of CD49f have an increased

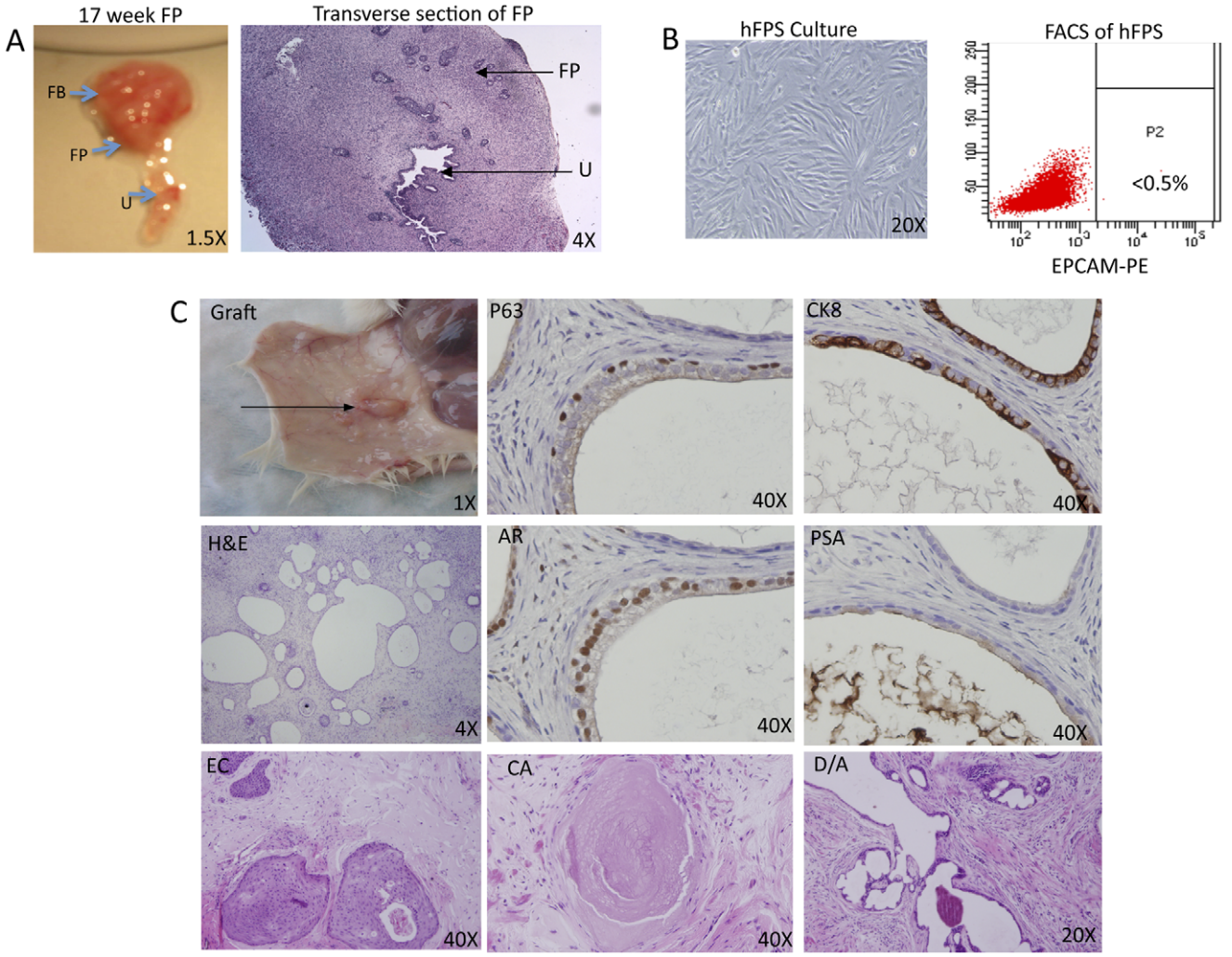

Figure 2. Isolation of human fetal prostate stroma (hFPS) for use in prostate tissue regeneration assays. A. Gross specimen containing 17-week fetal bladder (FB), prostate (FP), and urethra (U) en block with adjacent panel showing transverse hematoxylin and eosin (H&E) stained histological section. Developing prostate glands budding from the prostatic urethra are surrounded by abundant stroma. B. HFPS cells are cultured in DMEM supplemented with FBS. FACS analysis of cultured hFPS cells using antibodies that target Epcam demonstrates lack of (Epcam+) epithelial cell outgrowth. C. Regenerated graft induced by hFPS after recombination with freshly isolated adult human prostate cells and Matrigel®, followed by subcutaneous injection. H&E staining of paraffin-embedded graft demonstrates tubules with a distinct basal layer, containing cells that express tumor protein 63 (P63+) but lack luminal cell marker expression, including Androgen Receptor (AR), cytokeratin 8 (CK8), and Prostate Specific Antigen (PSA). A luminal layer is identified in the majority of outgrowths and contains cells that are P63−, AR+, CK8+, and PSA+. The bottom panel displays the different types of outgrowths identified in recombinant grafts, including epithelial cords (EC), corpora amylacea (CA), and epithelial cords/buds (EC).
doi:10.1371/journal.pone.0034219.g002

ability for tubule initiation compared to luminal ($Trop2^{+}CD49f^{Lo}$) cells [1,4,6].

In order to investigate the ability of cells fractionated based upon Epcam/CD44 expression to form tubules in vivo, human prostate tissue regeneration was performed. Approximately 1×10^5 unfractionated cells, $Epcam^{+}CD44^{+}$ cells, or $Epcam^{+}CD44^{-}$cells were combined with 2×10^5 hFPS and Matrigel®, followed by subcutaneous implantation into SCID-$NOD^{IL2grNULL}$ mice. Approximately twelve weeks following implantation, grafts were harvested and analyzed for tubule induction via histological analysis of paraffin embedded sections (Figure 3A). A table containing the rate of engraftment of unfractionated and fractionated cells is shown in Figure S2. Tubular structures were identified in grafts that developed from unfractionated cells and in $Epcam^{+}CD44^{+}$ recombinant grafts. Surprisingly, the $Epcam^{+}CD44^{-}$ luminal enriched/non-sphere-forming fractions yielded the largest number of tubular structures (Figure 3A and 3C). All grafts demonstrated a range of epithelial cord-like structures and more fully developed tubules with secretion-filled lumens (Figure 3A). Immunohistochemical staining confirmed the presence of basal ($p63^{+}$) and luminal ($CK8^{+}$) cells in regenerated tubules (Figure 3B). Although FACS and cytospin examination of fractionated cells confirmed $CD44^{-}$ status (data not shown), $CD44^{+}$ cord-like structures and tubules containing a distinct $CD44^{+}$ basal layer were identified in mature grafts induced by $Epcam^{+}CD44^{-}$ cell fractions (Figure 3B). This data suggests that $Epcam^{+}CD44^{-}$ cells may be precursors for $Epcam^{+}CD44^{+}$ cells found in regenerated tubular structures.

A functional role for a non-sphere-forming/luminal-enriched fraction appeared to contradict prior published results, in which fractionation of luminal cells based on Trop2/CD49f expression displayed no functional capabilities in vitro and in vivo[6]. To

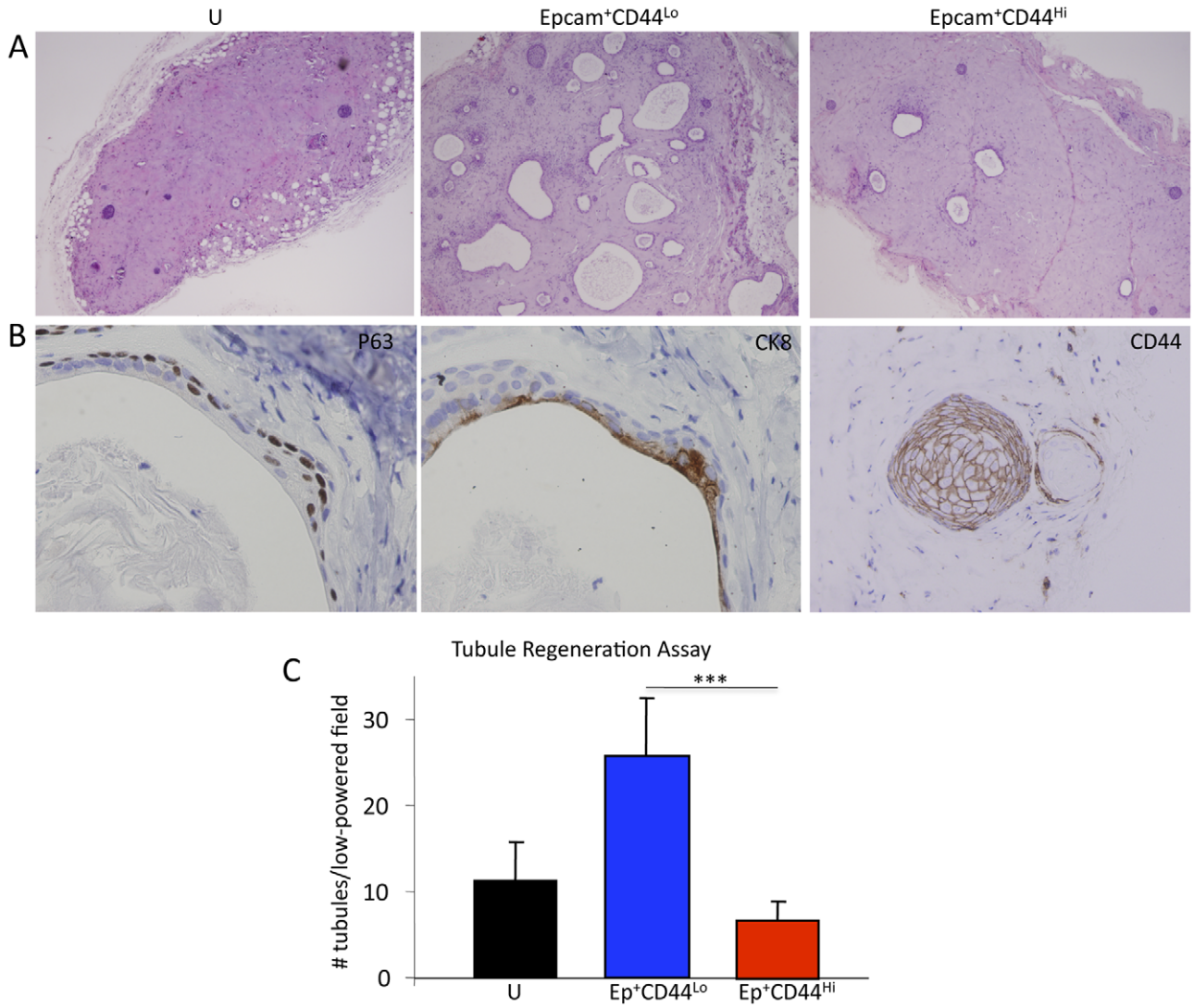

Figure 3. Tubule formation induced by unfractionated and fractionated (Epcam$^+$CD44$^+$ and Epcam$^+$CD44$^-$) prostate cells in human prostate tissue regeneration assays. A. H&E stained sections of paraffin-embedded 12-week grafts harvested from SCID-NOD$^{IL2\gamma rNULL}$ mice. Unfractionated (U) total prostate cells or Epcam$^+$CD44$^+$ and Epcam$^+$CD44$^-$ cell fractions combined with human fetal prostate stromal cells and Matrigel® were implanted subcutaneously into male SCID-NOD$^{IL2\gamma rNULL}$ mice. Testosterone was supplemented via pellets inserted subcutaneously. B. Example of secretion-filled ducts that display basal (p63 positive) and luminal (CK8 positive) cells induced by Epcam$^+$CD44$^-$ prostate cell fractions. Tubules and epithelial developed from cords containing CD44$^+$ cells also developed from the CD44$^-$ cell fraction. C. Comparison of the number of tubular structures identified in unfractionated, Epcam$^+$CD44$^+$, and Epcam$^+$CD44$^-$ grafts. After paraffin embedding, sections were made throughout the grafts. The two representative sections containing the highest number of tubules were identified and all tubules present in the low power (4X magnification) field were quantitated. The average numbers of tubules from total grafts obtained from unfractionated or fractionated cells are complied for the graph. Statistical analysis was performed using standard one-way ANOVA analysis; $P < 0.001$ (***).
doi:10.1371/journal.pone.0034219.g003

investigate this discrepancy, FACS analysis comparing Epcam and Trop2 expression was performed to evaluate co-expression of these surface markers. Indeed, there appeared to be almost complete overlap in expression of Trop2 and Epcam, with virtually all Trop2$^+$ cells co-expressing Epcam (Figure S3A). On the contrary, high expression CD49f did not appear to be confined to the CD44+ population, since a fraction of CD44$^-$ cells were CD49f^{Hi} (Figure S3B). This result suggests that Epcam$^+$CD44$^-$ prostate cells may be further subdivided based upon CD49f expression and may explain differential functional capabilities of basal/luminal cell fractions isolated based on Epcam/CD44 profile compared to Trop2/CD49f.

CD49f enables functional delineation of putative SCs, PCs, and LCs.

As described above, previous studies indicated that Trop2$^+$CD49f^{Hi} basal cells display both sphere forming and tubule regenerating capabilities, compared to the Trop2$^+$CD49f^{Lo} luminal cells, which lack these functional capabilities [4,6]. Given the surprising result that luminal-enriched Epcam$^+$CD44$^-$ cells display predominant tubule-initiation activity, we investigated whether or not CD49f^{Hi} cells present within this subpopulation may be responsible for tubule initiation in vivo. FACS analysis was performed on total prostate cells after incubation with antibodies targeting Epcam, CD44, and CD49f. Both CD49f^{Hi} and CD49f^{Lo} subpopulations were identified in Epcam$^+$CD44$^+$ and Ep-

cam^{+}CD44^{-} fractions (Figure 4A and S4). Cell sorting enabled isolation of prostate cells based upon Epcam/CD44/CD49 status. Prostasphere culture of Epcam^{+}CD44^{+}CD49f^{Hi} cells demonstrated enrichment of sphere-forming capability (10-fold over unfractionated cells and 3-fold over Epcam^{+}CD44^{+} cells) with 40–50% of cells within this fraction capable of forming spheres (Figure 4B). On the other hand, less than 1% of Epcam^{+}CD44^{+}CD49f^{Lo} or Epcam^{+}CD44^{-}CD49f^{Hi} cells were able to form spheres (Figure 4B and data not shown, respectively).

In order to evaluate tubule initiation activity of Epcam^{+}CD44^{-} non-sphere-forming cells subdivided by CD49f, in vivo tissue regeneration with hFPS was employed (Figure 4C). Recombinant grafts were retrieved from Epcam^{+}CD44^{-}CD49f^{Hi} cell fractions containing significantly more tubules than those induced by Epcam^{+}CD44^{-}CD49f^{Lo} cells (Figure 4C). FACS analysis of dissociated grafts induced by Epcam^{+}CD44^{-}CD49f^{Hi} cells demonstrated a similar composition of cells (based on Epcam/CD44/CD49f expression) as the original prostate surgical specimen (Figure 4E), indicating that this minority population could induce an intact prostate tissue profile.

As previously described, bright CD49f expression is associated with a basal cell profile, therefore, Epcam^{+}CD44^{-}CD49f^{Hi} and Epcam^{+}CD44^{-}CD49f^{Lo} cell fractions were evaluated by RT-PCR analysis to determine if the original Epcam^{+}CD44^{-} fraction contained a mix of luminal and basal cells [4,6,11]. RNA expression of p63 in association with a lack of AR and PSA indicated that Epcam^{+}CD44^{-}CD49f^{Hi} cells possessed a basal profile, while Epcam^{+}CD44^{-}CD49f^{Lo} cells exhibited a luminal profile, demonstrated by significant AR and PSA expression (Figure S5). This contrasting expression profile of Epcam^{+}CD44^{-}CD49f^{Hi} cells compared to RT-PCR analysis of Epcam^{+}CD44^{-} cells (in which fractionation with CD49f was not performed), indicates that the

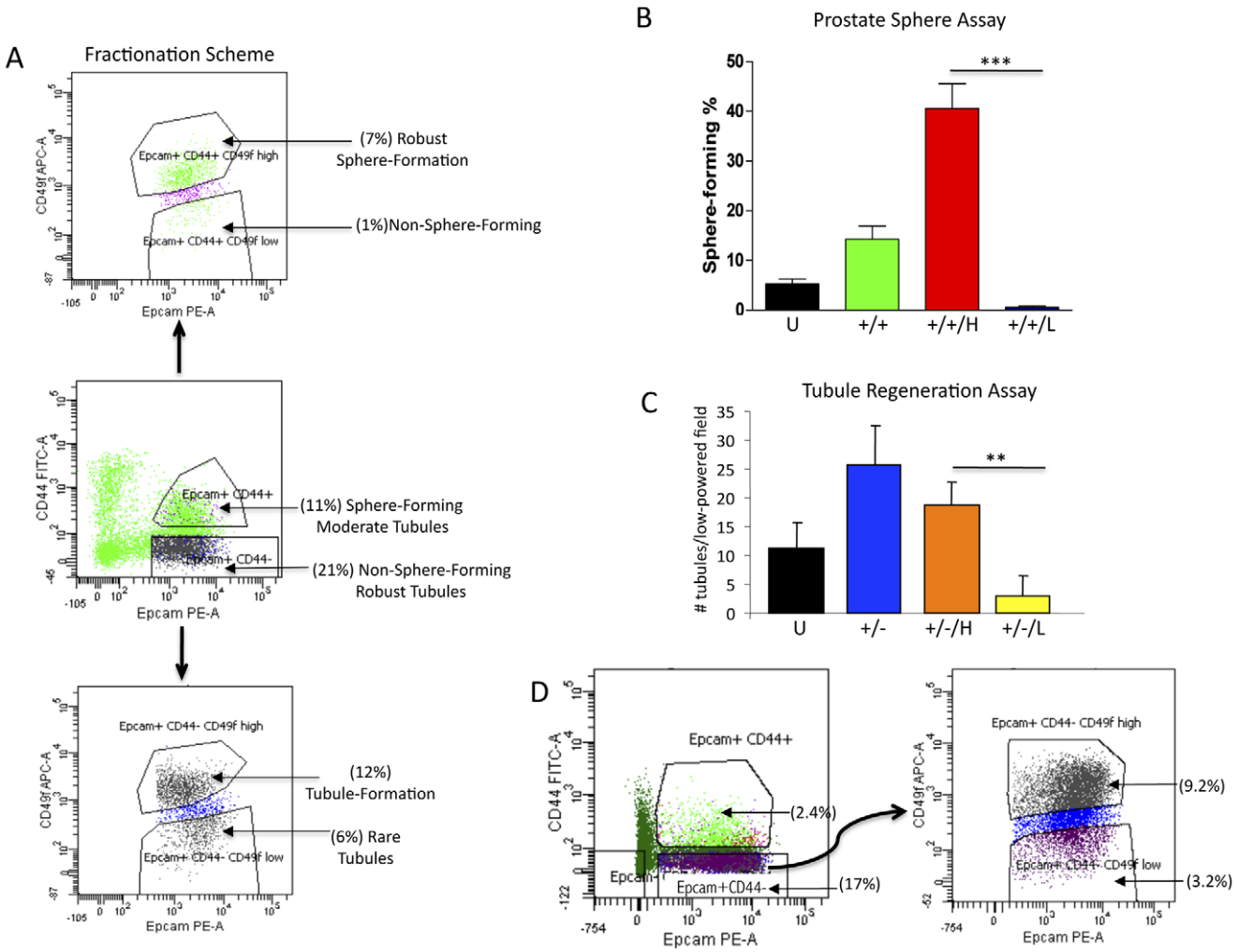

Figure 4. Identification and functional evaluation of CD49f$^{Hi/Lo}$ cells present in Epcam^{+}CD44^{+} and Epcam^{+}CD44^{-} fractions. A. FACS analysis of Epcam^{+}CD44^{+} and Epcam^{+}CD44^{-}for CD49f^{Hi} expression, with functionally distinct populations annotated. B. Sorting of Epcam^{+}CD44^{+} based on CD49f expression followed by sphere analysis in vitro (***P<0.001). Unfractionated (U), Epcam^{+}CD44^{+} (+/+), Epcam^{+}CD4+^{i}CD49f^{Hi} (+/+/H), Epcam^{+}CD44^{+}CD49f^{Lo} (+/+/L). C. Sorting of Epcam^{+}CD44^{-} based on CD49f expression followed by quantification of tubule initiation in vivo. After paraffin embedding, sections were made throughout the grafts. The two representative sections containing the highest number of tubules (4× magnification) were identified and quantitated. The average number of tubules from all the grafts retrieved is represented in the bar graph (**P<0.01). Epcam^{+}CD44−CD49f^{Hi} (+/−/H), Epcam^{+}CD44^{-}CD49f^{Lo} (+/−/L). D. FACS analysis of total cells obtained from three grafts induced by the Epcam^{+}CD44^{-}CD49f^{Hi} cell fraction. Grafts were mechanically and enzymatically digested to retrieve single cells that were pooled for FACS analysis. Although only highly enriched Epcam^{+}CD44^{-}CD49f^{Hi} cell fractions were combined with hFPS and Matrigel prior to injection, all of the cell types identified in the original prostate surgical specimens were found in regenerated tissue grafts.
doi:10.1371/journal.pone.0034219.g004

luminal expression profile observed with $Epcam^{+}CD44^{-}$ cell fractions was likely due to a masking effect by true luminal cells ($Epcam^{+}CD44^{-}CD49f^{Lo}$) that co-segregated with the non-sphere-forming basal subpopulation ($Epcam^{+}CD44^{-}CD49f^{Hi}$). Taken together, these results suggest that the human prostate basal cell population can be divided into populations with enriched sphere-forming activity ($Epcam^{+}CD44^{+}CD49f^{Hi}$) or tubule-initiating activity ($Epcam^{+}CD44^{-}CD49f^{Hi}$).

Discussion

Identifying functionally distinct populations of prostate epithelial cells could provide new insights about the cells of origin for human prostate cancer, by determining which cells within the hierarchy are susceptible to malignant transformation. Additionally, the mechanisms employed by normal prostate SCs that enable interaction with the niche and initiation of tubule development could lead to therapeutic approaches that interfere with similar pathways exploited by cancer cells or contributing to the development of benign prostatic hypertrophy (BPH). revious studies investigating human prostate S/P cells isolated from benign tissues have indicated that both general epithelial and basal antigens (Trop2, CD44, $alpha_2beta_1$-$integrin^{Hi}$, $alpha_6$-$integrin^{Hi}$ (CD49f)) are expressed [1,2,4]. In these studies, the ability to form self-renewing prostaspheres coincides with the potential to induce fully differentiated prostate tubules in vivo. In the current study, subpopulations of prostate basal cells with robust sphere-forming capability are distinguished from those with optimal tubule initiating capability based on specific antigenic profiles. Prostate epithelial cells with an increased potential to induce tubules inclusive of basal and luminal cell layers (putative SCs) are incapable of forming prostaspheres in vitro. On the other hand, highly proliferative sphere-forming cells (putative PCs) appear to have more limited potential for tubule initiation. This study is the first to functionally separate prostate epithelial cells based upon sphere-forming versus tubule initiating capabilities.

Combinations of antigens that subdivide the basal population and functionally distinguish prostate SCs from PCs have not been reported, with the exception of CD133, a rare surface marker found on less than 1% of basal cells [2]. A recent report regarding $\alpha_2\beta_1{}^{Hi}CD133^{+}$ cells indicated that these cells were incapable of forming spheres, but readily formed proliferative monolayer cultures [23]. Additional studies have demonstrated acinar-like outgrowths induced by $\alpha_2\beta_1{}^{Hi}CD133^{+}$ cells, in vivo [2]. This combined data suggests that $CD133^{+}$ cells are non-sphere-forming, but possess SC traits of self-renewal and differentiation capability, similar to the $Epcam^{+}CD44^{-}CD49f^{Hi}$ population reported here. In previous studies, we have also reported that CD133 expression did not enrich for sphere-forming cells [4]. However, given the surprising new finding of increased tubule formation induced by the non sphere-forming, $Epcam^{+}CD44^{-}CD49f^{Hi}$ cell fraction, analyzing concomitant expression of CD133 (and other putative SC markers) within this subset, including further fractionation and functional analysis, should be considered.

In previous studies of prostate S/P cells, Trop2, which has an almost identical pattern of expression as Epcam (Trop1) within prostate epithelial cells, was utilized to separate prostate epithelial from stromal and blood cells [1]. One advantage of using Epcam, as an alternative to Trop2, is stable and/or highly expressed Epcam is detected in most adenocarcinomas, as well as metastases, malignant effusions, and cancer stem cells [24]. Confirming the presence of Epcam within the human prostate S/P population may lead to investigations of therapeutic agents targeting Epcam and evaluation of specific effects on prostate SC and PC activity [24,25].

In the current study, CD44 expression appears to determine whether $Epcam^{+}$ prostate epithelial cells will form robust spheres ($CD44^{+}$) or remain quiescent in vitro, but induce robust tubule formation in vivo ($CD44^{-}$). In the neural system, it is a well-recognized limitation that quiescent neural SCs cannot be isolated using the neurosphere assay [26]. Additionally, it is emphasized that sphere-formation and self-renewal is a trait possessed by both SCs and PCs. In the current study, the antigenic profile of cells with the highest prostate sphere-forming capability is $Epcam^{+}CD44^{-}CD49f^{Hi}$. However, sphere-forming cells marked by $Epcam^{+}CD44^{+}$ expression can form tubules in vivo, but at a statistically significant lower rate than non-sphere-forming $Epcam^{+}CD44^{-}$ cells. Since previous in vivo studies clearly demonstrate that $CD49f^{Hi}$ is required for prostate tubule formation, we hypothesized that the $Epcam^{+}CD44^{-}CD49f^{Hi}$ antigenic profile designates non-sphere-forming cells capable of tubule regeneration in vivo. Indeed, this antigenic profile was confirmed in our study to represent a subpopulation of prostate basal cells with relatively robust tubule-initiating capability (compared to $Epcam^{+}CD44^{-}CD49f^{Hi}$ luminal cells) [6]. In contrast to our sphere results, sub-fractionation of $Epcam^{+}CD44^{-}$ cells with increased tubule initiation capability did not appear to further enrich for this activity. One factor that may have contributed to this observation is the fact that FACS sorting with three markers requires longer sort time, which could impact the long-term viability of these cells that is required for in vivo grafting. Despite enrichment with the more refined cell fraction, our results clearly demonstrate an advantage in tubule formation capability compared to luminal $Epcam^{+}CD44^{-}CD49f^{Lo}$ cells. Consequently, three distinct populations of prostate epithelial cells are revealed, including subdivided basal ($Epcam^{+}CD44^{+}CD49f^{Hi}$ and $Epcam^{+}CD44^{-}CD49f^{Hi}$) and luminal ($Epcam^{+}CD44^{-}CD49f^{Lo}$) fractions.

Bona fide SCs should be capable of residing in the quiescent state and become activated to differentiate and form new tubules as needed. With asymmetric cell division, progenitor daughter cells develop with less potential to induce new tubules. In the current study, although some sphere-forming cells retain the potential to induce new tubules, the proportion is far less than the in vitro quiescent $Epcam^{+}CD44^{-}$population. This result implies that prostaspheres contain both SCs and rapidly proliferating progenitors (possible transit-amplifying cells), resulting in an overall decreased potential to induce tubules compared to non-sphere-forming SCs. Hence, $Epcam^{+}CD44^{Hi}CD49f^{Hi}$ cells may be further along the developmental pathway and suggests a hierarchy of prostate epithelial cells.

Although the sphere-forming assays indicate that our putative SCs are quiescent, further studies are needed to evaluate this trait. It has been suggested that sphere-formation is an indicator of self-renewal, yet we have found that the non-sphere-forming ($Epcam^{+}CD44^{-}CD49f^{Hi}$) cells are capable of inducing differentiated tubules and regenerated grafts that include the full spectrum of prostate cells found in original surgical specimens, including putative SCs. This data indicates that in addition to differentiation and niche interaction capabilities, the putative SCs are self-renewing (despite the inability to form spheres).

Taken together, our results suggest that $Epcam^{+}CD44^{Lo}CD49f^{Hi}$ cells are non-sphere-forming SCs that may be activated to form tubules when exposed to inductive stroma cells in vivo. Lack of CD44 expression distinguishes non-sphere-forming SCs from the more proliferative state of the $CD44^{+}$ population, which may contain an increased proportion of PCs with limited

induction potential, relative to tubule-initiating SCs. Support for CD44 as a proliferative marker exists. The majority of primary prostate epithelial cells (transient amplifying cells) that grow as a monolayer, in vitro, express CD44 [27,28,29]. Examination of human prostate cancer cell lines and xenografts indicate that the $CD44^+$ population is more proliferative, clonogenic, tumorigenic, and metastatic than $CD44^-$ cells[30,31,32].

Future studies that may yield more insight into prostate SC/PC characteristics and function include gene expression array analysis comparing $Epcam^+CD44^-CD49f^{Hi}$ and $Epcam^+CD44^+CD49f^{Hi}$ cells. Such efforts could reveal novel antigens and genetic pathways that are unique to each subpopulation. Additionally, genetic manipulation of benign prostate cell fractions based on Epcam/CD44/CD49f expression, followed by in vivo regeneration may suggest mechanisms of tumorigenesis or benign proliferation (BPH) at different developmental stages.

Methods

Tissue Digestion and Cell Dissociation.

Human prostate tissue was obtained via a research protocol that was approved by the Office for the Protection of Research Subjects at UCLA and the Greater Los Angeles VA Medical Center. Informed written consent was obtained on all participants where identifying information was included. In cases where no identifying information was included and tissue was acquired in an anonymous fashion at UCLA, an approved Institutional Review Board protocol with written consent was not required by Office for the Protection of Research Subjects. Adjacent tissue specimens were snap frozen in liquid nitrogen or fixed in formalin and paraffin-embedded for histological analysis. Frozen sections were immediately examined by a genitourinary pathologist and cancer foci encircled. Fresh tissue specimens were matched with the frozen section slides to enable macrodissection of benign tissue away from tumor nodules. Typically, 2–10 grams of fresh tissue was allocated for research studies. Tissue specimens were then mechanically and enzymatically digested as previously described [16]. Dissociated tissue containing single cells and organoids was sequentially filtered through 100-μm and 40-μm cell strainer, and then passed repeatedly through a 23-gauge needle, in order to generate a single cell suspension. Cells were counted with a hemocytometer and resuspended in RPMI supplemented with 10% FBS prior to cell sorting or plating in prostasphere cultures. Approximately 1–2 million viable cells per gram of fresh tissue were routinely obtained.

Magnetic activated cell sorting(MACS).

Miltenyi auto MACS® was used to separate $Epcam^+CD44^+$ and $Epcam^+CD44^-$ prostate epithelial cells. For $Epcam^+$ cell separation, single cell suspensions obtained from freshly dissociated prostate tissue were stained with anti-human Epcam-PE antibody (Miltenyi Biotech), followed by incubation with anti-PE Multisort Microbeads (Miltenyi Biotech). Stained cells were separated through autoMACS (Miltenyi Biotech) with Mode POSSEL (Positive Selection). Positive fraction was collected as $Epcam^+$ cells and microbeads were removed using Multisort Release Reagents (Miltenyi Biotech). Cells were then stained with CD44 microbeads before separation through auto MACS® separator with POSSEL, with collection of positive ($Epcam^+CD44^+$) and negative ($Epcam^+CD44^-$) fractions. The negative fraction was separated further with Mode DEPLETES (Depletion in sensitive mode. The $Epcam^+CD44^+$ and $Epcam^+CD44^-$ cells were stained with anti-human CD44-PE-Cy-7 (eBioscience) and analyzed by FACS to evaluate the purity of sorted cells.

Fluorescence-activated cell sorting (FACS).

Prostate cells were suspended in PBS, 2 mM EDTA,0.5%BSA and stained with antibody for 15 minutes at 4°C. Fluorescence-activated cell sorting and analysis were performed on a BD Special Order FACS Aria II system and Diva v6.1.1 (BD Biosciences). Live single cells were gated based on scatter properties and analyzed for their surface marker expression. Cells were sorted and collected at 4°C using 100um nozzle and 23psi. Antibodies used for FACS include Epcam-PE (Miltenyi Biotech), CD44-FITC (ebioscience), and CD49f-APC (BioLegend).

In vitro prostasphere assay.

Prostate cells were counted and re-suspended in 50:50 Matrigel: PrEGM with a concentration of 5×10^3 cells/80microliters. This Matrigel/cellular suspension was plated at the edge of the well on 12-well plates and allowed to solidify by incubation at 37°C for 30 minutes. One milliliter of defined sphere media was then added to each well and plates were replaced in 37°C incubator, as previously described [4]. Quantitation of prostaspheres was performed approximately 10–14 days after plating.

Tissue acquisition, isolation and culture of fetal prostate cells.

Human fetal prostate tissue was acquired from 16–17 week specimens in accordance with federal and state guidelines. Adjacent prostate tissue was snap frozen in liquid Nitrogen or fixed in formalin and paraffin-embedded to evaluate anatomy and glandular architecture. The remainder of the tissue was mechanically and enzymatically digested as described (13). Dissociated prostate cell suspensions were sequentially filtered through 100-micron and 40-micron filters, and then passed through a 23-gauge needle. Cells were counted with a hemocytometer and resuspended in RPMI supplemented with 10% fetal bovine serum (FBS), penicillin/streptomycin (Mediatech Inc.), and Methyltrienolone R1881 (Sigma) for culture in vitro. After 3 passages, cells were analyzed via FACS to confirm purity of stromal cells (See below). HFBS is cryopreserved and thawed as needed for use in recombination assays.

In vivo tissue regeneration.

In vivo tissue experiments were performed in male SCID-$NOD^{IL2grNULL}$ mice in accordance with protocol number 2007-189-11A, approved by the Animal Research Committee within the Office for the Protection of Research Subjects at UCLA. Mice (6–8 weeks old) were subjected to subcutaneous injections of prostate epithelial cells. Approximately 1×10^5 epithelial cells were combined with 2×10^5 primary human fetal prostate stroma cells (hFPS). The epithelial and stromal cells were then suspended in 50 microliters 50:50 Matrigel®: PrEGM. Subcutaneous implantation of time-release testosterone pellets (Innovative Research of America) was simultaneously performed at the time of graft implantation. Subcutaneous nodules at the site of injection were removed after approximately 12 weeks of the implantation and frozen/paraffin-embedded sections were generated for immunohistochemical analysis. Fresh hFPS cells were cultured in RPMI supplemented with 10% FBS and R1881 (Sigma) and passaged three times prior to use in tissue regeneration assays.

Immunohistochemistry of tissue sections.

Prostate tissue was paraffin embedded as previously described [33]. Four-micron thick sections of frozen or paraffin embedded tissue were deparaffinized with xylene and rehydrated through a descending series of ethanol washes as described [4]. Antigen

retrieval and standard immunoperoxidase procedures were used in combination with primary antibodies, including CK5, CK8 (Convane), p63, androgen receptor (AR), Prostate Specific Antigen (PSA) (Santa Cruz), and CD44 (Abcam).

Real time RT-PCR Analysis.

RNA was extracted using Qiagen RNAeasy Micro Kit, following the manufacturer's instructions. The concentration and purity of total RNA was assessed spectrophotometrically at 260 and 280 nm. CDNA was generated from total RNA (up to 5 μg) using SuperScript III First-Strand Synthesis Kit (Invitrogen). For quantitative Real-time PCR, a Bio-Rad CFX Multicolor Real-time PCR detection system was employed, using the SYBR®-Green Supermix (Bio-Rad Laboratories). Real-time PCR primer pairs for CK8, PSA, AR and p63 were purchased from SABiosciences Corporation. The PCR reaction conditions included an initial step at 95°C for 3 min, followed by 40 cycles at 95°C for 15 s (Melt) and 60°C for 45 s (Anneal/Extend). Detection of PCR products was accomplished by measuring the emitting fluorescence at the end of each reaction step (reaction cycles). Threshold cycle corresponds with the cycle number required to detect a fluorescence signal above the threshold. Calculations were performed by Bio-Rad IQ5 software provided by the manufacturer. Gene expression analysis was performed using the comparative method.

Supporting Information

Figure S1 Comparison of prostate tissue grafts induced by rUGSM and hFPS. Total adult prostate cells (5×10^5) isolated from fresh benign surgical specimens were combined with either rUGSM or hFPS (1×10^6 cells). Grafts were retrieved approximately 12 weeks following subcutaneous injection into SCID-NOD$^{IL2\gamma rNULL}$ mice. H&E staining of paraffin-embedded sections demonstrated similar composition of tubular structures within grafts, including ductal/acini structures, corpora amylacea, and epithelial cords. Similar to previous studies with rUGSM, grafts that formed from hFPS without additive adult prostate epithelial cells (PCs) did not contain any tubular structures. All grafts with tubules (T) were found to have prominent vasculature (BV) throughout (Right panel).
(TIF)

Figure S2 Table depicting number of patient samples utilized for implants and grafts retrieved. A total of 29 implants yielded 20 grafts with tubules for comparative analysis (69% engraftment rate).
(TIF)

Figure S3 Epcam (Trop1) and Trop2 demonstrate overlapping expression in human prostate cells, while CD49f and CD44 demonstrate disparate expression. A. Total prostate cells were co-stained with antibodies recognizing Epcam and Trop2 and subjected to FACS analysis. The majority of Epcam$^+$ cells co-expressed Trop2. B. Total prostate cells were co-stained with antibodies recognizing CD44 and CD49f. A population of CD49f^{Hi} cells were identified that appear to be CD44$^-$, suggesting that a proportion of Epcam$^+$CD44$^-$cells may co-express CD49f.
(TIF)

Figure S4 FACS analysis of individual patient surgical specimens for Epcam/CD44/CD49f. Four patient specimens (A–D) are shown for comparative analysis of populations retrieved. After mechanical and enzymatic digestion, single cell suspensions are stained with antibodies targeting Epcam, CD44, and CD49f. High and low CD44-expressing populations of Epcam+ cells are gated and analyzed for CD49f expression. High and low CD49f-expressing cells are then isolated for functional analysis.
(TIF)

Figure S5 Quantitative RT-PCR demonstrates Epcam$^+$CD44$^-$CD49f^{Hi} cell fractions have a basal profile (p63$^+$AR^{Lo}PSA$^-$), while Epcam$^+$CD44$^-$CD49f^{Lo} cells display a luminal profile (p63^{Lo}AR^{Hi}PSA$^+$). Primers targeting p63, AR, and PSA were used in fractionated cells to compare expression relative to unfractionated cells (U). Epcam$^+$CD44$^-$CD49f^{Hi} (+/−/H), Epcam$^+$CD44$^-$CD49f^{Lo} (+/−/L). Statistical analysis was performed using standard one-way ANOVA analysis. $P<0.05$(*), $P<0.01$(**).
(TIF)

Acknowledgments

Flow cytometry/FACS was performed in the UCLA Jonsson Comprehensive Cancer Center (JCCC) and Center for AIDS Research Flow Cytometry Core Facility. We gratefully thank Donghui Cheng, who performed additional FACS sorting, Dr. Dong Sun An, who provided fetal prostate samples, and the genitourinary pathologists in the UCLA Tissue Procurement Clinical Laboratory and at the Greater Los Angeles Veterans Hospital for assisting with specimen retrieval and slide review. Additional thanks to Drs. Hong Wu and David Mulholland for manuscript review.

Author Contributions

Conceived and designed the experiments: CG HL IG. Performed the experiments: CG HL BZ RC. Analyzed the data: CG HL BZ AM IG RC. Contributed reagents/materials/analysis tools: AM. Wrote the paper: CG HL IG.

References

1. Goldstein AS, Lawson DA, Cheng D, Sun W, Garraway IP, et al. (2008) Trop2 identifies a subpopulation of murine and human prostate basal cells with stem cell characteristics. Proc Natl Acad Sci U S A 105: 20882–20887.
2. Richardson GD, Robson CN, Lang SH, Neal DE, Maitland NJ, et al. (2004) CD133, a novel marker for human prostatic epithelial stem cells. J Cell Sci 117: 3539–3545.
3. Vander Griend DJ, Karthaus WL, Dalrymple S, Meeker A, DeMarzo AM, et al. (2008) The role of CD133 in normal human prostate stem cells and malignant cancer-initiating cells. Cancer Res 68: 9703–9711.
4. Garraway IP, Sun W, Tran CP, Perner S, Zhang B, et al. (2010) Human prostate sphere-forming cells represent a subset of basal epithelial cells capable of glandular regeneration in vivo. Prostate 70: 491–501.
5. Collins AT, Habib FK, Maitland NJ, Neal DE (2001) Identification and isolation of human prostate epithelial stem cells based on alpha(2)beta(1)-integrin expression. J Cell Sci 114: 3865–3872.
6. Goldstein AS, Huang J, Guo C, Garraway IP, Witte ON (2010) Identification of a cell of origin for human prostate cancer. Science 329: 568–571.
7. Buzhor E, Harari-Steinberg O, Omer D, Metsuyanim S, Jacob-Hirsch J, et al. (2011) Kidney spheroids recapitulate tubular organoids leading to enhanced tubulogenic potency of human kidney-derived cells. Tissue Eng Part A.
8. Deleyrolle LP, Reynolds BA (2009) Identifying and enumerating neural stem cells: application to aging and cancer. Prog Brain Res 175: 43–51.
9. Deleyrolle LP, Reynolds BA (2009) Isolation, expansion, and differentiation of adult Mammalian neural stem and progenitor cells using the neurosphere assay. Methods Mol Biol 549: 91–101.
10. Farnie G, Clarke RB (2006) Breast stem cells and cancer. Ernst Schering Found Symp Proc. pp 141–153.
11. Lawson DA, Xin L, Lukacs RU, Cheng D, Witte ON (2007) Isolation and functional characterization of murine prostate stem cells. Proc Natl Acad Sci U S A 104: 181–186.
12. Xin L, Lukacs RU, Lawson DA, Cheng D, Witte ON (2007) Self-renewal and multilineage differentiation in vitro from murine prostate stem cells. Stem Cells 25: 2760–2769.
13. Went PT, Lugli A, Meier S, Bundi M, Mirlacher M, et al. (2004) Frequent EpCam protein expression in human carcinomas. Hum Pathol 35: 122–128.

14. Zoller M (2011) CD44: can a cancer-initiating cell profit from an abundantly expressed molecule? Nat Rev Cancer 11: 254–267.
15. Palapattu GS, Wu C, Silvers CR, Martin HB, Williams K, et al. (2009) Selective expression of CD44, a putative prostate cancer stem cell marker, in neuroendocrine tumor cells of human prostate cancer. Prostate 69: 787–798.
16. Tran CP, Lin C, Yamashiro J, Reiter RE (2002) Prostate stem cell antigen is a marker of late intermediate prostate epithelial cells. Mol Cancer Res 1: 113–121.
17. Epstein JI (2010) An update of the Gleason grading system. J Urol 183: 433–440.
18. van Leenders G, van Balken B, Aalders T, Hulsbergen-van de Kaa C, Ruiter D, et al. (2002) Intermediate cells in normal and malignant prostate epithelium express c-MET: implications for prostate cancer invasion. Prostate 51: 98–107.
19. van Leenders GJ, Aalders TW, Hulsbergen-van de Kaa CA, Ruiter DJ, Schalken JA (2001) Expression of basal cell keratins in human prostate cancer metastases and cell lines. J Pathol 195: 563–570.
20. Signoretti S, Loda M (2006) Prostate stem cells: From development to cancer. Semin Cancer Biol.
21. Cunha GR, Lung B (1978) The possible influence of temporal factors in androgenic responsiveness of urogenital tissue recombinants from wild-type and androgen-insensitive (Tfm) mice. J Exp Zool 205: 181–193.
22. Xin L, Ide H, Kim Y, Dubey P, Witte ON (2003) In vivo regeneration of murine prostate from dissociated cell populations of postnatal epithelia and urogenital sinus mesenchyme. Proc Natl Acad Sci U S A 100 Suppl 1: 11896–11903.
23. Lang SH, Anderson E, Fordham R, Collins AT (2010) Modeling the prostate stem cell niche: an evaluation of stem cell survival and expansion in vitro. Stem Cells Dev 19: 537–546.
24. Patriarca C, Macchi RM, Marschner AK, Mellstedt H (2011) Epithelial cell adhesion molecule expression (CD326) in cancer: A short review. Cancer Treat Rev.
25. Kurtz JE, Dufour P (2010) Adecatumumab: an anti-EpCAM monoclonal antibody, from the bench to the bedside. Expert Opin Biol Ther 10: 951–958.
26. Pastrana E, Silva-Vargas V, Doetsch F (2011) Eyes wide open: a critical review of sphere-formation as an assay for stem cells. Cell Stem Cell 8: 486–498.
27. Litvinov IV, Vander Griend DJ, Xu Y, Antony L, Dalrymple SL, et al. (2006) Low-calcium serum-free defined medium selects for growth of normal prostatic epithelial stem cells. Cancer Res 66: 8598–8607.
28. Peehl DM (2004) Are primary cultures realistic models of prostate cancer? J Cell Biochem 91: 185–195.
29. Peehl DM (2005) Primary cell cultures as models of prostate cancer development. Endocr Relat Cancer 12: 19–47.
30. Patrawala L, Calhoun T, Schneider-Broussard R, Li H, Bhatia B, et al. (2006) Highly purified CD44+ prostate cancer cells from xenograft human tumors are enriched in tumorigenic and metastatic progenitor cells. Oncogene 25: 1696–1708.
31. Patrawala L, Calhoun-Davis T, Schneider-Broussard R, Tang DG (2007) Hierarchical organization of prostate cancer cells in xenograft tumors: the CD44+alpha2beta1+ cell population is enriched in tumor-initiating cells. Cancer Res 67: 6796–6805.
32. Liu C, Kelnar K, Liu B, Chen X, Calhoun-Davis T, et al. (2011) The microRNA miR-34a inhibits prostate cancer stem cells and metastasis by directly repressing CD44. Nat Med 17: 211–215.
33. Garraway IP, Seligson D, Said J, Horvath S, Reiter RE (2004) Trefoil factor 3 is overexpressed in human prostate cancer. Prostate 61: 209–450.

OPEN ACCESS Freely available online

PLoS one

Identification of CD166 as a Surface Marker for Enriching Prostate Stem/Progenitor and Cancer Initiating Cells

Jing Jiao[1,2◑], Antreas Hindoyan[1,2◑], Shunyou Wang[1¤], Linh M. Tran[1,2], Andrew S. Goldstein[3,4], Devon Lawson[1], Donghui Chen[3,4], Yunfeng Li[1,2], Changyong Guo[5], Baohui Zhang[5], Ladan Fazli[6], Martin Gleave[6], Owen N. Witte[1,2,3,4,7], Isla P. Garraway[5]*, Hong Wu[1,2,7]*

1 Department of Molecular and Medical Pharmacology, University of California Los Angeles, Los Angeles, California, United States of America, **2** Institute for Molecular Medicine, University of California Los Angeles, Los Angeles, California, United States of America, **3** Howard Hughes Medical Institute, University of California Los Angeles, Los Angeles, California, United States of America, **4** Department of Microbiology and Molecular Genetics, University of California Los Angeles, Los Angeles, California, United States of America, **5** Department of Urology, University of California Los Angeles, Los Angeles, California, United States of America, **6** The Vancouver Prostate Centre and University of British Columbia, Vancouver, British Columbia, Canada, **7** Eli and Edythe Broad Center of Regenerative Medicine and Stem Cell Research, University of California Los Angeles, Los Angeles, California, United States of America

Abstract

New therapies for late stage and castration resistant prostate cancer (CRPC) depend on defining unique properties and pathways of cell sub-populations capable of sustaining the net growth of the cancer. One of the best enrichment schemes for isolating the putative stem/progenitor cell from the murine prostate gland is $Lin^-;Sca1^+;CD49f^{hi}$ (LSC^{hi}), which results in a more than 10-fold enrichment for *in vitro* sphere-forming activity. We have shown previously that the LSC^{hi} subpopulation is both necessary and sufficient for cancer initiation in the *Pten*-null prostate cancer model. To further improve this enrichment scheme, we searched for cell surface molecules upregulated upon castration of murine prostate and identified CD166 as a candidate gene. CD166 encodes a cell surface molecule that can further enrich sphere-forming activity of WT LSC^{hi} and *Pten* null LSC^{hi}. Importantly, CD166 could enrich sphere-forming ability of benign primary human prostate cells *in vitro* and induce the formation of tubule-like structures *in vivo*. CD166 expression is upregulated in human prostate cancers, especially CRPC samples. Although genetic deletion of murine CD166 in the *Pten* null prostate cancer model does not interfere with sphere formation or block prostate cancer progression and CRPC development, the presence of CD166 on prostate stem/progenitors and castration resistant sub-populations suggest that it is a cell surface molecule with the potential for targeted delivery of human prostate cancer therapeutics.

Citation: Jiao J, Hindoyan A, Wang S, Tran LM, Goldstein AS, et al. (2012) Identification of CD166 as a Surface Marker for Enriching Prostate Stem/Progenitor and Cancer Initiating Cells. PLoS ONE 7(8): e42564. doi:10.1371/journal.pone.0042564

Editor: Dean G. Tang, The University of Texas M.D. Anderson Cancer Center, United States of America

Received March 8, 2012; **Accepted** July 9, 2012; **Published** August 3, 2012

Funding: This work has been supported in part by an award from the Prostate Cancer Foundation (to OW, IPG and HW), Jean Perkins Foundation and Department of Defense (to IPG) and a grant from the National Institutes of Health (R01 CA107166 and RO1 CA121110 to HW). ONW is an Investigator of the Howard Hughes Medical Institute. The funders had no role in study design, data collection and analysis, decision to publish, or preparation of the manuscript.

Competing Interests: The authors have declared that no competing interests exist.

* E-mail: igarraway@mednet.ucla.edu (IG); hwu@mednet.ucla.edu (HW)

◑ These authors contributed equally to this work.

¤ Current address: Intellikine, Inc., La Jolla, California, United States of America

Introduction

Despite advances in the early detection and management of prostate cancer, castration resistant prostate cancer (CRPC) remains the second most common cause of male mortality in the United States [1]. Mounting evidence suggests that a subpopulation of prostate cells can initiate prostate cancer and may be responsible for the castration resistance [2,3,4,5]. Therefore, these cancer initiating cells [6] may serve as promising cellular targets for prostate cancer and identification of this subpopulation has become the necessary step toward future effective therapy.

The origins of prostate cancer initiating cells are controversial [7,8]. Normal prostate from human or mouse contains three different types of cells, namely luminal secretory, basal and neuroendocrine cells. Since human prostate cancer is characterized by loss of basal cells and expansion of luminal cells, several animal models posit that luminal-specific progenitors are the sources of prostate cancer initiation [9,10,11]. However, using the tissue regeneration approach, basal cells have proved to be more efficient oncogenic targets for both human and mouse prostate cancer initiation [12,13]. Interestingly, Xin's group demonstrated that adult murine prostate basal and luminal cells are self-sustained lineages that can both serve as oncogenic targets for prostate cancer initiation [14].

PTEN plays an important role in human prostate cancer and CRPC development [15] and is inactivated in 20% of primary and 60% of metastatic lesions [16]. The murine *Pten* prostate cancer model ($Pb\text{-}Cre^+;Pten^{L/L}$) recapitulates the disease progression seen in humans, including CRPC [17,18,19,20], and shares many signature genetic changes with human disease [17]. Importantly, the $Pb\text{-}Cre^+;Pten^{L/L}$ model provides a unique tool for studying tumor initiating cells as the majority of luminal cells and subpopulations of basal cells have *Pten* deletion [17,18]. Using this model, we demonstrated that *Pten* deletion causes an

expansion of basal and transient amplifying subpopulations and subsequent tumor initiation *in vivo* [18]. We further showed $Lin^-Sca\text{-}1^+CD49f^{hi}$ (LSC^{hi}) prostate stem/progenitor cells from the *Pten* null prostate are capable of initiating a cancerous phenotype that mimics the primary cancer in the *Pten* null prostate model [19].

Here, we report the identification of a cell surface marker, CD166 or Activated Leukocyte Cell Adhesion Molecule (CD166/ALCAM) that is highly upregulated in human and murine CRPC samples. CD166 can be used to enrich for stem/progenitor sphere-forming cells from both WT and *Pten* null mutant mouse prostates. In addition, CD166 can separate LSC^{hi} mouse stem/progenitor cells into $CD166^{hi}$ and $CD166^{lo}$ subpopulations, with the LSC^{hi};$CD166^{hi}$ subpopulation having much higher sphere-forming activity. We further demonstrate that CD166 can be used as an enrichment maker for isolating human prostate sphere-forming cells and tubule-forming cells.

Results

CD166 Expression is Upregulated in Murine Castrated Prostatic Epithelium and can be used for Enriching Stem/progenitor Cells

Rodent prostate contains stem-like cells that are enriched in the castrated prostate gland and can undergo more than 15 cycles of involution-regeneration in response to androgen withdrawal and replacement [21]. We reasoned that castration may also lead to upregulation or enrichment of those stem cell surface molecules that can potentially serve as marker for isolating stem/progenitor cells and for targeted drug delivery. We therefore mined publically available databases describing gene expression profiles of murine prostates at day 0 and day 3 post-castration [22,23]. We focused on those genes that fell in the gene ontology category of 'plasma membrane' and identified CD166/ALCAM as one of only two common castration-enriched cell surface molecules (Table S1). CD166 was significantly increased (1-tail t-test <0.015) 3 days after castration as compared to intact mice. While Cxcl12 is also upregulated, we chose not to focus on this gene as it is a chemokine and not amenable for FACS-mediated stem/progenitor cell enrichment.

CD166 is a type I transmembrane protein of the Ig superfamily that mediates cell-cell interactions via heterophilic (CD166-CD6) and/or homophilic (CD166-CD166) mechanisms [24,25]. We found that in the intact mice, CD166 is preferentially expressed in the stem/progenitor-enriched proximal region [21] but low in the stem/progenitor-poor distal region of the WT prostate (Figure 1A upper panels). CD166 protein levels are also up-regulated immediately following castration (Figure 1A lower panels; comparing day 0 and day 3 post- castration).

Prostate stem/progenitor cells are characterized by their ability to form spheres *in vitro* [26]. We performed the sphere-forming assay using sorted $CD166^{hi}$ and $CD166^{lo}$ cells and found that $CD166^{hi}$ cells have significantly higher sphere-forming activity compared to $CD166^{lo}$ cells (Figure 1B, left). Since we had previously developed the LSC^{hi} enrichment scheme [26], which yields 10-fold enrichment of WT sphere-forming cells, we tested whether CD166 can be used for further enriching sphere-forming activity. We gated LSC^{hi} cells according to their CD166 expression and found that LSC^{hi};$CD166^{hi}$ cells have 5-fold higher sphere-forming activity as compared to their LSC^{hi};$CD166^{lo}$ counterpart (Figure 1B, right). Therefore, CD166 can be used as a marker to further enrich sphere forming cells within the WT prostate. Serial passaging of the spheres generated from LSC^{hi};$CD166^{hi}$ cells demonstrated that this enhanced sphere-forming activity could be maintained *in vitro* through at least three passages (Figure S1A). In contrast, less spheres were generated from LSC^{hi};$CD166^{lo}$ cells (P0–P2) and cannot undergo continuous passage due to the limited cell number. We observed no significant difference in the sphere size distribution between LSC^{hi};$CD166^{hi}$ generated spheres and LSC^{hi};$CD166^{lo}$ generated spheres (Figure S1B and S1C). Similar to the LSC^{hi} subpopulation [26], castration also leads to significant enhancement of the LSC^{hi};$CD166^{hi}$ subpopulation (Figure 1C).

$CD166^{hi}$ Human Prostate Cells Have Higher Sphere Forming and Regeneration Potential

Certain cell surface markers, such as Sca-1, are only expressed in the mouse and therefore cannot be used for isolation of human stem/progenitor cells. CD166, on the other hand, is expressed in various human organs and upregulated in human cancers, including prostate cancer [27]. To determine whether CD166 can be used for enriching human prostate stem/progenitors, we first examined its expression and found that CD166 is highly expressed in the developing human fetal prostate epithelium (Figure 2A, left panel) and focally expressed in the benign adult prostate, which overlaps with a subset of TROP2 and CD49f – positive cells (Figure 2, middle and right panels).

We then evaluated whether CD166 could be used as a marker for enriching human stem/progenitor cells. Benign regions of prostate tissue were collected from multiple patients who underwent radical prostatectomy and dissociated to single cells. Consistent with our previous studies [13,28], the percentages of $CD166^+$ cells vary from patient to patient (data not shown). However, the majority of sphere forming activity was identified in the $CD166^{hi}$ population (Figure 2B), similar to our findings with murine prostate cells. Data are shown from 6 representative patients.

To evaluate whether CD166 can enrich human prostate tissue regeneration capacity *in vivo*, benign human prostate cells were dissociated and sorted according to cell surface CD166 expression levels. Equal number of viable $CD166^{hi}$ and $CD166^{lo}$ cells (2×10^5) was implanted subcutaneously into NOD-SCID/IL2rγ null mice, in combination with 2×10^5 rUGSM inductive mesenchymal cells. After 8–16 weeks, grafts were harvested, fixed and embedded in paraffin for quantification and analyses. $CD166^{hi}$ cells have more tissue regeneration capacity as evidenced by increased number of tubule-like epithelial structures found in the grafts, which is rarely seen in the $CD166^{lo}$ grafts (Figure 2C). Further analyses showed that the tubule-like structures initiated by $CD166^{hi}$ cells contain CK5 and p63 expressing basal cells, CK8 luminal cells and AR positive cells (Figure S2).

Combination of markers TROP2 and CD49f can separate lineage-negative human prostate epithelial cells into various subpopulations, with $TROP2^{hi}$;$CD49f^{hi}$ ($Lin^-T^{hi}C^{hi}$ or LTC) cells possessing the highest sphere forming capability *in vitro* [29]. Additionally, LTC cells can develop cancer-like phenotype *in vivo* following oncogenic transformation [13]. We tested whether CD166 can further segregate this LTC population. FACS analysis of benign human prostate cells indicated that more than 50% of LTC stem/progenitor cells also express the CD166 surface marker (Figure 2D, left and middle panel). Furthermore, we examined if differences in regeneration potential exist between these two subpopulations. Sorted LTC;$CD166^{hi}$ and LTC;$CD166^{lo}$ cells were injected subcutaneously into NOD-SCID/IL2rγ$^-$ null mice with 2×10^5 rUGSM cells and analyzed 8–16 weeks later. Our *in vivo* data suggest that LTC;$CD166^{hi}$ cells can induce more tubule-like structures, whereas LTC;$CD166^{lo}$ cells have less regeneration capacity (Figure 2D, right panel).

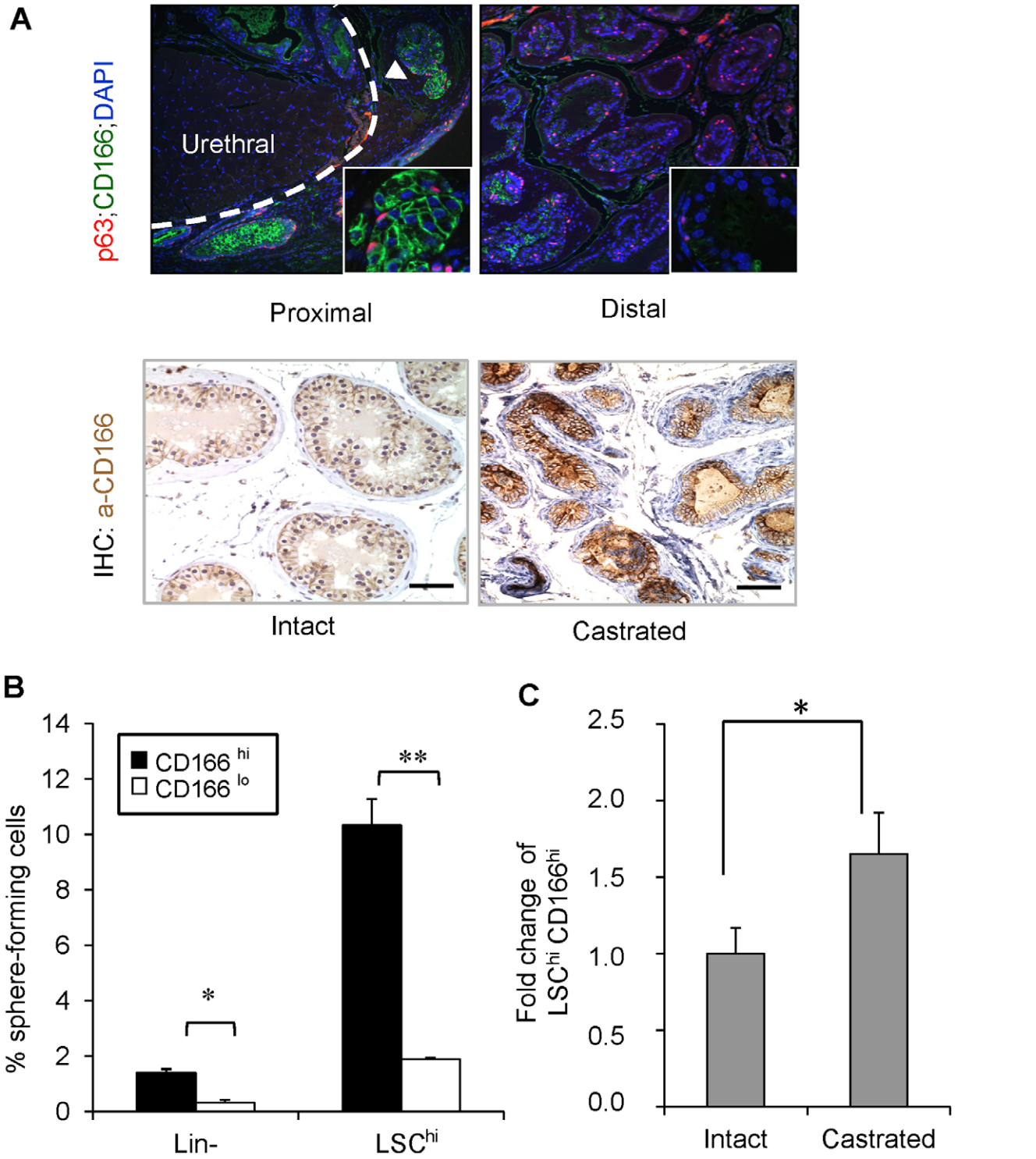

Figure 1. CD166 expression is upregulated in castrated prostate epithelium and CD166 can be used to enrich stem/progenitor cells in WT mice prostate. (A) Top: Comparison of p63 (red) and CD166 (green) co-IF staining between prostate proximal region and distal region. Bottom: IHC for CD166 expression from intact vs. castrated mouse prostate. Scale bar: 50 μm. (B) $Lin^-;CD166^{hi}$, $Lin^-;CD166^{lo}$, $LSC^{hi};CD166^{hi}$, and $LSC^{hi};CD166^{lo}$ cells were isolated by FACS from 8- to 12-week-old mice. Graph shows the percentage of sphere-forming cells, based on the spheres from each population per 2500 cells plated after 8 days of growth. Data shown as mean +/− STD (**, $p<0.001$, $n=3$). (C) Fold change of $LSC^{hi};CD166^{hi}$ content based on intact WT from FACS analysis (*, $p<0.05$, $n=3$).
doi:10.1371/journal.pone.0042564.g001

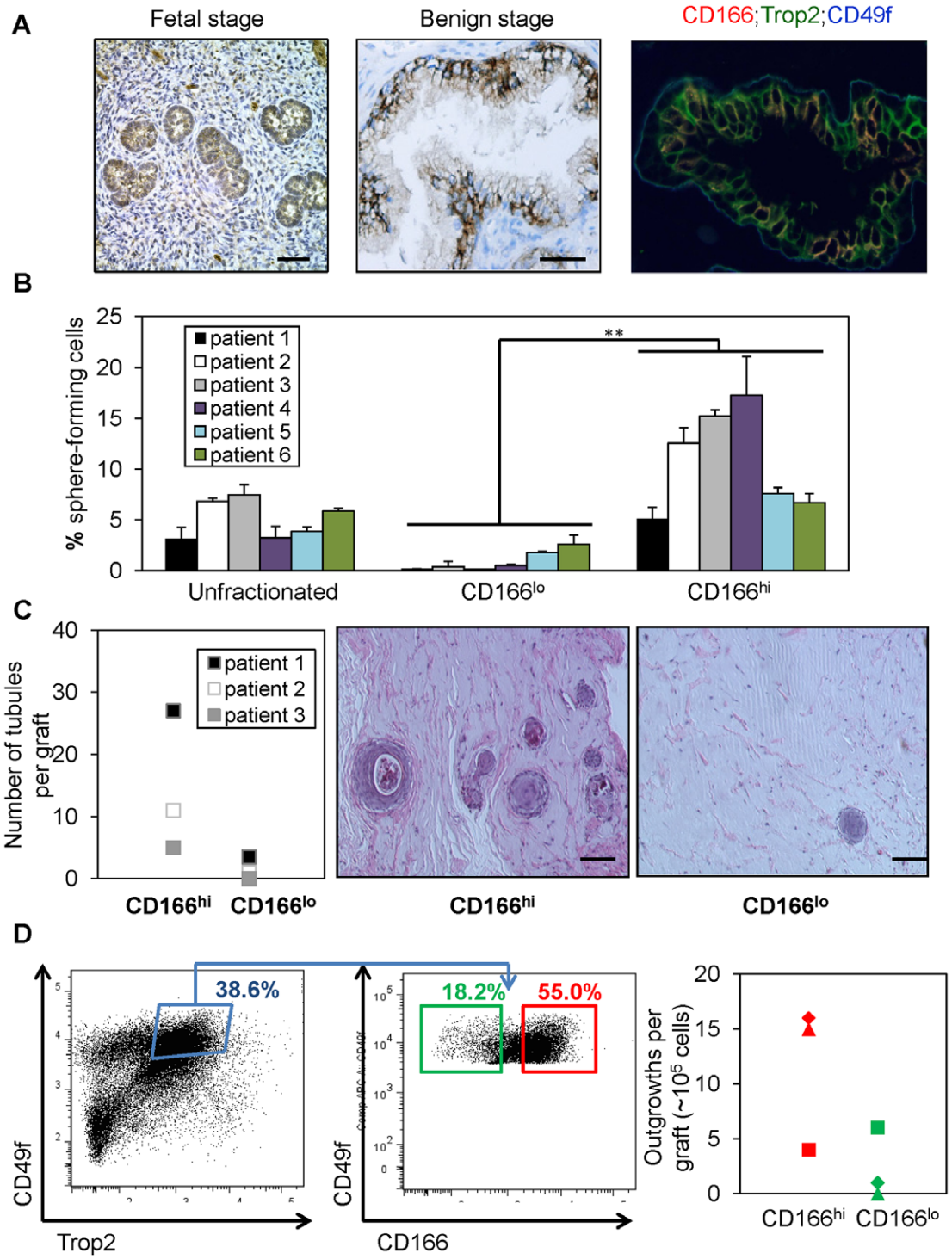

Figure 2. CD166^{hi} human prostate cells have higher sphere forming capacity *in vitro* and more graft outgrowth *in vivo*. (A) IHC staining of CD166 on human fetal prostate tissue and patient prostate cancer tissues. Scale bar: 50 μm. (B) Total dissociated prostate cells, CD166^{hi} and CD166^{lo} populations were isolated by FACS from 6 patient samples. Graph shows the percentage of sphere-forming cells, based on the spheres from each population per 5,000 cells plated after 7 days of culture. Data shown as mean +/− STD (**, $p<0.001$). (C) CD166^{hi}, and CD166^{lo} populations were isolated by FACS from 3 patient samples. CD166^{hi} and CD166^{lo} cells (2×10^5) were implanted subcutaneously into NOD-SCID/IL2rγ null mice, in combination with 2×10^5 rUGSM inductive mesenchymal cells. Grafts were harvested, fixed and analyzed after 8–16 weeks. Left, graph shows that CD166^{hi} human prostate cells can form more tubules in graft regeneration assay compared to CD166^{lo} human prostate cells. Right, H&E staining of representive graft. Scale bar: 100 μm. (D) Left, FACS plots show gates drawn for sorting of LTC (TROP2^{hi};CD49f^{hi}) CD166^{hi} and LTC;CD166^{lo} subpopulations from one patient. Right, representative graph shows that LTC;CD166^{hi} human prostate cells can form more tubules in graft regeneration assay compared to LTC;CD166^{lo} human prostate cells.
doi:10.1371/journal.pone.0042564.g002

CD166 can be used to Enrich Tumor Sphere-forming Cells in the *Pten* Null Prostate Cancer Model

To examine whether CD166 can enrich tumor initiating cells after castration, we compared the percentage of $CD166^{hi}$ subpopulation between intact and castrated *Pten* mutant mice and observed the expansion of $CD166^{hi}$ subpopulation after castration (Figure 3A). Next, we compared the sphere formation capabilities of LSC^{hi};$CD166^{hi}$, LSC^{hi};$CD166^{lo}$, LSC^{lo};$CD166^{hi}$, and LSC^{lo};$CD166^{lo}$ subpopulations at the pre-cancer PIN (6 weeks) and cancer stages (11 weeks). We found that the LSC^{hi};$CD166^{hi}$ subpopulation has much higher sphere-forming ability, and nearly all sphere-forming activity in the cancer stage resides in the LSC^{hi};$CD166^{hi}$ subpopulation (Figure 3B). Consistent with our previous observation that *Pten* mutant spheres are larger than WT control spheres [19], both LSC^{hi};$CD166^{hi}$ and LSC^{hi};$CD166^{lo}$ subpopulations form large prostate spheres (Figure S3). Our previous study suggested that *Pten* deletion promotes the expansion of LSC^{hi} prostate stem/progenitor cells [18,19]. Within the LSC^{hi} population, we observed selective expansion of LSC^{hi};$CD166^{hi}$ cells. *Pten* mutant mice have more than a 3-fold increase in the percentage of LSC^{hi};$CD166^{hi}$ subpopulation, compared to WT littermates (Figure 3C).

To further study the LSC^{hi};$CD166^{hi}$ subpopulation, we isolated RNA from LSC^{hi};$CD166^{hi}$, LSC^{hi};$CD166^{lo}$ subpopulations and the cell fraction depleted of LSC cells (non-LSC^{hi}) and compared their gene expressions by RT-PCR analysis. LSC^{hi};$CD166^{hi}$ subpopulation expresses similar levels of basal cell markers *Ck5* and *p63* as the LSC^{hi};$CD166^{lo}$ subpopulation (Figure 3D, left panel). However, LSC^{hi};$CD166^{hi}$ subpopulation expresses much higher level of luminal marker *Ck8* and *Trop2*, a new epithelial surface marker we recently identified for enriching stem cell activities in both murine and human prostates [13,29] (Figure 3D, right panel). Further examination of several other epithelial cell stem cells markers [10,30,31,32,33] showed that LSC^{hi};$CD166^{hi}$ cells have significantly higher *CD44* and *Nkx3.1* expression compared to LSC^{hi};$CD166^{lo}$ cells. Although compared to non-LSC population, LSC^{hi};$CD166^{hi}$ cells express less *Nkx3.1*. No significant differences were found in *CD117*, and *CD133* expressions between these two populations (Figure 3D, right panel).

CD166 Expression is Upregulated in Human Castration Resistant Prostate Cancer

Having found that CD166 can be used to enrich for human LTC cells and mouse tumor in itiating cells, we then examined the relationship between CD166 expression and human prostate cancer progression. In clinically annotated data of 218 prostate tumors [34], CD166 gene expression significantly correlates with increased prostate cancer aggressiveness, as indicated by Gleason score, with highest expression in metastasis samples (Figure 4A). We further surveyed CD166 expression on human prostate cancer tissue microarrays, which consist of 14 castration resistant (CRPC) metastasis samples and 98 hormone naïve primary cancer samples from patients receiving either neoadjuvant hormone treatment (NHT) for various periods or receiving no treatment. CD166 is significantly enhanced in CRPC samples (Figure 4B for representative images). Compared to the predominant membrane localization of CD166 in hormone naïve primary cancer samples, we observed intense cytoplasmic localization of CD166 in CRPC bone metastasis samples (Figure 4B, high magnification). CD166 expression levels were scored and p values are computed by Mann-Whitney test. CD166 protein expression level is significantly higher in CRPC samples as compared with primary cancers with ($p<0.0001$) or without ($p<0.02$) NHT (Figure 4C). These data suggest that CD166 is a castration-enriched marker for both murine and human prostate cancer.

Loss of CD166 does not Interfere with WT Prostate Development and Prostate Sphere Formation

While expressed in a wide variety of tissues, CD166 is usually restricted to subsets of cells involved in dynamic growth and/or migration, including neural development, branching organ development, hematopoiesis and immune response [27]. To test whether CD166 plays an intrinsic role in regulating prostate stem/progenitor cells, we analyzed *CD166* knockout mice ($CD166^{-/-}$). Genetic deletion of *CD166* gene was achieved by replacing its first exon with a cDNA encoding EGFP [35]. *CD166* null mice are phenotypically normal and fertile [35]. We examined the prostate at 8 and 20 weeks of age and found no difference in gross anatomy and histology among WT (data not shown), $CD166^{+/-}$ and $CD166^{-/-}$ mouse prostates (Figure 5A).

To further examine whether loss of CD166 has any effect on prostate stem/progenitor cells, we compared sphere formation activities of $CD166^{+/-}$ and $CD166^{-/-}$ prostate epithelium and found there is no significant difference (Figure 5B). In addition, spheres generated from $CD166^{-/-}$ prostate have similar size distribution compare to those from $CD166^{+/-}$ prostate epithelium (data not shown). Similarly, FACS analysis demonstrated that loss of CD166 does not affect LSC^{hi} content of prostates isolated from the $CD166^{-/-}$ mice (Figure 5C), suggesting that CD166 does not play an essential role in normal prostate gland development or prostate stem/progenitor number and function.

Genetic Deletion of *CD166* does not Block Prostate Cancer Progression

It has been postulated that CD166 functions as a cell surface sensor for cell density and controls the transition between local cell proliferation and tissue invasion during melanoma progression [36]. To examine whether CD166 plays an essential role in prostate cancer development, especially in the tumor initiating cells, we crossed $CD166^{-/-}$ mice with the *Pten* conditional knockout mice [17]. Histopathologic analysis indicated that loss of CD166 did not significantly change the kinetics of prostate cancer development in *Pten* null model and all $Pb\text{-}Cre^{+};Pten^{L/L};CD166^{-/-}$ mice developed adenocarcinoma around 9 weeks of age (Figure 6A and data not shown). We observed similar levels of $Ki67^{+}$ cells between $Pb\text{-}Cre^{+},Pten^{L/L},CD166^{+/+}$ *and* $Pb\text{-}Cre^{+};Pten^{L/L};CD166^{-/-}$ prostates (Figure 6A). SMA staining also demonstrated that loss of CD166 does not block prostate cancer cells from local invasion (Figure 6A, right panels).

We then compared the sphere formation between $Pb\text{-}Cre^{+};Pten^{L/L};CD166^{+/-}$ and $Pb\text{-}Cre^{+};Pten^{L/L};CD166^{-/-}$ prostates and found that loss of CD166 does not interfere with sphere-forming activity of *Pten* null epithelium (Figure 6B). Moreover, $CD166^{-/-}$ prostates have similar LSC^{hi} content as compared to $CD166^{+/-}$ *Pten* null prostates (Figure 6C). Since PI3K/AKT pathway activation is a driving force for cell proliferation and prostate cancer progression in $Pb\text{-}Cre^{+};Pten^{L/L}$ prostate cancer [17,20], we then examined whether there is any alteration of AKT activation after genetic deletion of *CD166*. Western blot analysis demonstrated that $Pb\text{-}Cre^{+};Pten^{L/L};CD166^{-/-}$ prostate has no CD166 expression, but has similar P-AKT levels compared to $Pb\text{-}Cre^{+};Pten^{L/L};CD166^{+/+}$ and $Pb\text{-}Cre^{+};Pten^{L/L};CD166^{+/-}$ prostate (Figure 6D). We further confirmed that there is no negative selection against $Pten^{-/-};CD166^{-/-}$ cells since equal intensity of knockin-GFP protein can be detected in all cohorts except $CD166^{+/+}$ mice.

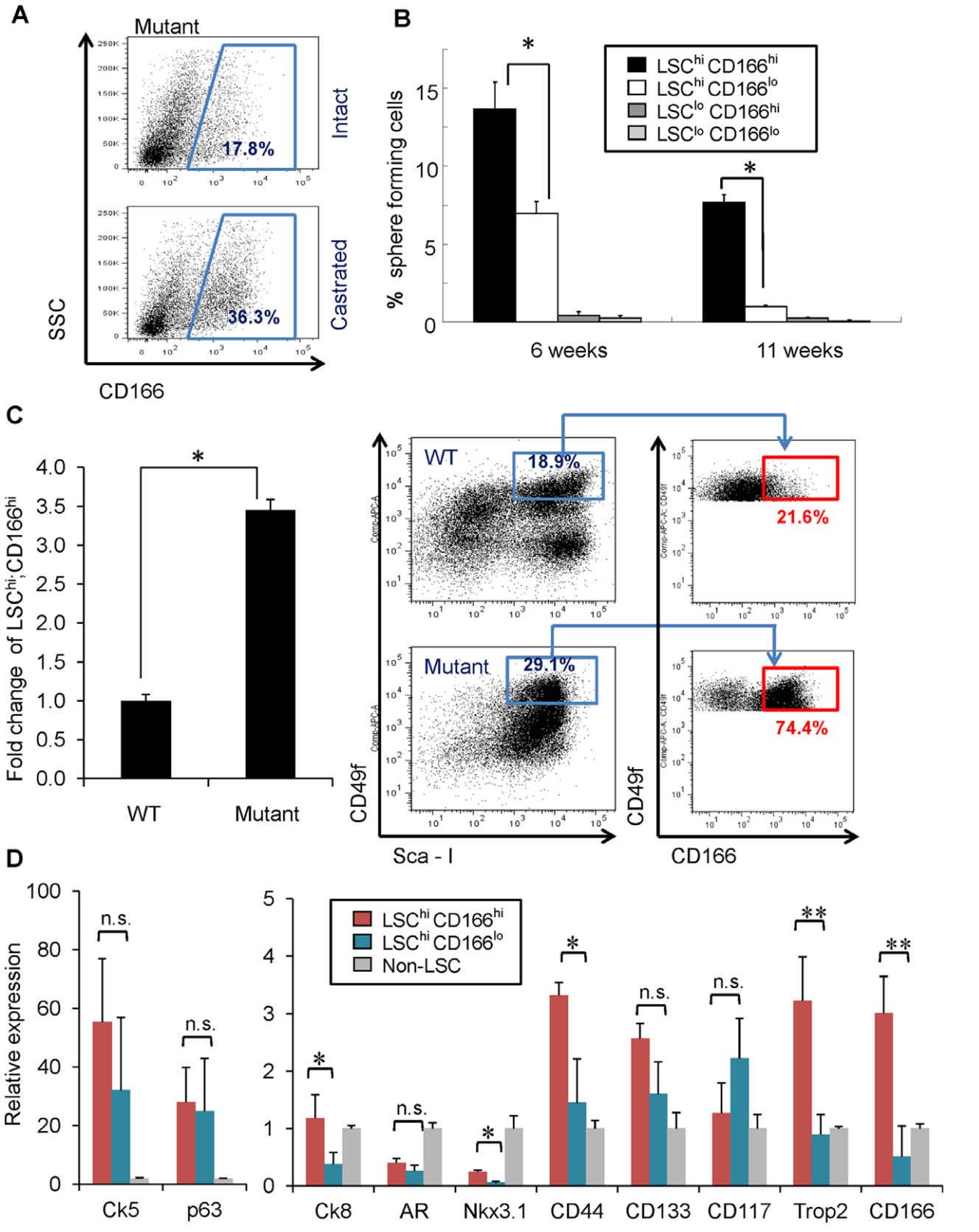

Figure 3. CD166 can be used to enrich tumor initiating cells in *Pten* mutant prostate. (A) FACS blots show increased Lin$^-$CD166^{hi} population after castration of *Pten* mutant mice compared to intact *Pten* mutant mice. (B) Four subpopulations (LSC^{hi}CD166^{hi}, LSC^{hi}CD166^{lo}, LSC^{lo}CD166^{hi}, LSC^{lo}CD166^{lo}) were isolated from *Pten* mutant prostate from either 6 weeks or 11 weeks old mice. Graph shows the percentage of sphere-forming cells. Data from several experiments were pooled. Data shown as mean +/− STD (*, $p<0.05$, $n=3$). (C) Left: bar graph shows fold

change of *Pten* mutant LSC^{hi}CD166^{hi} content compared to WT; right, FACS blots show the expansion of LSC^{hi} CD166^{hi} cells within LSC population on *Pten* mutant compared to WT. (D) RNA was isolated from non-LSC, LSC^{hi}CD166^{hi}, and LSC^{hi}CD166^{lo} fractions in duplicate experiments. RNA was synthesized into cDNA and subjected to qRT-PCR. Graph shows fold-enrichment over the non-LSC cells for each gene. Gadph was used as the reference gene (*, $p<0.05$; **, $p<0.01$; n.s., not significant).
doi:10.1371/journal.pone.0042564.g003

Since we see significant overexpression of CD166 in human CRPC samples, we next investigated whether CD166 would influence the development of CRPC in the *Pten* null prostate cancer model. *Pb-Cre*$^{+}$;*Pten*$^{L/L}$;*CD166*$^{+/-}$ and *Pb-Cre*$^{+}$;*Pten*$^{L/L}$;*CD166*$^{-/-}$ males were castrated at 12 weeks and prostates were isolated 8 weeks later. As shown in Figure 7, deletion of CD166 does not significantly influence the formation of CRPC, as evidenced by similar pathohistology (Figure 7A), CK5/CK8 marker distribution, BrdU pulse labeling and SMA staining in both cohorts (Figure 7B). Taken together, our genetic studies indicate that CD166 has limited intrinsic function in the prostate, even in the tumor initiating cells.

Discussion

Few surface markers are currently available for enriching both murine and human prostate tissue stem/progenitor cells and for identifying prostate cancer initiating cells. By searching for those cell surface molecules that are upregulated in castrated murine prostate and castration resistant prostate cancers (CRPC) of murine and human origins, we identified CD166 as a surface marker for enriching both murine and human prostate tissue stem/progenitor cells based on *in vitro* sphere forming and *in vivo* tissue regeneration analyses. Importantly, upregulated CD166 expression and expansion of CD166^{hi} cells correlate with *Pten* null CRPC progression as well as human CRPC development, although genetic deletion of *CD166* does not interfere with normal murine prostate development or *Pten* null prostate cancer progression. Together, our study suggests CD166 can be used as a potential surface marker for identifying castration resistant tumor cells for targeted drug delivery.

CD166 expression has been proposed as a prognostic marker for several cancers, including breast [37], prostate [38], ovarian [39], pancreatic [40], colon [41], oral cancers [42], melanoma [36] and gastric cancers [43]. Importantly, our microarray and TMA studies demonstrate the association of increased CD166 expression with human prostate cancer metastasis and CRPC development. Moreover, within both murine and human prostates, we show that the CD166-high expressing subpopulation encompasses prostate stem/progenitor and cancer initiating cells.

To investigate human prostate tissue stem/progenitor cell properties, we evaluated adult human prostate epithelium dissociated from benign prostate, rather than cell lines and xenografts. The advantage of this approach is to maintain the original heterogeneity in human prostate samples by avoiding the effect of long-term *in vitro* selection. However, there appears to be greater variability among patient samples in the tissue regeneration assays. This may be due to the difference in sample variability (i.e., ischemia time prior to tissue processing and cell retrieval), individual variability in CD166 expression, and technical challenges related to the tissue regeneration assays using human prostate cells. Therefore, analysis of sufficient patient samples is essential in order to draw a valid conclusion. In the current study, 6 human samples were utilized for the *in vitro* sphere forming and another 6 samples were used for *in vivo* regeneration assays. Using this system, we have previously defined TROP2^{hi};CD49f^{hi} as a cancer initiating cell (cell of origin) for human prostate cancer [13]. In the current study, CD166^{hi} population demonstrated significantly increased sphere-forming capacity compared to the patient-matched CD166^{lo} population. In addition, our study demonstrates that CD166 can not only enrich human sphere-forming cells, but also segregate TROP2^{hi};CD49f^{hi} into two functionally different populations, with TROP2^{hi};CD49f^{hi};CD166^{hi} having higher regeneration capacity *in vivo*, compared to TROP2^{hi}CD49f^{hi}CD166^{lo}. CD166 is also highly upregulated in CRPC based on our gene expression analysis and tissue microarray study. Therefore, CD166 may enrich both human prostate tissue stem/progenitor cells and castration resistant prostate cancer cells.

LSC^{hi} subpopulation has been defined as the murine prostate tissue stem/progenitor cells and expands significantly following castration [12,19,26]. LSC^{hi} cells express basal markers and demonstrated robust sphere-forming activity *in vitro* and prostate regeneration capability *in vivo* [26]. In contrast to luminal cells, LSC^{hi} cells respond efficiently to multiple oncogenic insults for prostate cancer initiation using a transplantation-based prostate regeneration assay [12]. We and others have demonstrated that the LSC^{hi} population, isolated from *Pten* null prostate tissue, is sufficient to regenerate cancerous morphology upon transplantation that closely mimics that of primary cancers [19,44]. In this study, we further separated LSC^{hi} subpopulation into CD166^{hi} and CD166^{lo} subsets and found that most of sphere-forming activities are associated with the LSC^{hi};CD166^{hi} cells. Importantly, this LSC^{hi};CD166^{hi} population was demonstrated to have self-renewal activity as spheres from this population could be passaged at least 3 generations with a high rate of sphere formation. Moreover, LSC^{hi};CD166^{hi} cells are expanded upon castration as well as *Pten* deletion in comparison to LSC^{hi};CD166^{lo} cells. Therefore, CD166 can further enrich murine prostate cancer initiating cells and castration resistant cells.

The relationship of LSC^{hi};CD166^{hi} cancer initiating cells described here to other cell populations is of obvious interest [45]. Using lineage tracing and cell type-specific Cre lines, a recent report demonstrates that both luminal cells and basal cells can initiate prostate cancer upon *Pten* deletion [14]. This new observation is not in conflict with our previous studies: we showed that *Pten* deletion mediated by *Pb-Cre* happens in both basal and luminal cells [18]. In addition, we observed significant expansion of a subset of prostate cancer cells positive for basal cell markers CK5 and p63 and luminal cell marker CK8, suggestive of transient amplifying/intermediate cells [18,46]. Compared to LSC^{hi};CD166^{lo} cells, one of the distinguishing features of LSC^{hi};CD166^{hi} cells is the higher *Trop2* expression, a cell surface marker we have used for enriching both murine and human tissue stem cells [13,29]. TROP2 can functionally segregate mouse LSC population but there is no cytokeratin phenotypic difference between LSC^{hi};Trop2^{hi} and LSC^{hi};Trop2^{lo} population [29]. CD166, on the other hand, can enrich *Pten* null LSC^{hi} population with CK5^{+}/p63^{+}/CK8^{+}/AR$^{-/}$TROP2^{hi} characteristics, suggesting that CD166 may preferentially enrich for CK5^{+}/CK8^{+} transient amplifying/intermediate cells, which currently cannot be prospectively purified. Increased CK5^{+};CK8^{+} cells have been observed in the *Pten* conditional knockout model [18,47] as well as *Pten*$^{-/-}$;*TP53*$^{-/-}$ prostates cancer model [48]. A recent study also identified a subset of tumor-initiating stem-like cells in human prostate cancer cell lines and xenografts based on co-expression of the human pluripotent stem cell marker TRA-1-60, CD151 and

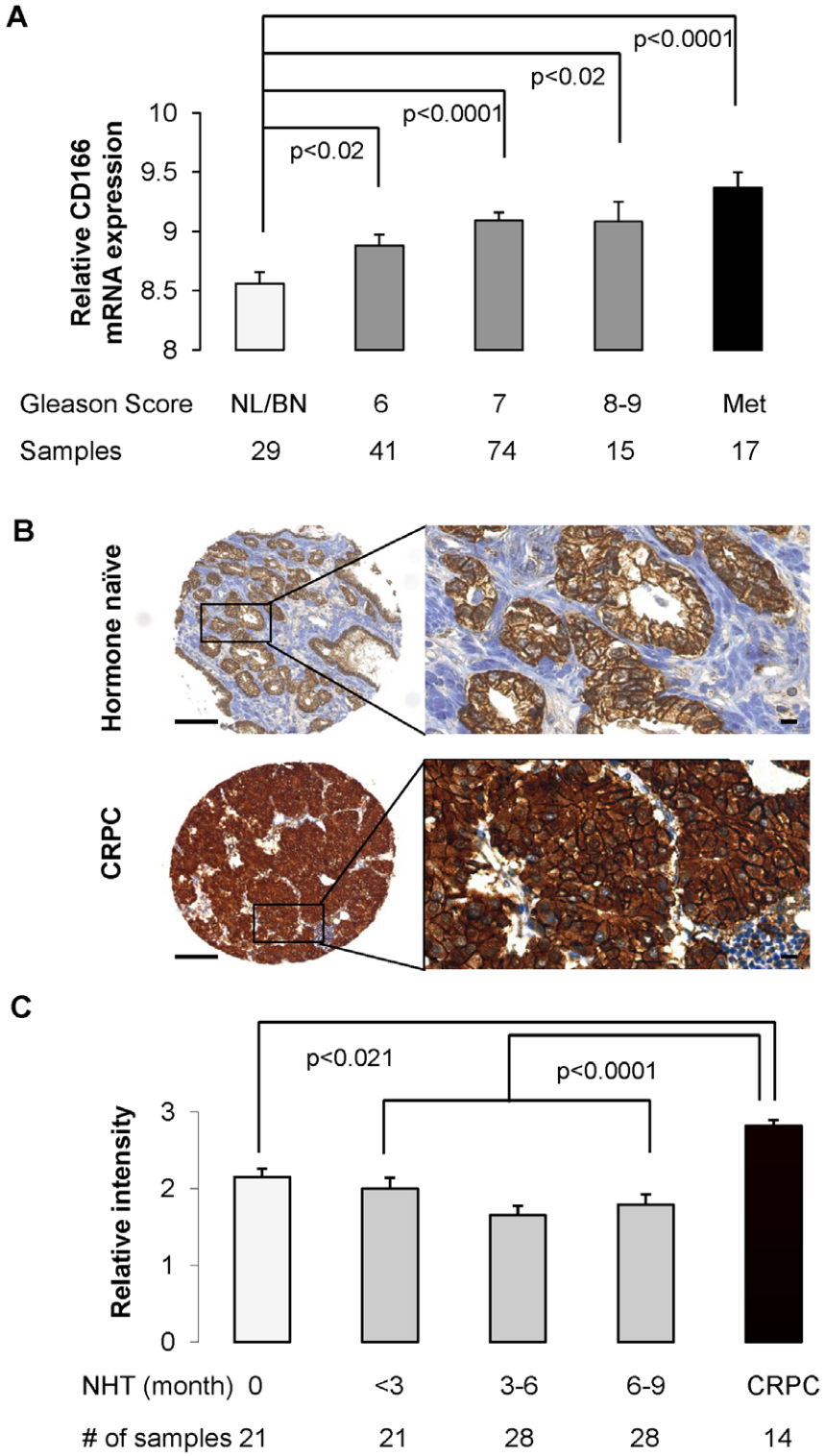

Figure 4. Gene expression profiling and tissue microarray (TMA) demonstrates that increased CD166 expression is correlated with high Gleason score and human castration resistant prostate cancer. (A) CD166 gene expression from 147 human prostate tumors was analyzed by comparing different Gleason score groups to normal/benign (NL/BN) prostate. (B) Representative IHC staining of CD166 expression from human prostate TMA. Top: hormone naïve primary prostate cancer; Low: castration resistant prostate cancer showing highly intensive immunostaining. Scale bar: 100 μm (left); 10 μm (right). (C) Data from 112 samples were calculated and statistical analysis of CD166 expression of human TMA conducted. NHT: neoadjuvant hormone therapy; CRPC: castrate resistant prostate cancer. Column, mean CD166 staining in NHT and CR tissues. Samples were graded from 0 to +3 representing the range from no staining to heavy staining by visual scoring. Error bar: standard error. Immunoreactivity of CD166 is significantly higher in CRPC group compared with untreated group ($p<0.021$) or NHT with different treatment times ($p<0.0001$).

doi:10.1371/journal.pone.0042564.g004

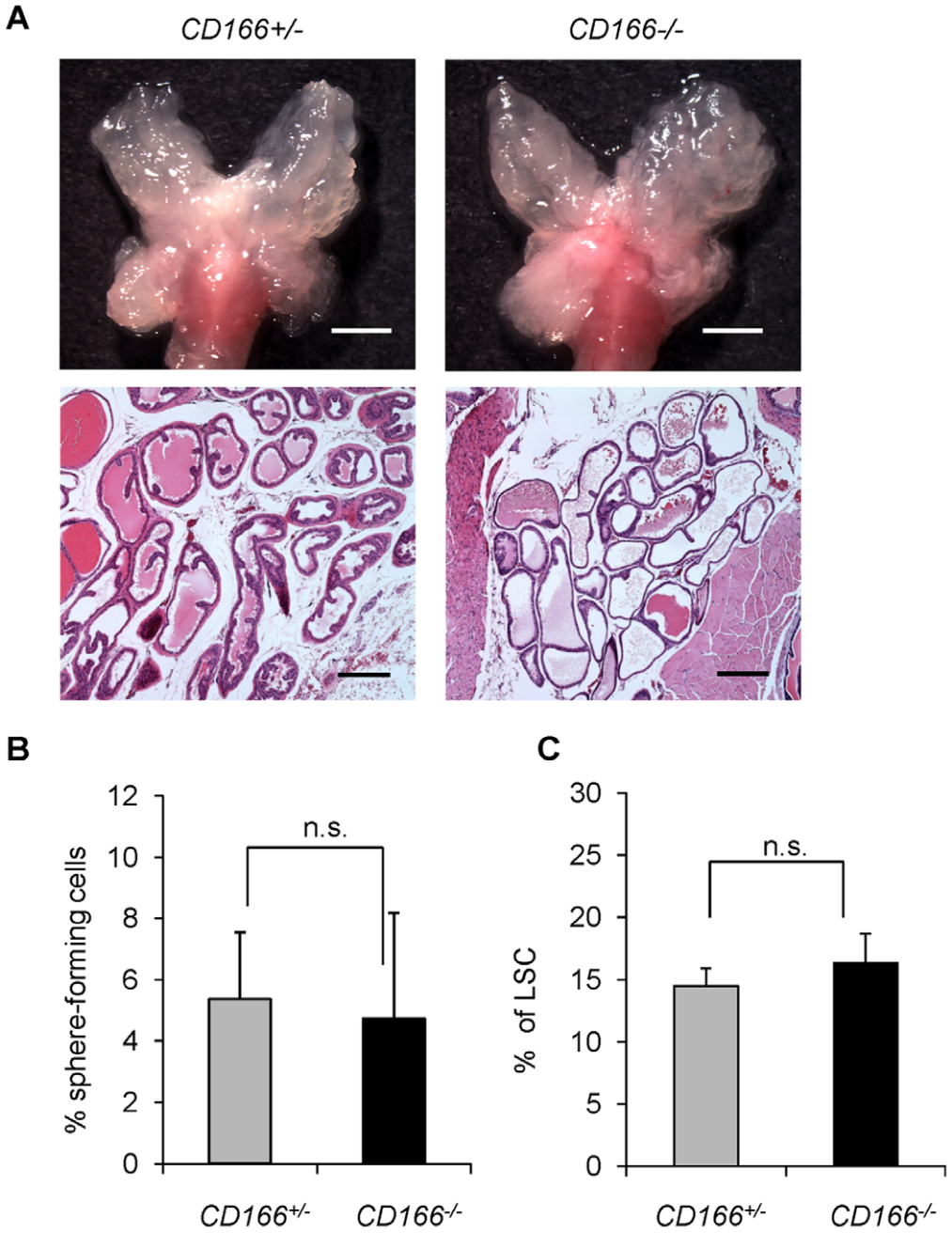

Figure 5. Loss of CD166 does not block WT prostate development and stem/progenitor cell function. (A) Top: The gross anatomy of the prostate of *WT* and *CD166−/−* mice at 8 weeks of age, scale bar: 2 mm. Bottom: HE staining of DLP section from WT and $CD166^{-/-}$ mice at 8 weeks of age, scale bar: 200 μm. (B) Comparison of sphere formation from total unsorted prostate cells (5000 per 12-well) between $CD166^{+/-}$ and $CD166^{-/-}$ prostates. Data represented as mean +/− STD ($p>0.05$, $n=3$). (C) Comparison of LSC^{hi} content between $CD166^{+/-}$ and $CD166^{-/-}$ prostates at 8–12 weeks age ($p>0.05$, $n=5$).
doi:10.1371/journal.pone.0042564.g005

CD166 [49]. Interestingly, this subtype of human prostate tumor initiating cells also have the AR^{-};$CK5^{+}$;$CK8^{+}$ phenotype [49]. Another characteristic of LSC^{hi};$CD166^{hi}$ cells is relatively higher CD44 expression. Since knockdown of CD44 was very effective to suppress cancer stem cell regeneration and metastasis [30], it will be interesting to examine whether there is any functional role for CD44 in LSC^{hi};$CD166^{hi}$ tumor initiating cells.

As an adhesion molecule, CD166 can initiate homophilic (CD166-CD166) or heterophilic interaction (CD166-CD6), and play important roles in neural guidance and the immune system [27]. CD166 has also been suggested to play a critical role in various human cancers and as a potential therapeutic target for cancer initiating cells, similar to CD44 [30] and CD47 [50]. A truncated CD166 variant has been shown to block melanoma metastasis by interfering with the CD166-CD166 homophilic interaction [51]. Similarly, novel human recombinant single-chain anti-CD166 antibodies have been shown to inhibit colorectal carcinoma growth as well as breast cancer cell invasion [52].

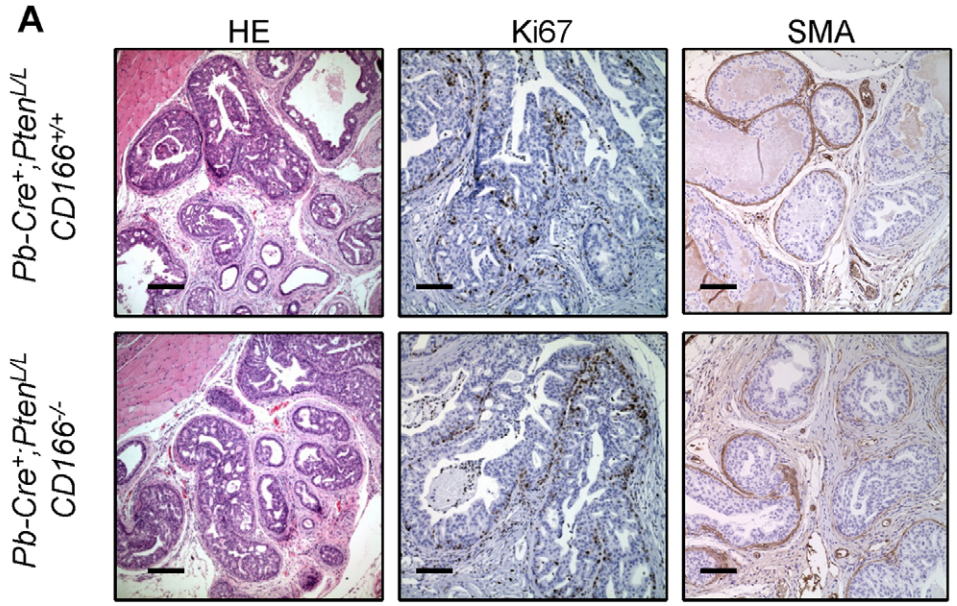
A
HE
Ki67
SMA
Pb-Cre+;PtenL/L CD166+/+
Pb-Cre+;PtenL/L CD166-/-

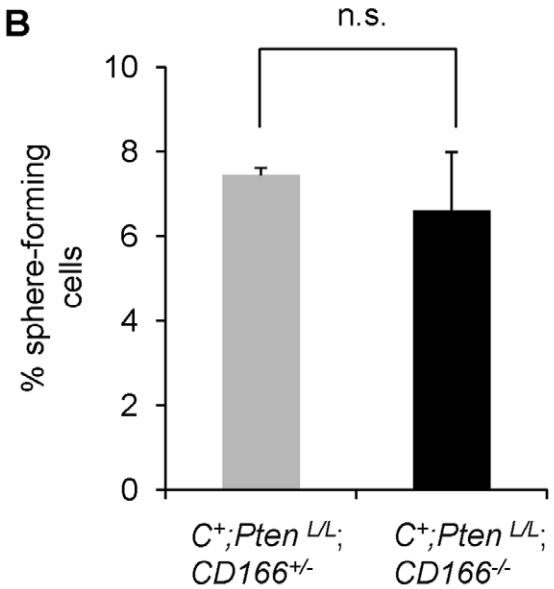
B
n.s.
% sphere-forming cells
10
8
6
4
2
0
C+;Pten L/L; CD166+/-
C+;Pten L/L; CD166-/-

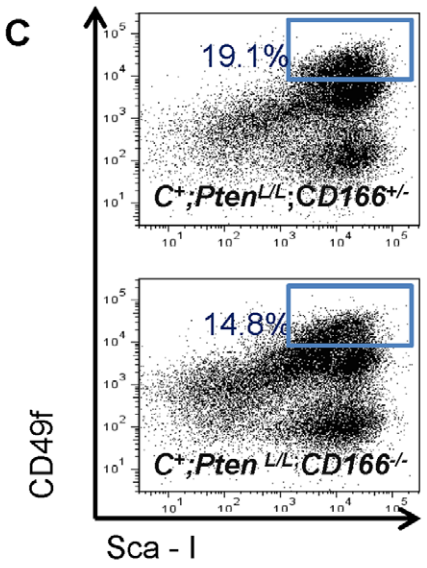
C
19.1%
C+;PtenL/L;CD166+/-
14.8%
C+;Pten L/L;CD166-/-
CD49f
Sca - I

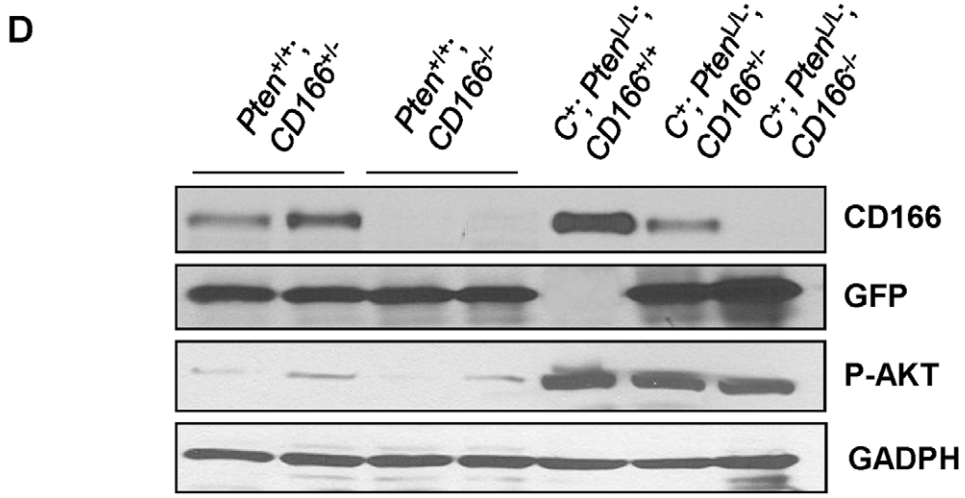
D
Pten+/+; CD166+/-
Pten+/+; CD166-/-
C+; PtenL/L; CD166+/+
C+; PtenL/L; CD166+/-
C+; PtenL/L; CD166-/-
CD166
GFP
P-AKT
GADPH

Figure 6. Loss of CD166 does not block prostate tumor progression and tumor initiating cell function in *Pb-Cre*$^{+}$;*Pten*$^{L/L}$;*CD166*$^{-/-}$ mice. (A) Evaluation of *CD166* deletion on prostate cancer progression (HE staining, scale bar: 200 μm), cell proliferation (Ki67 staining, scale bar: 100 μm), and prostate tumor invasion (SMA staining, scale bar: 100 μm) by comparing age matched *Pb-Cre*$^{+}$, *Pten*$^{L/L}$, *CD166*$^{+/+}$ and *Pb-Cre*$^{+}$, *Pten*$^{L/L}$, *CD166*$^{-/-}$ prostate tissue at 20 weeks of age. (B) Comparison of sphere formation from total unsorted prostate cells (5000 per 12-well) between *Pb-Cre*$^{+}$, *Pten*$^{L/L}$, *CD166*$^{+/-}$ and *Pb-Cre*$^{+}$, *Pten*$^{L/L}$, *CD166*$^{-/-}$ prostate (9 weeks of age). (C) A representative FACS blot shows LSC content between *Pb-Cre+*, *Pten*$^{L/L}$, *CD166*$^{+/-}$ and *Pb-Cre*$^{+}$, *Pten*$^{L/L}$, *CD166*$^{-/-}$. (D) Examination of protein levels of CD166, P-AKT and GFP among different prostate tissue with indicated genotype by Western blotting. GADPH is included as an equal loading control.
doi:10.1371/journal.pone.0042564.g006

Unlike subcutaneous allograft or xenograft models used in above studies, we defined the functions of CD166 in prostate cancer initiating cells and prostate cancer development in immune competent mice within the natural prostate environment. By generating the *Pb-Cre*$^{+}$;*Pten*$^{L/L}$;*CD166*$^{-/-}$ line, our study demonstrates that loss of CD166 within LSC^{hi} population does not change their ability to form spheres *in vitro* and block prostate cancer initiation and progression *in vivo*. As it is possible that other members of the Cell Adhesion Molecule (CAM) family can compensate for the role of CD166 in murine prostate cancer development, we cannot conclude that CD166 has no *in vivo* function on prostate cancer initiation. Nevertheless, since cancer initiating cell surface markers can be used for molecular imaging [53] and/or for internalizing a death-inducing compound for targeted therapies [54], our work suggests that CD166 may be for a suitable surface marker for future targeted drug delivery [55]. Recently, a promising study showed substantial cytotoxic effects of the CD166 scFv-condugated drugs on three human prostate cancer cell lines (Du-145, PC3, and LNCaP) [55]. Since CD166 is highly expressed on both human and mouse tissue stem/progenitor cells, it will be interesting to examine the effect of this targeted drug delivery on their prostate sphere forming activity and prostate regeneration potential. The *Pb-Cre*$^{+}$;*Pten*$^{L/L}$;*CD166*$^{+/-}$ and *Pb-Cre*$^{+}$;*Pten*$^{L/L}$;*CD166*$^{-/-}$ mouse models generated in this study, therefore, can be used to investigate the efficiency of CD166 - mediated drug delivery to prostate cancer initiating cells *in vivo*, especially during CRPC development.

Materials and Methods

Mouse Strains

Mutant mice with prostate-specific deletion of *Pten* were generated as described previously under a mixed background [17]. The 129/C57 background CD166 knockout (*CD166*$^{-/-}$) was generously provided by the laboratory of Dr. Weiner of University of Iowa [35]. *Pten*$^{L/L}$ mice on a 129/Balb/c background were first crossed to the *CD166*$^{-/-}$ mice [35] to get F2 female *Pten*$^{L/L}$;*CD166*$^{-/-}$. *Pb-Cre*$^{+}$; *Pten*$^{L/L}$;*CD166*$^{-/-}$ mice were then generated by crossing female Cre^{-};*Pten*$^{L/L}$;*CD166*$^{-/-}$ with male *Pb-Cre*$^{+}$;*Pten*$^{L/L}$;*CD166*$^{+/-}$. All animal experiments were performed following Institutional Approval for Appropriate Care and use of Laboratory animals by the UCLA Institutional Animal Care and Use Committee (Chancellor's Animal Research Committee (ARC)), Animal Welfare assurance number A3196-01.

Tissue Collection and FACS

The preparation of prostate epithelial cell suspensions from male mice were described previously [20]. Dissociated prostate cells were suspended in DMEM/10% FBS and stained with antibody for 15 min at 4°C. Antibodies are listed in Table S2. FACS analysis was performed by using BD FACS Canto (BD Biosciences, San Jose, CA). Cell sorting was done by using BD FACS Vantage and the BD FACS Aria II.

In vitro Prostate Sphere-forming Assays

Prostate spheres were cultured and passaged as described previously [56,57]. FACS-isolated prostate cells or unsorted prostate cells were counted and suspended into a 100 μL mixture of 1:1 Matrigel (BD Biosciences, San Jose, CA) and PrEGM (Lonza, Walkersville, MD). Samples were plated around the rims of wells in a 12-well plate and allowed to solidify at 37°C for 45 minutes, before 1 ml of PrEGM was added. Sphere media was changed every three days. Spheres were counted after 8 days. To passage spheres, medium was aspirated off and matrigel was digested with 1 mL Dispase solution (Invitrogen, Carlsbad, CA, 1 mg/ml, dissolved in PrEGM medium) for 30 minutes at 37°C. Spheres were collected, incubated in 1 ml warm Trypsin/0.05% EDTA at 37°C for 5 minutes, passed through a 27-gauge syringe 5 times, and filtered through a 40 μm filter. Cells were counted by hemocytometer and replated.

RNA Isolation and qRT-PCR

Sorted cells were collected and spun down. RNAs from sorted cells were extracted using TRIzol® Reagent (Invitrogen, Carlsbad, CA). RNAs were reverse transcribed into cDNA with SuperScript III First-Strand Synthesis System for qRT-PCR (Invitrogen, Carlsbad, CA), and quantitative PCR was done in the iQ thermal cycler (Bio-Rad) using the iQSYBR Green Supermix (Bio-Rad) in triplicate. Primers used for study are Ck5 (F5′-ACCTTCGAAA-CACCAAGCAC-3′; R5′-TTGGCACACTGCTTCTTGAC-3′), Ck8 (F5′-ATCGAGATCACCACCTACCG-3′; R5′-TGAAGC-CAGGGCTAGTGAGT-3′), p63 (F5′-CCCACAGACTGCAG-CATTG-3′; R 5′-GAGATGAGGAGGTGAGGAGAAG-3′), AR (F5′-AACCAACCAGATTCCTTTGC-3′; R5′-ATTAGT-GAAGGACCGCCAAC-3′), CD166 (F 5′-CCTAAGAGAG-GAGCGGATTG-3′; R5′-CAGCCACTCCCAGAACAAAG-3′), Trop2 (F5′- AGACCAAAGCCTGCGCTGCG-3′; R 5′-AGCTGGGGTGCAGCTTGTAG-3′), Gadph (F5′-ACTGG-CATGGCCTTCCG-3′; R5′-CAGGCGGCACGTCAGATC-3′), CD117 (F5- AGAAGCAGATCTCGGACAGC-3′; R5′-GACTTGGGTTTCTGCTCAGG-3′), CD133 (F5-ACCAA-CACCAAGAACAAGGC-3′; R5′-GGAGCTGACTTGAATT-GAGG-3′), CD44 (F5- GTCAACCGTGATGGTACTCG-3′; R5′-AGTGCACAGTTGAGGCAATG-3′), Nkx3.1 (F5'-TCCGTCTTTTGGCTCTGAGT-3′; R5′- GTGAAAGTG-CACGCTGAAAA-3′).

Immunofluorescence and Immunohistochemistry Analyses

Tissue analysis was carried out using standard techniques as described previously [17]. Sections (4 μm) were stained with hematoxylin and eosin (H&E) or with specified antibodies (Table S2).

Western Blot Analysis

Total protein was extracted with RIPA buffer (20 mM Tris-HCl, pH 7.5, 150 mM NaCl, 1 mM Na_2EDTA, 1 mM EGTA, 1% NP-40, 1% sodium deoxycholate) with fresh added phosphatase inhibitors (Sigma, St. Louis, MO) and protease inhibitors

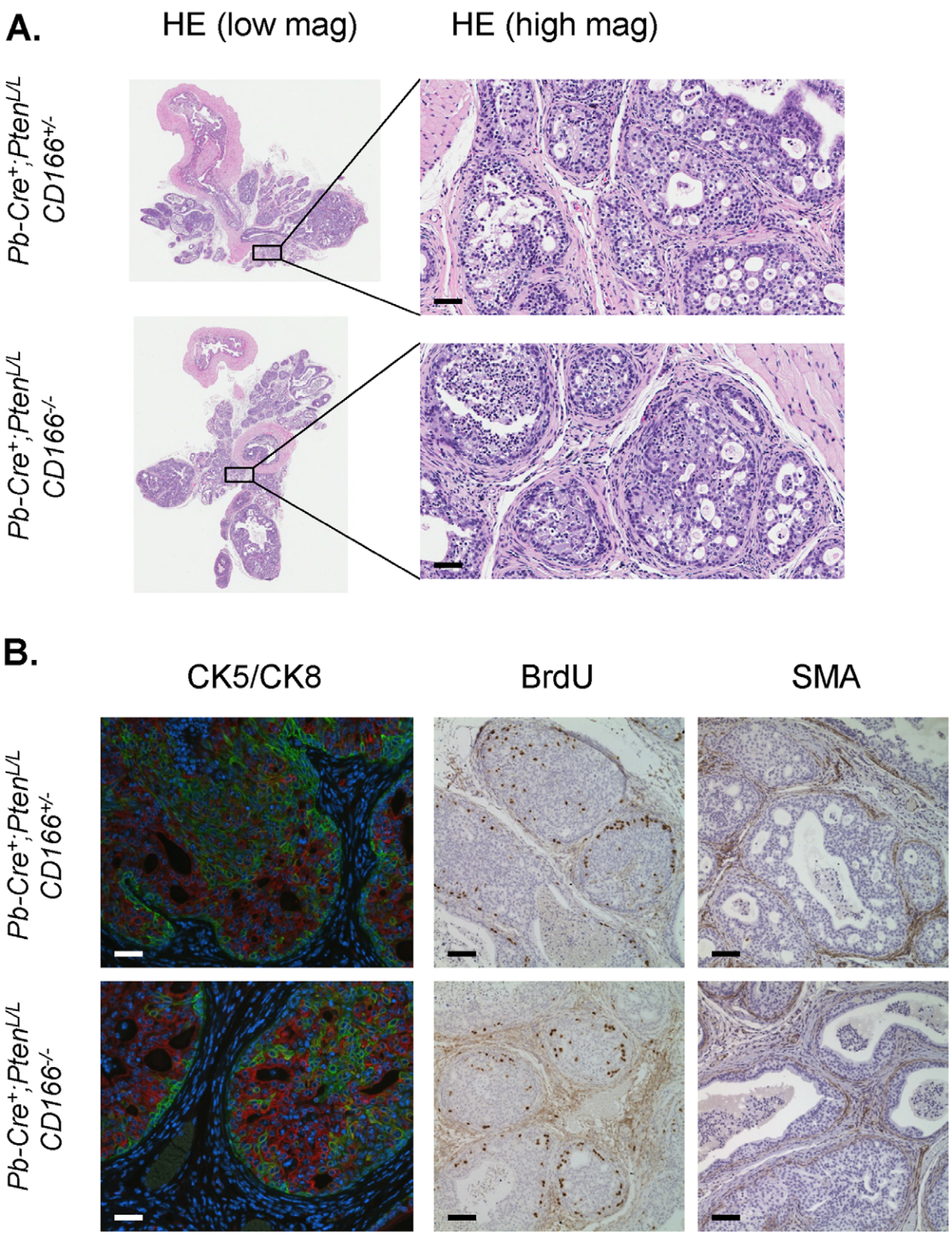

Figure 7. Loss of CD166 does not block castration resistant prostate tumor progression in *Pb-Cre*$^{+}$;*Pten*$^{L/L}$;*CD166*$^{-/-}$ mice. *Pb-Cre*$^{+}$, *Pten*$^{L/L}$, *CD166*$^{+/-}$ and *Pb-Cre*$^{+}$, *Pten*$^{L/L}$, *CD166*$^{-/-}$ mice were castrated at the age of 12 weeks using standard techniques. At 8 weeks post-castration, mice were intraperitoneal injected with a single dose of 100 µl (1 mg) of BrdU solution and sacrificed 4 hour later for analysis. Evaluation of the effects of *CD166* deletion on (A) castration resistant prostate cancer progression (HE), and (B) cell lineage composition (CK5/CK8), cell proliferation (BrdU) and prostate tumor invasion (SMA) were performed. Scale bar: 50 µm.
doi:10.1371/journal.pone.0042564.g007

(Roche, Indianapolis, IN). Protein concentrations were determined by Bradford Assay kit (BioRad, Hercules, CA). Protein was separated by 4–15% gradient SDS/PAGE (BioRad, Hercules, CA) and transferred onto a PVDF membrane (Amersham Biosciences, Arlington Heights, IL). The membrane was blocked in 5% skim milk, and subsequently incubated with primary antibodies against CD166 and GADPH (Santa Cruz Biotechnology, Santa Cruz, CA), GFP (Abcam, Cambridge, MA), phospho-AKT Ser473 (Cell Signaling Technology, Beverly, MA) at 4°C overnight followed by incubation with peroxidase-conjugated goat anti-mouse IgG or goat anti-rabbit IgG (Jackson ImmunoResearch, Inc., West Grove, PA), and developed with Pierce ECL reagent (Thermal Scientific, Rockford, IL).

Human Prostate Cancer Tissue Microarray (TMA)

TMA used to survey CD166 expression is composed of 112 patient samples. Written consent was obtained from the patient as well as ethics approval from University of British Columbia-British Columbia Cancer Agency Research Ethics Board (UBC BCCA REB), Vancouver, Canada. The 112 patient specimens were spotted in triplicate to create a tissue microarray with 336 cores as described previously in [58]. Scoring method was based on the intensity of the staining in each core on a 4-point scale from none (0) to high (3). Mann-Whitney test was used to compare CD166 protein expression difference between different groups. p values <0.05 were considered significant.

Human Prostate Tissue Acquisition and Dissociation

Human prostate tissue was obtained via a research protocol that was approved by the Office for the Protection of Research Subjects at UCLA and the Greater Los Angeles VA Medical Center. Informed written consent was obtained on all participants where identifying information was included. A frozen section was prepared from an adjacent slice of prostate tissue in order to determine the location of tumor nodules. Tumor areas were encircled and dissected away from benign regions within the fresh tissue slice. Benign tissue specimens were placed on ice and brought immediately to the laboratory for mechanical and enzymatic digestion [28]. Prostate tissue was minced into small fragments (1 mm^3) in RPMI-1640 medium supplemented with 10% FBS and went through through enzymatic digestion (12 h in 0.25% type I collagenase followed by TripLE (Invitrogen) for 5 min at 37°C). Cell suspensions were passed through a 23-gauge needle and were filtered through 40- μm filters. Cells were plated overnight in PrEGM as described above for sphere formation assay or tissue regeneration assay.

Tissue Regeneration Assay

In vivo tissue experiments were performed in male NOD-SCID/IL2rγ null mice in accordance with protocol number 2007-189-11A, approved by the Animal Research Committee within the Office for the Protection of Research Subjects at UCLA. Cells of interest were collected from FACS sorting. 2×10^5 viable cells were then mixed with 2×10^5 rat urogenital sinus mesenchyme (rUGSM) and suspended in 100 μL with 50:50 matrigel:PREGM [4,28,59]. Cell/Matrigel mixtures were then injected subcutaneously into NOD-SCID/IL2rγ null mice. Animals were supplemented with a 12.5 mg 90-day release testosterone pellet under the skin (Innovative Research of America, Sarasota, FL). Grafts were harvested 8–16 weeks later and subjected to further analysis.

Supporting Information

Figure S1 WT LSC^{hi}; $CD166^{hi}$ prostate cells demonstrate higher self-renewal activity. (A) LSC^{hi};$CD166^{hi}$ and LSC^{hi}; $CD166^{lo}$ cells were isolated by FACS from 8- to 10-week-old mice and plated for sphere formation assay. Spheres from the each subpopulation (P0) were dissociated and replated for 3 successive generations (P1–P3). Graph shows the percentage of sphere-forming cells, based on the spheres from each population per 5000 cells plated after 8 days of growth. Error bars represent means and STD from triplicates of one of the two independent experiments (**, $P<0.001$). (B) Comparison of sphere size distribution between LSC^{hi}; $CD166^{hi}$ and LSC^{hi}; $CD166^{lo}$ formed spheres. n.s., not significant. (C) Representative sphere images of LSC^{hi};$CD166^{hi}$ and LSC^{hi}; $CD166^{lo}$ cells generated spheres. Scale bar: 100 μm.
(TIF)

Figure S2 Immunohistochemical analysis of $CD166^{hi}$ human prostate epithelium-derived graft demonstrates nuclear expression of AR and p63, CK5 and CK8 positive cells and Ki67 positive cells within tubule structure. Scale bar: 50 μm.
(TIF)

Figure S3 LSC^{hi};$CD166^{hi}$ and LSC^{hi}; $CD166^{lo}$ cells isolated from *Pten* mutant prostate form spheres with similar size distribution. Representative sphere images of LSC^{hi};$CD166^{hi}$ and LSC^{hi}; $CD166^{lo}$ cells generated spheres. Top: spheres maintained in matrigel. low: spheres released from matrigel after dispase treatment. Scale bar: 200 μm.
(TIF)

Table S1 Compared to intact prostate epithelium WT CD166 gene expression is significantly increased at day 3 post-castration.
(TIF)

Table S2 Antibodies used for FACS, IHC and IF.
(TIF)

Acknowledgments

We thank Dr. Joshua Weiner for generously supplying the *CD166* knockout line. We thank Dr. Rita Lukacs for technical help and scientific discussions; Ying Wang and Jenifer Lau for technical assistance; and colleagues in our laboratories for helpful comments. We appreciate the assistance of Dr. Dong Sung Anh in acquisition of fetal prostate samples.

Author Contributions

Conceived and designed the experiments: JJ AH IG HW. Performed the experiments: JJ AH SW AG DC YL CG BZ LF. Analyzed the data: JJ AH SW LT AG DL MG LF. Contributed reagents/materials/analysis tools: MG OW IG HW. Wrote the paper: JJ AH IG HW.

References

1. Jemal A, Siegel R, Xu J, Ward E (2010) Cancer statistics, 2010. CA Cancer J Clin 60: 277–300.
2. Taylor RA, Toivanen R, Risbridger GP (2010) Stem cells in prostate cancer: treating the root of the problem. Endocr Relat Cancer 17: R273–285.
3. Wang ZA, Shen MM (2011) Revisiting the concept of cancer stem cells in prostate cancer. Oncogene 30: 1261–1271.
4. Goldstein AS, Stoyanova T, Witte ON (2010) Primitive origins of prostate cancer: in vivo evidence for prostate-regenerating cells and prostate cancer-initiating cells. Mol Oncol 4: 385–396.
5. Tang DG, Patrawala L, Calhoun T, Bhatia B, Choy G, et al. (2007) Prostate cancer stem/progenitor cells: identification, characterization, and implications. Mol Carcinog 46: 1–14.
6. Visvader JE (2011) Cells of origin in cancer. Nature 469: 314–322.

7. Maitland NJ, Collins A (2005) A tumour stem cell hypothesis for the origins of prostate cancer. BJU Int 96: 1219–1223.
8. Moscatelli D, Wilson EL (2010) PINing down the origin of prostate cancer. Sci Transl Med 2: 43ps38.
9. Korsten H, Ziel-van der Made A, Ma X, van der Kwast T, Trapman J (2009) Accumulating progenitor cells in the luminal epithelial cell layer are candidate tumor initiating cells in a Pten knockout mouse prostate cancer model. PLoS One 4: e5662.
10. Wang X, Kruithof-de Julio M, Economides KD, Walker D, Yu H, et al. (2009) A luminal epithelial stem cell that is a cell of origin for prostate cancer. Nature 461: 495–500.
11. Kurita T, Medina RT, Mills AA, Cunha GR (2004) Role of p63 and basal cells in the prostate. Development 131: 4955–4964.
12. Lawson DA, Zong Y, Memarzadeh S, Xin L, Huang J, et al. (2010) Basal epithelial stem cells are efficient targets for prostate cancer initiation. Proc Natl Acad Sci U S A 107: 2610–2615.
13. Goldstein AS, Huang J, Guo C, Garraway IP, Witte ON (2010) Identification of a cell of origin for human prostate cancer. Science 329: 568–571.
14. Choi N, Zhang B, Zhang L, Ittmann M, Xin L (2012) Adult Murine Prostate Basal and Luminal Cells Are Self-Sustained Lineages that Can Both Serve as Targets for Prostate Cancer Initiation. Cancer Cell 21: 253–265.
15. Sarker D, Reid AH, Yap TA, de Bono JS (2009) Targeting the PI3K/AKT pathway for the treatment of prostate cancer. Clin Cancer Res 15: 4799–4805.
16. McMenamin ME, Soung P, Perera S, Kaplan I, Loda M, et al. (1999) Loss of PTEN expression in paraffin-embedded primary prostate cancer correlates with high Gleason score and advanced stage. Cancer Res 59: 4291–4296.
17. Wang S, Gao J, Lei Q, Rozengurt N, Pritchard C, et al. (2003) Prostate-specific deletion of the murine Pten tumor suppressor gene leads to metastatic prostate cancer. Cancer Cell 4: 209–221.
18. Wang S, Garcia AJ, Wu M, Lawson DA, Witte ON, et al. (2006) Pten deletion leads to the expansion of a prostatic stem/progenitor cell subpopulation and tumor initiation. Proc Natl Acad Sci U S A 103: 1480–1485.
19. Mulholland DJ, Xin L, Morim A, Lawson D, Witte O, et al. (2009) Lin-Sca-1+CD49fhigh stem/progenitors are tumor-initiating cells in the Pten-null prostate cancer model. Cancer Res 69: 8555–8562.
20. Mulholland DJ, Tran LM, Li Y, Cai H, Morim A, et al. (2011) Cell autonomous role of PTEN in regulating castration-resistant prostate cancer growth. Cancer Cell 19: 792–804.
21. Tsujimura A, Koikawa Y, Salm S, Takao T, Coetzee S, et al. (2002) Proximal location of mouse prostate epithelial stem cells: a model of prostatic homeostasis. J Cell Biol 157: 1257–1265.
22. Wang XD, Wang BE, Soriano R, Zha J, Zhang Z, et al. (2007) Expression profiling of the mouse prostate after castration and hormone replacement: implication of H-cadherin in prostate tumorigenesis. Differentiation 75: 219–234.
23. Carver BS, Chapinski C, Wongvipat J, Hieronymus H, Chen Y, et al. (2011) Reciprocal feedback regulation of PI3K and androgen receptor signaling in PTEN-deficient prostate cancer. Cancer Cell 19: 575–586.
24. Swart GW (2002) Activated leukocyte cell adhesion molecule (CD166/ALCAM): developmental and mechanistic aspects of cell clustering and cell migration. Eur J Cell Biol 81: 313–321.
25. van Kempen LC, Nelissen JM, Degen WG, Torensma R, Weidle UH, et al. (2001) Molecular basis for the homophilic activated leukocyte cell adhesion molecule (ALCAM)-ALCAM interaction. J Biol Chem 276: 25783–25790.
26. Lawson DA, Xin L, Lukacs RU, Cheng D, Witte ON (2007) Isolation and functional characterization of murine prostate stem cells. Proc Natl Acad Sci U S A 104: 181–186.
27. Ofori-Acquah SF, King JA (2008) Activated leukocyte cell adhesion molecule: a new paradox in cancer. Transl Res 151: 122–128.
28. Garraway IP, Sun W, Tran CP, Perner S, Zhang B, et al. (2010) Human prostate sphere-forming cells represent a subset of basal epithelial cells capable of glandular regeneration in vivo. Prostate 70: 491–501.
29. Goldstein AS, Lawson DA, Cheng D, Sun W, Garraway IP, et al. (2008) Trop2 identifies a subpopulation of murine and human prostate basal cells with stem cell characteristics. Proc Natl Acad Sci U S A 105: 20882–20887.
30. Liu C, Kelnar K, Liu B, Chen X, Calhoun-Davis T, et al. (2011) The microRNA miR-34a inhibits prostate cancer stem cells and metastasis by directly repressing CD44. Nat Med 17: 211–215.
31. Leong KG, Wang BE, Johnson L, Gao WQ (2008) Generation of a prostate from a single adult stem cell. Nature 456: 804–808.
32. Burger PE, Gupta R, Xiong X, Ontiveros CS, Salm SN, et al. (2009) High aldehyde dehydrogenase activity: a novel functional marker of murine prostate stem/progenitor cells. Stem Cells 27: 2220–2228.
33. Richardson GD, Robson CN, Lang SH, Neal DE, Maitland NJ, et al. (2004) CD133, a novel marker for human prostatic epithelial stem cells. J Cell Sci 117: 3539–3545.
34. Taylor BS, Schultz N, Hieronymus H, Gopalan A, Xiao Y, et al. (2010) Integrative genomic profiling of human prostate cancer. Cancer Cell 18: 11–22.
35. Weiner JA, Koo SJ, Nicolas S, Fraboulet S, Pfaff SL, et al. (2004) Axon fasciculation defects and retinal dysplasias in mice lacking the immunoglobulin superfamily adhesion molecule BEN/ALCAM/SC1. Mol Cell Neurosci 27: 59–69.
36. van Kempen LC, van den Oord JJ, van Muijen GN, Weidle UH, Bloemers HP, et al. (2000) Activated leukocyte cell adhesion molecule/CD166, a marker of tumor progression in primary malignant melanoma of the skin. Am J Pathol 156: 769–774.
37. King JA, Tan F, Mbeunkui F, Chambers Z, Cantrell S, et al. (2010) Mechanisms of transcriptional regulation and prognostic significance of activated leukocyte cell adhesion molecule in cancer. Mol Cancer 9: 266.
38. Kristiansen G, Pilarsky C, Wissmann C, Kaiser S, Bruemmendorf T, et al. (2005) Expression profiling of microdissected matched prostate cancer samples reveals CD166/MEMD and CD24 as new prognostic markers for patient survival. J Pathol 205: 359–376.
39. Mezzanzanica D, Fabbi M, Bagnoli M, Staurengo S, Losa M, et al. (2008) Subcellular localization of activated leukocyte cell adhesion molecule is a molecular predictor of survival in ovarian carcinoma patients. Clin Cancer Res 14: 1726–1733.
40. Kahlert C, Weber H, Mogler C, Bergmann F, Schirmacher P, et al. (2009) Increased expression of ALCAM/CD166 in pancreatic cancer is an independent prognostic marker for poor survival and early tumour relapse. Br J Cancer 101: 457–464.
41. Weichert W, Knosel T, Bellach J, Dietel M, Kristiansen G (2004) ALCAM/CD166 is overexpressed in colorectal carcinoma and correlates with shortened patient survival. J Clin Pathol 57: 1160–1164.
42. Sawhney M, Matta A, Macha MA, Kaur J, DattaGupta S, et al. (2009) Cytoplasmic accumulation of activated leukocyte cell adhesion molecule is a predictor of disease progression and reduced survival in oral cancer patients. Int J Cancer 124: 2098–2105.
43. Ishigami S, Ueno S, Arigami T, Arima H, Uchikado Y, et al. (2011) Clinical implication of CD166 expression in gastric cancer. J Surg Oncol 103: 57–61.
44. Liao CP, Adisetiyo H, Liang M, Roy-Burman P (2010) Cancer-associated fibroblasts enhance the gland-forming capability of prostate cancer stem cells. Cancer Res 70: 7294–7303.
45. De Marzo AM, Nelson WG, Bieberich CJ, Yegnasubramanian S (2010) Prostate cancer: New answers prompt new questions regarding cell of origin. Nat Rev Urol 7: 650–652.
46. Sato C, Matsuda T, Kitajima K (2002) Neuronal differentiation-dependent expression of the disialic acid epitope on CD166 and its involvement in neurite formation in Neuro2A cells. J Biol Chem 277: 45299–45305.
47. Lu TL, Chang JL, Liang CC, You LR, Chen CM (2007) Tumor spectrum, tumor latency and tumor incidence of the Pten-deficient mice. PLoS One 2: e1237.
48. Abou-Kheir WG, Hynes PG, Martin PL, Pierce R, Kelly K (2010) Characterizing the contribution of stem/progenitor cells to tumorigenesis in the Pten−/−TP53−/− prostate cancer model. Stem Cells 28: 2129–2140.
49. Rajasekhar VK, Studer L, Gerald W, Socci ND, Scher HI (2011) Tumour-initiating stem-like cells in human prostate cancer exhibit increased NF-kappaB signalling. Nat Commun 2: 162.
50. Chao MP, Alizadeh AA, Tang C, Jan M, Weissman-Tsukamoto R, et al. (2011) Therapeutic antibody targeting of CD47 eliminates human acute lymphoblastic leukemia. Cancer Res 71: 1374–1384.
51. Lunter PC, van Kilsdonk JW, van Beek H, Cornelissen IM, Bergers M, et al. (2005) Activated leukocyte cell adhesion molecule (ALCAM/CD166/MEMD), a novel actor in invasive growth, controls matrix metalloproteinase activity. Cancer Res 65: 8801–8808.
52. Wiiger MT, Gehrken HB, Fodstad O, Maelandsmo GM, Andersson Y (2010) A novel human recombinant single-chain antibody targeting CD166/ALCAM inhibits cancer cell invasion in vitro and in vivo tumour growth. Cancer Immunol Immunother 59: 1665–1674.
53. Hart LS, El-Deiry WS (2008) Invincible, but not invisible: imaging approaches toward in vivo detection of cancer stem cells. J Clin Oncol 26: 2901–2910.
54. Wang CH, Chiou SH, Chou CP, Chen YC, Huang YJ, et al. (2011) Photothermolysis of glioblastoma stem-like cells targeted by carbon nanotubes conjugated with CD133 monoclonal antibody. Nanomedicine 7: 69–79.
55. Roth A, Drummond DC, Conrad F, Hayes ME, Kirpotin DB, et al. (2007) Anti-CD166 single chain antibody-mediated intracellular delivery of liposomal drugs to prostate cancer cells. Mol Cancer Ther 6: 2737–2746.
56. Lukacs RU, Goldstein AS, Lawson DA, Cheng D, Witte ON (2010) Isolation, cultivation and characterization of adult murine prostate stem cells. Nat Protoc 5: 702–713.
57. Xin L, Lukacs RU, Lawson DA, Cheng D, Witte ON (2007) Self-renewal and multilineage differentiation in vitro from murine prostate stem cells. Stem Cells 25: 2760–2769.
58. Narita S, So A, Ettinger S, Hayashi N, Muramaki M, et al. (2008) GLI2 knockdown using an antisense oligonucleotide induces apoptosis and chemosensitizes cells to paclitaxel in androgen-independent prostate cancer. Clin Cancer Res 14: 5769–5777.
59. Goldstein AS, Drake JM, Burnes DL, Finley DS, Zhang H, et al. (2011) Purification and direct transformation of epithelial progenitor cells from primary human prostate. Nat Protoc 6: 656–667.

ELSEVIER

Urologic Oncology: Seminars and Original Investigations xx (2011) xxx

UROLOGIC ONCOLOGY

News and topics

Will identification of a prostate cancer stem cell lead to its cure?

There is abundant evidence in mouse and man that the prostate contains normal tissue stem cells within the epithelium that are capable of self-renewal and inducing benign tubule formation [1–5]. The premise that prostate tumors contain cancer stem cells (CSCs) that ultimately lead to development of castration-resistant prostate cancer remains to be determined. The basic theory of CSCs is that they represent a small fraction of tumor cells possessing biological characteristics that render an exceptional propensity for tumor initiation and resilience to traditional therapy [6–9]. CSCs self-renew, but also generate more differentiated progeny that comprise the bulk and heterogeneity of tumors. CSCs may be transformed normal tissue stem cells with inherent self-renewal capability or deranged progenitor cells with reactivated stem cell pathways, resulting in limitless self-renewal potential. In the case of prostate cancer, it is postulated that CSCs are relatively androgen insensitive. Similar to normal prostate tissue stem cells, CSCs may respond to androgen, but not require it for survival. CSCs may be the seeds for local recurrence and metastasis, by spreading from niche to niche. Hence, if CSCs are not eliminated, the cancer cannot be cured. But do prostate CSCs really exist?

Evidence supporting CSC populations is based on functional evaluation of fractionated tumor cells. In order to be characterized as a CSC, self-renewal must be demonstrated. Putative CSCs, isolated according to a particular antigenic profile, must also be capable of seeding and propagating heterogeneous tumors. CSCs reside in niches and have biologic regulatory mechanisms that induce chemo- and radioresistance. Abundant evidence for CSCs exist for hematologic malignancies, (acute myeloblastic leukemia) as well as, glioblastoma, breast cancer, and colon cancer [10–16].

Evidence for the existence of prostate CSCs has lagged because of technical hurdles associated with human prostate tumor modeling [17]. Primary prostate cancer cells obtained from human prostatectomy specimens are extremely difficult to culture in vitro, even for brief periods [18,19]. Cells with luminal profiles (including tumor cells) are difficult to recover following tissue dissociation, with the majority of the cells retrieved being of basal, stromal, and blood lineage [3,20]. Metastatic tumors are rarely available for live cell investigations. Without isolation of viable prostate cancer cells, fractionation and engraftment studies that evaluate tumor regeneration capability cannot be done. Even if viable tumor cells can be successfully isolated, xenograft formation in immunocompromised mice remains a challenge. Highly immunodeficient mouse models are required, and it is likely that species-specific prostatic growth factors and support cells may also be essential for recreation of the niche and efficient tumorigenesis [17,21].

Studies that have advocated for the existence of human prostate CSCs are limited in number and scope. The first reports of prostate CSCs indicated that CD133+ cells isolated from tumors were more proliferative and could produce heterogeneous progeny [22]. These studies, however, did not demonstrate tumor regeneration in vivo, an important component supporting CSC function. Evaluation of prostate cancer xenografts and cell lines indicate that CD44 may be a marker of prostate cancer CSCs [23,24]. Serially passaged xenografts and cell lines, however, may not accurately reflect primary tumor cell biology. Without confirmatory studies with primary prostate tumors or metastases, the relevance of these observations comes into question.

Recent reports have identified a human cancer cell of origin from benign prostate tissue [20]. Prostate cells from dissociated tissues were fractionated based on surface marker expression and genetically manipulated to overexpress AR, in combination with the oncogenes, AKT and ERG. Only prostate cellular fractions containing $Trop2^{+}Cd49f^{Hi}$ basal cells were able to induce tumors in immunocompromised mice. Whether or not the cell of origin for prostate cancer and CSCs (the cancer cells that propagate tumor and metastasize) share a common antigenic profile remains to be determined.

If there are CSCs in human prostate cancer, would their targeting and elimination lead to cure of castration resistant disease? If the hypothesized CSC in prostate cancer is indeed androgen insensitive and equipped with anti-apoptotic mechanisms, specific targeting may achieve clinical benefit in patients with metastatic disease. CSCs may be targeted by interference of self-renewal and other pathways involved in CSC maintenance, aptamer, or antibody-mediated toxin-linked agents, or by disrupting the niche [25–27].

An alternative approach to curing prostate cancer is to inhibit its initiation. Targeting the cells of origin for prostate cancer (normal prostate stem cells) before cancer develops or spreads should be considered. As prostate imaging mo-

1078-1439/$ – see front matter
doi:10.1016/j.urolonc.2011.01.015

dalities improve, it is conceivable that small lesions could be susceptible to treatment with agents targeting stem cells.

In order to make progress in the isolation and characterization of prostate cancer stem cells, improved methodologies are needed to retrieve viable cells from primary prostate tumors and metastases for evaluation of CSC activity. In the meantime, further characterization of the role of normal stem cells in tumorigenesis is warranted, in order to determine if genetic profiling or targeting of these cells will make a diagnostic and/or prognostic impact.

Isla P. Garraway, M.D., Ph.D.
Department of Urology
Jonsson Comprehensive Cancer Center
Broad Center of Regenerative Medicine and Stem Cell Research
David Geffen School of Medicine at UCLA
Los Angeles, CA, USA

References

[1] Isaacs JT, Coffey DS. Etiology and disease process of benign prostatic hyperplasia. Prostate 1989;2(Suppl):33–50.
[2] Xin L, Ide H, Kim Y, et al. In vivo regeneration of murine prostate from dissociated cell populations of postnatal epithelia and urogenital sinus mesenchyme. Proc Natl Acad Sci U S A 2003;100(Suppl 1):11896–903.
[3] Garraway IP, Sun W, Tran CP, et al. Human prostate sphere-forming cells represent a subset of basal epithelial cells capable of glandular regeneration in vivo. Prostate 2010;70:491–501.
[4] Burger PE, Xiong X, Coetzee S, et al. Sca-1 expression identifies stem cells in the proximal region of prostatic ducts with high capacity to reconstitute prostatic tissue. Proc Natl Acad Sci U S A 2005;102:7180–5.
[5] Hayward SW, Haughney PC, Rosen MA, et al. Interactions between adult human prostatic epithelium and rat urogenital sinus mesenchyme in a tissue recombination model. Differentiation 1998;63:131–40.
[6] Reya T, Morrison SJ, Clarke MF, et al. Stem cells, cancer, and cancer stem cells. Nature 2001;414:105–11.
[7] Al-Hajj M, Clarke MF. Self-renewal and solid tumor stem cells. Oncogene 2004;23:7274–82.
[8] Jordan CT, Guzman ML, Noble M. Cancer stem cells. N Engl J Med 2006;355:1253–61.
[9] Polyak K, Hahn WC. Roots and stems: Stem cells in cancer. Nat Med 2006;12:296–300.
[10] Dontu G, Abdallah WM, Foley JM, et al. In vitro propagation and transcriptional profiling of human mammary stem/progenitor cells. Genes Dev 2003;17:1253–70.
[11] Dontu G, Al-Hajj M, Abdallah WM, et al. Stem cells in normal breast development and breast cancer. Cell Prolif 2003;36(Suppl 1):59–72.
[12] Dontu G, El-Ashry D, Wicha MS. Breast cancer, stem/progenitor cells and the estrogen receptor. Trends Endocrinol Metab 2004;15:193–7.
[13] O'Brien CA, Pollett A, Gallinger S, et al. A human colon cancer cell capable of initiating tumour growth in immunodeficient mice. Nature 2007;445:106–10.
[14] Singh SK, Clarke ID, Terasaki M, et al. Identification of a cancer stem cell in human brain tumors. Cancer Res 2003;63:5821–8.
[15] Singh SK, Hawkins C, Clarke ID, et al. Identification of human brain tumour initiating cells. Nature 2004;432:396–401.
[16] Lapidot T, Sirard C, Vormoor J, et al. A cell initiating human acute myeloid leukaemia after transplantation into SCID mice. Nature 1994;367:645–8.
[17] Li H, Jiang M, Honorio S, et al. Methodologies in assaying prostate cancer stem cells. Methods Mol Biol 2009;568:85–138.
[18] Peehl DM. Are primary cultures realistic models of prostate cancer? J Cell Biochem 2004;91:185–95.
[19] Peehl DM. Primary cell cultures as models of prostate cancer development. Endocr Relat Cancer 2005;12:19–47.
[20] Goldstein AS, Huang J, Guo C, et al. Identification of a cell of origin for human prostate cancer. Science 2010;329:568–71.
[21] Ito M, Kobayashi K, Nakahata T. NOD/Shi-scid IL2rgamma(null) (NOG) mice more appropriate for humanized mouse models. Curr Top Microbiol Immunol 2008;324:53–76.
[22] Collins AT, Berry PA, Hyde C, et al. Prospective identification of tumorigenic prostate cancer stem cells. Cancer Res 2005;65:10946–51.
[23] Patrawala L, Calhoun T, Schneider-Broussard R, et al. Highly purified CD44+ prostate cancer cells from xenograft human tumors are enriched in tumorigenic and metastatic progenitor cells. Oncogene 2006;25:1696–708.
[24] Li H, Chen X, Calhoun-Davis T, et al. PC3 human prostate carcinoma cell holoclones contain self-renewing tumor-initiating cells. Cancer Res 2008;68:1820–5.
[25] Takebe N, Harris PJ, Warren RQ, et al. Targeting cancer stem cells by inhibiting Wnt, Notch, and Hedgehog pathways. Nat Rev Clin Oncol 2011;8:97–106.
[26] Guise T. Examining the metastatic niche: Targeting the microenvironment. Semin Oncol 2010;37(Suppl 2):S2–14.
[27] Min K, Jo H, Song K, et al. Dual-aptamer-based delivery vehicle of doxorubicin to both PSMA (+) and PSMA (−) prostate cancers. Biomaterials 2011;32:2124–32.

JBC Papers in Press. Published on September 18, 2012 as Manuscript M112.389015
The latest version is at http://www.jbc.org/cgi/doi/10.1074/jbc.M112.389015

Secreted Hsp90 is a novel regulator of the epithelial to mesenchymal transition (EMT) in prostate cancer

Michael W. Hance[1], Krystal Dole[§1], Udhayakumar Gopal[§1], Jessica E. Bohonowych[1], Agnieszka Jezierska-Drutel[1], Carola A. Neumann[1], Haibo Liu[2], Isla P. Garraway[2], and Jennifer S. Isaacs[1*]

From the Departments of [1]Cell and Molecular Pharmacology, Medical University of South Carolina, Charleston, SC 29425 and [2]Urology, David Geffen School of Medicine, University of California, LA, CA 90095

Running Title: eHsp90 is a novel effector of prostate tumor cell EMT.

[*]To whom correspondence should be addressed: Department of Cell and Molecular Pharmacology, Medical University of South Carolina, Hollings Cancer Center, 86 Jonathan Lucas St, Charleston, SC, 29425. Tel: 843-792-8393; Fax: 843-792-3200; email:isaacsj@musc.edu.

Key words: extracellular Hsp90, prostate cancer, epithelial to mesenchymal transition, MMP, ERK, cell motility

Background: EMT correlates with increased metastatic potential and poor prognosis
Results: Secreted eHsp90 induces EMT, MMP activity and cell motility.
Conclusions: EMT inducing activity of eHsp90 provides a mechanistic basis for its tumorigenic and metastatic function.
Significance: The requirement for eHsp90 in supporting tumorigenic events indicates that targeting eHsp90 may represent a therapeutic approach to improve prostate cancer patient survival.

SUMMARY

Prostate cancer (PCa) is the most frequently diagnosed malignancy in men, and the second highest contributor of male cancer related lethality. Disease mortality is due primarily to metastatic spread, highlighting the urgent need to identify factors involved in this progression. Activation of the genetic epithelial to mesenchymal transition (EMT) program is implicated as a major contributor of PCa progression. Initiation of EMT confers invasive and metastatic behavior in preclinical models and is correlated with poor clinical prognosis. Extracellular Hsp90 (eHsp90) promotes cell motility and invasion in cancer cells and metastasis in preclinical models, however the mechanistic basis for its widespread tumorigenic function remains unclear. We have identified a novel and pivotal role for eHsp90 in driving EMT events in PCa. In support of this notion, more metastatic PCa lines exhibited increased eHsp90 expression relative to their lineage related non-metastatic counterparts. We demonstrate that eHsp90 promoted cell motility in an ERK and MMP-2/9-dependent manner, and shifted cellular morphology towards a mesenchymal phenotype. Conversely, inhibition of eHsp90 attenuated pro-motility signaling, blocked PCa migration, and shifted cell morphology towards an epithelial phenotype. Lastly, we report that surface eHsp90 was found in primary PCa tumor specimens, and elevated eHsp90 expression was associated with increased levels of MMP-2/9 transcripts. We conclude that eHsp90 serves as a driver of EMT events, providing a mechanistic basis for its ability to promote cancer progression and metastasis in preclinical models. Further, its newly identified expression in PCa specimens, and potential regulation of pro-metastatic genes, supports a putative clinical role for eHsp90 in PCa progression.

INTRODUCTION

One of the greatest challenges associated with the widespread and early diagnosis of prostate cancer (PCa) in men (1-3) is the inability to accurately distinguish which subset of patients with apparently

localized disease will progress to metastatic disease. The propensity of tumor cells to metastasize to bone, rendering the disease incurable (4), is largely responsible for PCa as the second leading cause of male cancer associated lethality (5). Although rising levels of the serum protein prostate specific antigen (PSA) are indicative of tumor growth, its expression can be nonspecifically modulated by a number of benign conditions (6,7) such that this metric alone risk cannot accurately predict risk for progression. Similarly, Gleason score cannot accurately predict disease progression, relapse, or response to treatment (8,9). These clinical limitations illustrate the pressing need to utilize new and improved molecular indicators of PCa progression.

Activation of the evolutionarily conserved developmental epithelial to mesenchymal transition (EMT) genetic program (10,11) is implicated as a significant contributor to PCa progression. A universal hallmark of EMT is loss of epithelial cell polarity and acquisition of elongated mesenchymal morphology, concomitant with disruption of cell adhesion, increased cell migration, invasion and metastasis (12). The adherens junction protein E-cadherin acts as a gatekeeper in suppressing EMT events, and corresponding cell motility and dissemination, by maintaining the cuboidal phenotype and architecture that defines the morphology of normal epithelium (10,11,13). As such, loss of E-cadherin function is a conserved and fundamental hallmark associated with early EMT events (10,11).

Multiple preclinical models provide strong support for EMT in mediating PCa progression. Pathological EMT events have been shown to potentiate the transition from localized prostate adenocarcinoma to invasive carcinoma and subsequent metastasis (14-19). Conversely, repression of EMT events blocks the metastatic potential of PCa cells (20). In clinical specimens, measures of cancer progression correlate with loss of E-cadherin and upregulation of EMT-inducing transcriptional factors (18,20-23). EMT events are correlated with metastatic recurrence following surgery (18,24), and have recently been observed concurrently following androgen withdrawal therapy (25). Therefore, the ability to identify primary tumor cells with an increased propensity to undergo EMT-like events would improve diagnostic approaches to discriminate patients at risk for progression.

Hsp90 is a well known intracellular chaperone responsible for mediating the ATP dependent folding and signaling function of numerous client proteins, many of which exhibit pro-tumorigenic functions (26-28). In addition to its intracellular localization, Hsp90 is also a secreted and cell surface protein. Extracellular Hsp90 (eHsp90) exhibits distinct function from the intracellular chaperone with its signal transducing activity, in tandem with its receptor low density lipoprotein related protein (LRP1) (29,30). eHsp90 supports cell motility and invasion in several cancer cell lines (31-34), and promotes metastatic spread in preclinical models (35-38). Clinically, eHsp90 was first reported as a tumor antigen (39,40), and more recently found in the serum from patients afflicted with a variety of tumor types (37), including metastatic PCa (41). Although these reports strongly implicate eHsp90 in disease progression, a mechanistic basis for this putative function remains largely unknown.

The present study identifies eHsp90 as a pivotal regulator of E-cadherin function in PCa. Importantly, we demonstrate that modest, physiologically relevant expression of secreted eHsp90 reduces the expression and alters the localization of E-cadherin in phenotypically epithelial cell lines. In addition, eHsp90 modulates numerous genetic events consistent with activation of EMT, as well as promoting diminished cell adhesion, conversion to a more mesenchymal morphology and increased cell motility. In addition to its role in initiating

EMT events, eHsp90 is also essential for sustaining the mesenchymal properties and behavior of more aggressive PCa cell types. Finally, we report that surface eHsp90 is found in primary PCa tumor specimens and is correlated with markedly elevated expression of a subset of pro-tumorigenic eHsp90 regulated transcripts. This newly identified role for eHsp90 as a mediator of EMT events provides a mechanistic basis for its ability to promote cancer progression and metastasis in a variety of preclinical models. Moreover, the newly identified expression of eHsp90 in PCa specimens, coupled with its potential role in modulating gene expression, implicates a clinical role for eHsp90 in PCa progression.

Materials and Methods

Western blot and Antibodies: Cell extracts for Western blot analysis were prepared and performed as described (30) and all blots are representative of a minimum of two independent experiments. Antibodies for N-cadherin (ab12221), Slug (ab27568), Snail (ab63371), and Vimentin (ab8978) were purchased from Abcam. Mouse and rabbit Hsp90 antibodies (ADI-SPA-830, ADI-SPS-771) were from Enzo Lifesciences. E-cadherin (3195), ERK 1/2 (4695), P-ERK 1/2 (4370), MEK1/2 (9122), P-MEK1/2 (9121) and ZO-1(5406) were from Cell Signaling. FAK (AHO0502) and P-FAK (44-624G) were from Invitrogen/Life Technologies. V5 antibody (NB600-381) was from Novus Biologicals. Twist (sc-15393) was from Santa Cruz Biotechnology, and anti-alpha tubulin antibody (T6074) was from Sigma. Mouse monoclonal LRP1 antibody (11H4) was purified from a hybridoma cell line (CRL 1936) purchased from ATCC. The hybridoma supernatant was concentrated with a Vivacell 70 concentrator (Sartorius Biolab products) and purified with an NAb protein G antibody purification kit (Thermo Scientific) according to the manufacturer's instructions, and aliquots were stored at −20°C.

Reagents: Recombinant Hsp90 alpha protein was obtained from Enzo Life Sciences (ADI-SPP-776). Geldanamycin was obtained from the Experimental Therapeutics Branch, National Cancer Institute, DMAG-N-oxide modified geldanamycin, (or non-permeable GA, NPGA used at 1μM) was synthesized by Chris Lindsey and Craig Beeson (Pharmaceutical Sciences, Medical University of South Carolina). MMP inhibitors GM6001 (CC1010 used at 1μM), MMP-2/9 inhibitor IV (444274 used at 1μM) and MMP-3 inhibitor IV (444243 used at 5μM) were obtained from EMD Millipore Chemicals. MEK inhibitor U0126 (V112A used at 10μM) was obtained from Promega.

Cell Culture, Plasmids, and Transfection: The prostate cancer cell lines DU145 and LNCaP were obtained from ATCC, the ARCaP cell pair was purchased from Novicure Biotechnology, and C4-2B was obtained from Viromed. The P69/M12 cell pair was a gift from Joy Ware. The ARCaP pair and P69/M12 cell pair was maintained in T-media supplemented with 5% heat inactivated fetal bovine serum, and the LNCaP and C4-2B pair was maintained in their specified media supplemented with 1% HEPES and 1% penicilin/streptomycin in a 5% CO_2-humidified atmosphere. The plasmid for shLRP1 was as previously described (29,30). The sequence for Hsp90 alpha was cloned in frame to a 5' signal peptide to direct its extracellular localization, and 3' to a V5 tag and 6X His epitope, with each epitope separated by a flexible linker. The product was assembled in a Gateway entry vector and recombined (CRE) into Plenti6.3V5-Dest (Invitrogen). To obtain viral particles for LRP1 suppression and constitutive eHsp90 secretion, 293FT cells (Invitrogen) were co-transfected with the viral packaging plasmids VSVG and PΔR 8.71, along with the corresponding lentiviral vector. All plasmid transfections were performed with Lipofectamine 2000 (Invitrogen) according to the manufacturer's specifications. Following viral plasmid transfection, cell medium was harvested at

48 hr, the lentiviral supernatant was concentrated by ultracentrifugation, titered, and 5×10^4 particles were used to infect the recipient cells in the presence of polybrene (8 μg/ml). Cells transduced with eHsp90 virus were selected in blasticidin (Invivogen), while GFP-shLRP1 transduced cells were selected by flow cytometry to isolate the highest GFP expressing cells. Selection for eHsp90 transduced cells was performed for two weeks, whereupon surviving cells were pooled.

Patient Samples: Human prostate tissue was obtained via an approved research protocol with informed written consent of all participants. Adjacent tissue specimens were snap frozen in liquid nitrogen or fixed in formalin and paraffin-embedded for histological analysis. Tumor tissue specimens were mechanically and enzymatically digested as previously described (42) and dissociated tissue filtered and passed repeatedly through a 23-gauge needle to generate single cell suspensions. Cells were resuspended and incubated (15 min at 4˚C) with either isotype matched control or anti-Hsp90 antibody (SPS-771-PE, 1:50), and subjected to FACS analysis (BD FACS Aria II system). Cell populations corresponding to $eHsp90^{high}$ and $eHsp90^{low}$ subtypes were gated and isolated (minimum signal threshold set at 10e2).

RNA isolation and real time PCR analysis: RNA purification from patient samples was performed according to the manufacturer's recommendations (Qiagen RNeasy Plus Micro kit; 74034). RNA purification from cells was performed following a trizol/chloroform extraction (Qiagen miRNeasy kit; 217004). mRNA from cells and patient material was converted into complimentary DNA (OriGene first strand cDNA synthesis kit; NP100042), and (BioRad iScript advanced cDNA synthesis kit; 170-8842), respectively, and amplified. Array samples were prepared according to the manufacturer's instructions (Qiagen RT^2 first strand kit; 330401), and further analyzed using an EMT profiler array (Qiagen; PAHS-090A). Biological replicates were utilized for the initial array analysis, and select results validated with additional biological replicates. Primers (supplemental table 1) were purchased from IDT.

Cell motility assays: Wounding assays were performed as previously described (30). Briefly, a thin sterile pipette tip was used to create a scratch wound in confluent cell monolayers. Pictures were taken at 0 and 16 -20 hrs with an inverted Nikon eclipse TE 2000-S microscope with 10× magnification, and the extent of migration was calculated by measurement of the gap area using Image J software. For all motility experiments, mitomycin C (5 ug/ml) (Sigma) was added at the time of plating to suppress proliferation.

Gelatin zymography assay: The gelatinolytic activity of MMP-2 and MMP-9 was determined by gelatin zymography in 0.1% gelatin-10% acrylamide gels. Samples were prepared by plating cells at 50% confluency, and conditioned medium (0.25% serum in DMEM) was collected after 36 hr. 1 mM o-phenanthroline monohydrate was added to halt MMP activity. Conditioned medium was incubated with gelatin-sepharose beads (GE Healthcare, 17-0956-01) and eluted samples run in non-reducing conditions. Gels were washed with 2.5% Triton X-100 renaturing buffer, incubated in a Tris-HCL/Brij35 developing buffer (42˚C for 24 hours), and subsequently stained with a 5% Comassie solution.

Hsp90α ELISA: To detect expression of secreted Hsp90α, equivalent cell numbers (7.5×10^5) were plated overnight and replenished with complete media 24 hr prior to harvest. Conditioned medium was collected, debris removed by centrifugation (5 min, 1200 x g) and Hsp90α levels detected by ELISA (Enzo Life Sciences). Values are presented as fold change of Hsp90 per ml of conditioned medium with the standard deviation shown.

Immunofluorescence: To evaluate cellular localization of E-cadherin and ZO-1, equivalent cell numbers (2.5×10^4) were plated overnight and replenished with complete media for 24 hr. Cells were then treated with either NPGA, GM6001, MMP-2/9 and MMP-3 inhibitors for specified times. Cells were fixed with 4% paraformaldehyde and permeabilized with 0.1% Triton X-100 in PBS. Immunofluorescence was performed as described (30).

Statistical analysis: All cell motility and quantitative real time PCR were performed in triplicate. Data shown are presented as means and SD; differences in treatment groups are defined as statistically significant at $P<0.05$ value, as calculated from Student's t test.

RESULTS

An eHsp90-LRP1 signaling pathway initiates prostate cancer cell motility

Although eHsp90 has been implicated in promoting cancer cell motility, invasion and metastasis in several models (30-34,36-38,43), its role in PCa has not yet been explored. To investigate whether eHsp90 supports PCa motility, we examined the effects of eHsp90 inhibition in PC3 cells. To inhibit eHsp90, PC3 cells were treated with two different anti-Hsp90 antibodies, an effective approach to neutralize eHsp90 activity and diminish eHsp90 driven cell motility (30,35-37). As an additional means to inhibit eHsp90 function, cells were treated with NPGA specific for eHsp90 (30,36,44). Exposure of PC3 cells to either NPGA or blocking antibodies to Hsp90α and β isoforms or to Hsp90α similarly suppressed cell migration over 50% (Fig. 1A and S1A). The similar results elicited by these three distinct eHsp90 targeted approaches validate the importance of eHsp90 in PCa motility.

It has been shown that eHsp90 elicits autocrine signaling through LRP1 (29,30). We reasoned that if eHsp90 was eliciting its pro-motility effects through LRP1, then treatment of cells with either NPGA or suppression of LRP1 would similarly impair cell migration. In support of this notion, treatment of DU145 PCa cells with either NPGA or shLRP1 comparably blocked cell motility (Fig 1B and Fig. S1B). NPGA did not further block cell motility in LRP1 suppressed cells, indicating impairment of a similar pathway.

LRP1 has been shown to be required for activation of the pro-motility proteins extracellular-signal-regulated kinase (ERK) and focal adhesion kinase (FAK) (45-47). Treatment of DU145 with NPGA inhibited phosphorylation of both FAK and ERK (Fig. 1C). To provide further evidence for an eHsp90-LRP1 signaling pathway, the activation status of FAK and ERK was evaluated in LRP1 suppressed cells. As shown, LRP1 suppression in DU145 cells dramatically diminished both FAK and ERK phosphorylation, with no further effect elicited by NPGA treatment (Fig. 1D). These data indicate that eHsp90-LRP1 plays an essential role in regulating the activation status of pro-motility effectors and supporting the migratory potential of PCa cells.

eHsp90 is elevated in more aggressive PCa cell types and is essential for cell motility

Increased cell motility is commonly associated with cells adopting a mesenchymal morphology (11,48). We therefore next investigated whether increased eHsp90 expression was associated with more highly motile mesenchymal cell types. To examine this, we analyzed 3 sets of lineage related prostate cancer cell pairs, with the mesenchymal derivative of each pair representing a more tumorigenic and metastatic derivative of its epithelial counterpart. The ARCaP model, consisting of ARCaPE and ARCaPM subtypes, recapitulates many of the pathological

features of PCa (49), and is one of the best characterized cell pairs for investigating EMT events (14,15,50). The epithelial ARCaPE disseminates at low frequency, while its mesenchymal counterpart ARCaPM is highly aggressive and metastatic (14,15,17). EMT events in ARCaPE can be initiated following exposure to a variety of soluble growth factors (22,51,52), and sustained EMT activation increases its metastatic potential (19,52). The cell pair represented by P69 and M12 is another useful model for monitoring EMT events. P69 is a normal nontumorigenic immortalized prostate epithelial cell line, whereas M12 a highly tumorigenic and metastatic subline (53). P69 expresses E-cadherin and is responsive to EMT inducing stimuli that confer tumorigenic properties (54), while M12 expresses mesenchymal markers such as vimentin (17,54). We confirmed the epithelial and mesenchymal nature of these two cell pairs (Supplemental Fig. S2A). We included LNCaP and C4-2B as an additional lineage related model with differential metastatic potential. LNCaP is weakly tumorigenic (55,56), while C4-2B is an osteogenic derivative that is highly metastatic and efficiently forms bone metastases (57). Strikingly, we demonstrate that each of the three metastatic derivatives express several fold higher expression of eHsp90 relative to their less metastatic epithelial counterparts (Fig. 2A).

We next evaluated whether the secretion of eHsp90 in these cell pairs influenced tumor cell motility. To assess this, exogenous Hsp90 protein (to mimic eHsp90 secretion) was added to ARCaPE, while eHsp90 in ARCaPM was targeted by NPGA. Addition of eHsp90 elicited a greater than threefold increase in ARCaPE cell motility, while inhibition of eHsp90 function in ARCaPM resulted in a fivefold reduction of cell motility (Fig. 2B and Fig. S2B). Similar trends were noted in the P69/M12 pair (Fig. 2C and Fig. S2C). These findings solidify a causal relationship between eHsp90 expression and cell motility.

To establish whether eHsp90 elicited its effects via autocrine signaling through LRP1, we evaluated the impact of LRP1 suppression upon eHsp90 driven cell motility in ARCaPE. We show that downregulation of LRP1 suppressed ARCaPE basal migration, and completely blocked eHsp90 mediated cell motility (Fig. 2D and Fig. S2D). To provide further support for eHsp90 initiated pro-motility signaling events, we evaluated the ability of eHsp90 to stimulate the MEK-ERK axis, a critical component of cell motility (58). Our results indicate that eHsp90 elicits a rapid activation of MEK-ERK signaling (Fig. S2E), supporting an autocrine eHsp90 directed signaling pathway in promoting cell motility.

eHsp90 induces molecular and morphological changes consistent with an epithelial to mesenchymal transition

Our data are consistent with the premise that increased eHsp90 expression is associated with migratory potential and mesenchymal morphology. Given this correlation, we next examined whether eHsp90 functionally regulated molecular and morphologic events consistent with activation of an epithelial to mesenchymal transition (EMT). We utilized ARCaPE cells as an EMT responsive model representative of early disease. Our data indicate that eHsp90 suppressed E-cadherin, while increasing the mesenchymal proteins N-cadherin and Twist (Fig. 3A). Strikingly, addition of eHsp90 also induced morphological changes consistent with a mesenchymal phenotype, such as an elongated fibroblastic morphology, and conversion from a tightly packed epithelial cobblestone pattern to a loosely packed scattered phenotype. To assess the possible role of eHsp90 in supporting the mesenchymal phenotype of ARCaPM, eHsp90 was pharmacologically targeted by NPGA. This treatment reduced the mesenchymal marker N-cadherin, concomitantly reduced the extent of cell elongation and increased cell cohesiveness (Fig. 3B). E-cadherin is repressed in

ARCaPM (51) and NPGA treatment was unable to restore this expression.

To solidify these trends, we next examined the role of eHsp90 in the P69/M12 cell pair. Addition of eHsp90 to P69 recapitulated a similar transition toward mesenchymal-like characteristics, with a modest reduction of E-cadherin and increased expression N-cadherin and Twist (Fig. 3C). Addition of eHsp90 elicited similar EMT-like morphological changes, such as cell elongation and increased cell scattering. Targeting eHsp90 in the mesenchymal counterpart M12 resulted in decreased N-cadherin and a less dispersive phenotype, resulting in tight cellular clusters resembling epithelial cell types. These data indicate that targeting eHsp90 in mesenchymal cell types facilitates a reversal of a subset of EMT events, resulting in at least a partial mesenchymal to epithelial (MET) conversion.

Modest elevation of eHsp90 is sufficient to suppress E-cadherin function and promote cell motility.

Although treatment of cells with eHsp90 consistently elicited EMT-like events, use of bacterially produced protein is a less than ideal system, due to confounding factors such as batch variation, protein instability, the potential presence of endotoxin, or additional minor protein species in the preparations. To address these concerns and to create a more physiologically relevant and reproducible model, we designed a genetic approach for eHsp90 secretion by fusing a signal peptide to the N-terminus of Hsp90α. This approach has been shown to direct the extracellular localization of proteins (59), including the chaperone protein Hsp70 (60). Expression of Hsp90α was chosen due to the relative lack of activity of the Hsp90β isoform in our model (data not shown). Lentivirus expressing V5 tagged Hsp90 (V5-eHsp90) was used to infect ARCaPE cells, while ARCaPE cells transduced with V5-lacZ served as the control. Stably transduced ARCaPE (ARCaPE-eHsp90) exhibited a 3-fold increase in eHsp90 secretion, as determined by ELISA analysis for Hsp90α protein (Fig. 4A). The increased secretion was further confirmed by immunoblot analysis of conditioned media for Hsp90α, and by V5 detection, the latter of which is specific for exogenous V5-eHsp90 (Fig. 4A). Intracellular Hsp90 protein levels were not appreciably elevated in ARCaPE-eHsp90 (Fig. 4B). This model replicated the molecular effects of exogenously added protein, and was able to elicit the characteristic cadherin switch associated with EMT events (Fig. 4B). Furthermore, relative to control (ARCaPE-Lacz) cells, ARCaPE-eHsp90 demonstrated a sustained activation of the pro-motility kinase ERK, demonstrated a more mesenchymal morphology, and an approximately 2.5 fold increase in cell motility, the latter of which was suppressed by NPGA (Fig. 4C). Consistent with a pro-EMT role, blockade of eHsp90 reduced E-cadherin to control levels (Fig. 4D).

We next investigated whether eHsp90 affected the integrity of cellular junctional complexes. Loss of membrane localization of the gap junction protein ZO-1 frequently accompanies the disruption of cell polarity during EMT (51,61,62). As clearly demonstrated, diminished expression and protein mislocalization of both E-cadherin and ZO-1 was observed in ARCaPE-eHsp90 compared to control cells (Figs. 4E and 4F). A similar mislocalization of E-cadherin and ZO-1 was observed in a parallel genetic model of eHsp90 transduced P69 cells (P69-eHsp90) (Fig. S3A). To confirm the specific role of eHsp90 in modulating junctional complexes, we evaluated the ability of NPGA to normalize these structures in the ARCaPE model. As shown, both E-cadherin and ZO-1 protein localization was restored to regions of cell-cell contact, corresponding with the restoration of tightly packed cells with epithelial morphology (Figs. 4E and F).

To explore the possible therapeutic implications of eHsp90 treatment, we next examined whether eHsp90 inhibition in more aggressive mesenchymal cell lines might restore junctional complex integrity. Although NPGA did not elicit a re-expression of E-cadherin in ARCaPM, it partially restored membrane localization of ZO-1 (Fig. S3B). Pharmacologic targeting of eHsp90 in M12 cells dramatically restored the junctional localization of E-cadherin and elicited a modest effect upon ZO-1 (Fig. S3B). Taken together, our results indicate that eHsp90 is a pivotal regulator of the junctional complexes that influence epithelial and mesenchymal morphology.

eHsp90 modulates the expression of multiple genes associated with EMT activation

To further strengthen the EMT-initiating role of eHsp90, we evaluated its ability to modulate additional EMT-associated transcripts. To monitor the temporal effects of eHsp90 action, RNA was harvested from ARCaPE cells following exposure to eHsp90 protein for the indicated times. The resultant heat map from a qRT-PCR array demonstrates that eHsp90 regulates a large number of EMT transcripts (Fig. 5A), including N-cadherin, as supported by our protein expression data. Longer eHsp90 protein treatments most effectively increased the core EMT mediators Snail, Slug, Zeb1 and Zeb2. Changes were also observed in cytoskeletal, integrin/ECM proteins, and proteolytic proteins.

To confirm these results, and to more carefully interrogate temporal effects, a subset of these targets was validated in ARCaPE in response to protein exposure for 1, 3, or 5 days. As shown, E-cadherin was progressively suppressed in a time dependent manner (Fig. 5B). Transcriptional upregulation of the key EMT mediators Snail, Slug, Zeb1, and Zeb2 was also validated by qRT-PCR. Our findings indicate that Slug and Zeb1 are early responders to eHsp90, whereas Snail and especially Zeb2 exhibit a delayed response. We next evaluated expression of these transcripts in our ARCaPE-eHsp90 genetic model. Whereas the suppression of E-cadherin was consistent, there was a less dramatic, but statistically significant increase in both Snail and Zeb1. Transcripts for Slug were decreased, implicating this effector as eliciting an early and possibly transient role. A robust increase in Zeb2 suggests that this EMT factor may be required for later events, a finding in accordance with the later elevation of this transcript following protein exposure. In addition to these core EMT transcripts, we also evaluated expression of matrix metalloproteinases (MMPs), zinc-dependent endopeptidases that degrade components of the basement membrane, promote EMT events and support metastatic spread (63,64). We found that MMP-9 transcript expression was upregulated greater than three-fold in both protein treated ARCaPE and ARCaPE-eHsp90 cells (Fig. 5C). In contrast, MMP-3, which also plays an important role in EMT events (65), was preferentially elevated at earlier time points in the protein treated model, whereas MMP-2 was only upregulated in the ARCaPE-eHsp90 genetic model.

MMP and ERK activity are required for eHsp90 mediated motility and EMT events

It has been demonstrated that eHsp90 directly interacts with MMP-2/9 to modulate proteolytic activity and subsequent cell motility (35,66-68). We therefore utilized a standard zymogen gelatinase assay to determine whether the elevated levels of eHsp90 in ARCaPE-eHsp90 would be sufficient to increase MMP activity. As shown, MMP-2 and MMP-9 activity was increased in ARCaPE-eHsp90 cells relative to ARCaPE-LacZ control (Fig. 6A). As expected, this increase was abrogated by NPGA, demonstrating that eHsp90 is the initiating stimulus for increased MMP-2/9 activity. Given that eHsp90 activates ERK in ARCaPE-eHsp90, and the demonstrated

ability of ERK to regulate MMP-2/9 activity (69,70), we evaluated the effects of ERK upon MMP-2/9. ERK inhibition most effectively blocked this activity, supporting the premise that eHsp90 mediated ERK activation is an initiating event for MMP-2/9 activation.

We next evaluated the effect of MMP-2/9, MMP-3 and ERK upon E-cadherin transcript levels in ARCaPE-eHsp90. As indicated, broad spectrum targeting with GM60001 or MMP-2/9 inhibition robustly increased (approximately 10-fold) E-cadherin message levels, comparably to NPGA (Fig. 6B). MMP-3 inhibition weakly induced transcript expression, while UO126 elicited a potent (approximately 35-fold) increase. We further investigated whether these trends correlated with changes in E-cadherin protein expression. Inhibition of either MMP-2/9 or MMP-3 comparably restored E-cadherin protein expression by 3 days, whereas UO126 promoted the most dramatic restoration, in accordance with its effects upon message levels (Fig. 6C). It is unclear why MMP inhibition diminished E-cadherin at 5 days, as this trend was not supported via immunofluorescence microscopy (Fig 6D). It has been shown that E-cadherin may be found in an insoluble membrane fraction (71,72) when associated with the cytoskeletal matrix at apical junctions, offering a potential explanation. Interestingly, inhibition of either MMP-2/9 or MMP-3 attenuated ERK activity, with a more dramatic effect elicited by the former, indicating that these MMPs collaborate with eHsp90-ERK mediated suppression of E-cadherin.

Given that inhibition of MMP-2/9, MMP-3 and ERK increased E-cadherin expression, we assessed whether this effect trended with the restoration of E-cadherin at cellular junctions, a hallmark of its EMT suppressive epithelial function. As shown (Fig. 6D), pan MMP inhibition, or targeted inhibition of MMP-3, MMP-2/9, or ERK, comparably re-established E-cadherin expression at the cell membrane in ARCaPE-eHsp90. Functional restoration of junctional complexes was further confirmed by the membrane expression ZO-1. These findings demonstrate that eHsp90 mediated activation of ERK and MMPs is required for the loss in cell polarity that accompanies the transition to a mesenchymal morphology.

We next evaluated whether MMP and ERK activity were important for eHsp90 directed pro-motility function. As shown, pan MMP inhibition with GM6001 blocked eHsp90 mediated cell motility (Fig. 6E). Interestingly, specific targeting of MMP-2/9 or MMP-3 elicited a similar inhibition, highlighting a prominent role for MMP signaling in eHsp90 directed pro-motility function. ERK inhibition comparably diminished cell migration. Therefore, MMP and ERK are critical regulators of eHsp90's coordinate effects upon junctional integrity and cell motility.

Detection of eHsp90 protein and regulated transcripts in human prostatectomy tumor specimens

The ability of eHsp90 to initiate EMT events has important clinical ramifications. We therefore investigated the potential translational relevance of our results and determined whether eHsp90 was found in primary PCa tumors. We reasoned that tumor cells with autocrine eHsp90 function would be represented by a subpopulation exhibiting higher cell surface eHsp90. Therefore, prostatectomy specimens from high risk, locally advanced patients were subjected to FACS sorting, and tumor cell populations isolated by either high or low surface eHsp90α expression. Interestingly, this approach reproducibly detected a subpopulation of eHsp90^{high} cells corresponding to approximately 5% of the total cell number (Fig. 7A). We next investigated whether surface eHsp90 could be utilized as a marker to define a genetically distinct subpopulation of tumor cells. A modest increase in MMP-2 and a marked induction of MMP-9 was evident in these specimens, when comparing the

eHsp90^{high} population of tumor cells, relative to each tumor matched eHsp90^{low} population (Fig. 7B). No increases were observed in MMP-3 transcript expression. Intriguingly, these data parallel the trends observed in our constitutively expressing ARCaPE-eHsp90 genetic model (Fig. 5C). Importantly, these findings validate the clinical presence of eHsp90 in primary patient tumors, and further support the notion that eHsp90 may drive genetic events associated with increased risk for tumor progression. A working model for eHsp90 mediated EMT events and tumor promotion is depicted in Fig. 7C.

DISCUSSION

Although reports demonstrate the ability of eHsp90 to promote cell motility (30-34) and facilitate metastatic spread in preclinical models (36-38,43), a unifying mechanistic basis for eHsp90 tumorigenic function has not yet been clearly defined. To our knowledge, we are the first to identify eHsp90 as a pivotal initiator of EMT-like events. We demonstrate that eHsp90 increases the cell motility of epithelial ARCaPE and P69 several fold. This pro-motility function of eHsp90 is dependent upon its impairment of E-cadherin, manifest as diminished protein expression and aberrant cellular localization. Strikingly, eHsp90 elicited dramatic changes in cell morphology, converting cells from an epithelial cuboidal clustered morphology to an elongated mesenchymal morphology with loss of cell-cell contacts. Thus, eHsp90 coordinates a multitude of key events associated with cancer progression, including impaired E-cadherin function, loss of junctional integrity, initiation of EMT, and increased cell motility. Importantly, these events were achieved with relatively modest increases in eHsp90 expression comparable to levels observed in metastatic PCa tumor cells and patient sera, further underscoring that eHsp90 is a potent driver of these processes.

The EMT initiating activity of eHsp90 was further supported by its ability to modulate a wide array of genetic events consistent with this program, including upregulation of the EMT effectors Snail, Twist, Zeb, and Slug. Not surprisingly, these factors also serve as transcriptional repressors of E-cadherin (74-77), in accordance with diminished E-cadherin message observed in ARCaPE-eHsp90. The finding that eHsp90 increases transcript expression of the proteolytic enzymes MMP-2, MMP-3 and MMP-9 is relevant given that sustained MMP-2/9 activity increases the tumorigenic and metastatic properties of ARCaPE (19), and initiates EMT events and tumor progression in preclinical models of PCa (19,78). While a causal role for MMPs in tumor progression is well known, the relation between eHsp90 and MMPs is still unfolding. Reports demonstrate that eHsp90 increases the proteolytic activity of MMP-2/9 via direct protein-protein interactions (35,66-68). Our results indicate that eHsp90 plays a dual role in upregulating MMP-2/9 transcript expression, as well as increasing proteolytic function. Given that the eHsp90 regulated EMT transcriptional effectors additionally contribute to MMP expression (79-81), MMP proteolytic activity may be further influenced by these factors, as well as by direct eHsp90-chaperone mediated mechanisms (82).

Collectively, our data support a model (Fig. 7C) whereby an eHsp90-LRP1 signaling axis activates ERK and MMP activity to promote increased cell motility, impairment of E-cadherin function, and initiation of EMT events. The ability of eHsp90 to sustain ERK activation is significant, given the reported role of ERK as a potent effector of EMT, motility, malignant invasion, and metastasis (58,83-86). Our data indicate that the relationships among ERK, MMPs, and EMT are complex. eHsp90 rapidly initiates ERK activation, which is required for increased MMP-2/9 activity, supporting ERK as an upstream regulator of MMP function. In addition, it

was shown that ERK may be activated by MMP-2/9 in ARCaPE and other cancer models (19). Our data also indicate that ERK may additionally function downstream of MMP-2/9. We therefore propose that eHsp90 mediated MMP-2/9 activity is required to potentiate and sustain ERK activity, implicating a feed-forward mechanism. Our data support a contributory role for MMP-3, and MMP-3 has been implicated in promoting cell motility (65), at least in part via activation of MMP-9 (87).

Further work is required to clarify the precise contribution of these proteins to eHsp90 mediated ERK activation and E-cadherin suppression. Additional functions for MMP-2/9 may be considered (Fig 7C). First, MMP-2/9 signaling may induce ERK activation via growth factor initiated receptor activation (19). Although we cannot exclude this possibility, LRP1 silencing precludes ERK activation, indicating that LRP1 plays a dominant role in this process. Second, MMP-2/9 may cleave E-cadherin, thereby attenuating its tumor suppressive function (88). Although this is possible, we did not observe cleavage products (unpublished), and MMP suppressive activity is at least partially due to its modulation of E-cadherin transcript expression. Third, MMP-9 is a ligand for LRP1 (89) and may signal through LRP1 in a non-proteolytic manner to regulate ERK activity (90). Nonetheless, our data conclusively establish that MMP-2/9 and ERK are critical regulators of eHsp90's coordinate effects upon junctional integrity and cell motility.

Hsp90 has been detected from patient serum and ascites fluid in a number of cancer types (37,41,91,92), yet the source of this protein remains unclear. In support of a regulated secretory pathway, surface eHsp90 is detected from patients with metastatic melanoma tumors (93). Our discovery that Hsp90α is found on the surface of a subpopulation of primary tumor cells further reinforces a regulated pathway for Hsp90 secretion. A striking finding is the increased expression of MMP-2 and MMP-9 transcripts associated with the eHsp90^{high} population of tumor cells, which supports trends from our cell based models. Although it is possible that non-tumorigenic and/or stromal cells may be present in these preparations, this does not change the interpretation of our results that eHsp90 appears to mark a distinct (presumably tumor) population of cells exhibiting transcripts associated with protumorigenic properties. Our finding that a relatively small subpopulation of eHsp90 expressing tumor cells may contribute to PCa progression also highlights the challenges in identifying a unifying genetic signature indicative of EMT events clinical samples.

Despite its EMT inducing activity, eHsp90 was unable to enforce a permanent EMT, demonstrated by the ability of NPGA to reverse EMT like events in ARCaPE-eHsp90. Within this context, it was remarkable that continued eHsp90 expression was also required to sustain the aggressive properties of metastatic PCa cell types, including cell motility, expression of N-cadherin, and mesenchymal morphology. This constitutive reliance upon eHsp90 may be widespread, supported by the reported ability of eHsp90 targeting to suppress the metastatic potential of breast and other tumor types (35-38). Although the eHsp90 mediated induction of MMP-2/9 has been implicated in several of these models, (35,37), the precise eHsp90 directed molecular events driving metastatic potential remain unresolved. A recent report has also implicated a role for N-cadherin in the invasion and metastasis of PCa (94). In light of these reports, the ability of eHsp90 targeting to attenuate a subset of EMT events may have clinical utility in blocking or delaying cancer progression. Although more mechanistic details need to be elucidated, our data conclusively position eHsp90 as a novel and pivotal effector of tumor cell EMT plasticity.

REFERENCES

1. Arya, M., Bott, S. R., Shergill, I. S., Ahmed, H. U., Williamson, M., and Patel, H. R. (2006) *Surg Oncol* **15**, 117-128
2. Crawford, E. D. (2009) *Urology* **73**, S4-10
3. Jemal, A., Siegel, R., Ward, E., Hao, Y., Xu, J., and Thun, M. J. (2009) *CA Cancer J Clin* **59**, 225-249
4. Efstathiou, E., and Logothetis, C. J. (2010) *Clin Cancer Res* **16**, 1100-1107
5. Siegel, R., Naishadham, D., and Jemal, A. (2012) *CA Cancer J Clin* **62**, 10-29
6. Culp, S., and Porter, M. (2009) *BJU Int* **104**, 1457-1461
7. Strope, S. A., and Andriole, G. L. (2010) *Nat Rev Urol* **7**, 487-493
8. Andriole, G. L. (2009) *Nat Rev Urol* **6**, 188-189
9. Markert, E. K., Mizuno, H., Vazquez, A., and Levine, A. J. (2011) *Proc Natl Acad Sci U S A* **108**, 21276-21281
10. Polyak, K., and Weinberg, R. A. (2009) *Nat Rev Cancer* **9**, 265-273
11. Thiery, J. P., Acloque, H., Huang, R. Y., and Nieto, M. A. (2009) *Cell* **139**, 871-890
12. Hanahan, D., and Weinberg, R. A. (2011) *Cell* **144**, 646-674
13. Onder, T. T., Gupta, P. B., Mani, S. A., Yang, J., Lander, E. S., and Weinberg, R. A. (2008) *Cancer Res* **68**, 3645-3654
14. Zhau, H. E., Li, C. L., and Chung, L. W. (2000) *Cancer* **88**, 2995-3001
15. Xu, J., Wang, R., Xie, Z. H., Odero-Marah, V., Pathak, S., Multani, A., Chung, L. W., and Zhau, H. E. (2006) *Prostate* **66**, 1664-1673
16. Acevedo, V. D., Gangula, R. D., Freeman, K. W., Li, R., Zhang, Y., Wang, F., Ayala, G. E., Peterson, L. E., Ittmann, M., and Spencer, D. M. (2007) *Cancer Cell* **12**, 559-571
17. Zhang, X., Fournier, M. V., Ware, J. L., Bissell, M. J., Yacoub, A., and Zehner, Z. E. (2009) *Mol Cancer Ther* **8**, 499-508
18. Mak, P., Leav, I., Pursell, B., Bae, D., Yang, X., Taglienti, C. A., Gouvin, L. M., Sharma, V. M., and Mercurio, A. M. (2010) *Cancer Cell* **17**, 319-332
19. Lue, H. W., Yang, X., Wang, R., Qian, W., Xu, R. Z., Lyles, R., Osunkoya, A. O., Zhou, B. P., Vessella, R. L., Zayzafoon, M., Liu, Z. R., Zhau, H. E., and Chung, L. W. (2011) *PLoS One* **6**, e27720
20. Xie, D., Gore, C., Liu, J., Pong, R. C., Mason, R., Hao, G., Long, M., Kabbani, W., Yu, L., Zhang, H., Chen, H., Sun, X., Boothman, D. A., Min, W., and Hsieh, J. T. (2010) *Proc Natl Acad Sci U S A* **107**, 2485-2490
21. Kwok, W. K., Ling, M. T., Lee, T. W., Lau, T. C., Zhou, C., Zhang, X., Chua, C. W., Chan, K. W., Chan, F. L., Glackin, C., Wong, Y. C., and Wang, X. (2005) *Cancer Res* **65**, 5153-5162
22. Graham, T. R., Zhau, H. E., Odero-Marah, V. A., Osunkoya, A. O., Kimbro, K. S., Tighiouart, M., Liu, T., Simons, J. W., and O'Regan, R. M. (2008) *Cancer Res* **68**, 2479-2488
23. Contreras, H. R., Ledezma, R. A., Vergara, J., Cifuentes, F., Barra, C., Cabello, P., Gallegos, I., Morales, B., Huidobro, C., and Castellon, E. A. (2010) *Urol Oncol* **28**, 534-540
24. Zhang, Q., Helfand, B. T., Jang, T. L., Zhu, L. J., Chen, L., Yang, X. J., Kozlowski, J., Smith, N., Kundu, S. D., Yang, G., Raji, A. A., Javonovic, B., Pins, M., Lindholm, P., Guo, Y., Catalona, W. J., and Lee, C. (2009) *Clin Cancer Res* **15**, 3557-3567
25. Sun, Y., Wang, B. E., Leong, K. G., Yue, P., Li, L., Jhunjhunwala, S., Chen, D., Seo, K., Modrusan, Z., Gao, W. Q., Settleman, J., and Johnson, L. (2012) *Cancer Res* **72**, 527-536
26. Isaacs, J. S., Xu, W., and Neckers, L. (2003) *Cancer Cell* **3**, 213-217
27. Whitesell, L., and Lindquist, S. L. (2005) *Nat Rev Cancer* **5**, 761-772

28. Bohonowych, J. E., Gopal, U., and Isaacs, J. S. (2010) *J Oncol* **2010**, 412985
29. Cheng, C. F., Fan, J., Fedesco, M., Guan, S., Li, Y., Bandyopadhyay, B., Bright, A. M., Yerushalmi, D., Liang, M., Chen, M., Han, Y. P., Woodley, D. T., and Li, W. (2008) *Molecular and cellular biology* **28**, 3344-3358
30. Gopal, U., Bohonowych, J. E., Lema-Tome, C., Liu, A., Garrett-Mayer, E., Wang, B., and Isaacs, J. S. (2011) *PLoS One* **6**, e17649
31. Becker, B., Multhoff, G., Farkas, B., Wild, P. J., Landthaler, M., Stolz, W., and Vogt, T. (2004) *Exp Dermatol* **13**, 27-32
32. Eustace, B. K., Sakurai, T., Stewart, J. K., Yimlamai, D., Unger, C., Zehetmeier, C., Lain, B., Torella, C., Henning, S. W., Beste, G., Scroggins, B. T., Neckers, L., Ilag, L. L., and Jay, D. G. (2004) *Nat Cell Biol* **6**, 507-514
33. Sidera, K., Gaitanou, M., Stellas, D., Matsas, R., and Patsavoudi, E. (2008) *J Biol Chem* **283**, 2031-2041
34. Yang, Y., Rao, R., Shen, J., Tang, Y., Fiskus, W., Nechtman, J., Atadja, P., and Bhalla, K. (2008) *Cancer Res* **68**, 4833-4842
35. Stellas, D., El Hamidieh, A., and Patsavoudi, E. (2010) *BMC Cell Biol* **11**, 51
36. Tsutsumi, S., Scroggins, B., Koga, F., Lee, M. J., Trepel, J., Felts, S., Carreras, C., and Neckers, L. (2008) *Oncogene* **27**, 2478-2487
37. Wang, X., Song, X., Zhuo, W., Fu, Y., Shi, H., Liang, Y., Tong, M., Chang, G., and Luo, Y. (2009) *Proc Natl Acad Sci U S A* **106**, 21288-21293
38. Sahu, D., Zhao, Z., Tsen, F., Cheng, C. F., Park, R., Situ, A. J., Dai, J., Eginli, A., Shams, S., Chen, M., Ulmer, T. S., Conti, P., Woodley, D. T., and Li, W. (2012) *Mol Biol Cell* **23**, 602-613
39. Ullrich, S. J., Robinson, E. A., Law, L. W., Willingham, M., and Appella, E. (1986) *Proc Natl Acad Sci U S A* **83**, 3121-3125
40. Luo, L. Y., Herrera, I., Soosaipillai, A., and Diamandis, E. P. (2002) *Br J Cancer* **87**, 339-343
41. Burgess, E. F., Ham, A. J., Tabb, D. L., Billheimer, D., Roth, B. J., Chang, S. S., Cookson, M. S., Hinton, T. J., Cheek, K. L., Hill, S., and Pietenpol, J. A. (2008) *Proteomics Clin Appl* **2**, 1223-1233
42. Garraway, I. P., Sun, W., Tran, C. P., Perner, S., Zhang, B., Goldstein, A. S., Hahm, S. A., Haider, M., Head, C. S., Reiter, R. E., Rubin, M. A., and Witte, O. N. (2010) *Prostate* **70**, 491-501
43. Stellas, D., El Hamidieh, A., and Patsavoudi, E. (2010) *BMC Cell Biol* **11**, 51
44. Qin, Z., DeFee, M., Isaacs, J. S., and Parsons, C. (2010) *Virology* **403**, 92-102
45. Orr, A. W., Pedraza, C. E., Pallero, M. A., Elzie, C. A., Goicoechea, S., Strickland, D. K., and Murphy-Ullrich, J. E. (2003) *J Cell Biol* **161**, 1179-1189
46. Shi, Y., Mantuano, E., Inoue, G., Campana, W. M., and Gonias, S. L. (2009) *Sci Signal* **2**, ra18
47. Langlois, B., Perrot, G., Schneider, C., Henriet, P., Emonard, H., Martiny, L., and Dedieu, S. (2010) *PLoS One* **5**, e11584
48. Polyak, K., and Weinberg, R. A. (2009) *Nat Rev Cancer* **9**, 265-273
49. Zhau, H. Y., Chang, S. M., Chen, B. Q., Wang, Y., Zhang, H., Kao, C., Sang, Q. A., Pathak, S. J., and Chung, L. W. (1996) *Proc Natl Acad Sci U S A* **93**, 15152-15157
50. He, H., Yang, X., Davidson, A. J., Wu, D., Marshall, F. F., Chung, L. W., Zhau, H. E., and Wang, R. (2010) *Prostate* **70**, 518-528
51. Zhau, H. E., Odero-Marah, V., Lue, H. W., Nomura, T., Wang, R., Chu, G., Liu, Z. R., Zhou, B. P., Huang, W. C., and Chung, L. W. (2008) *Clin Exp Metastasis* **25**, 601-610
52. Josson, S., Nomura, T., Lin, J. T., Huang, W. C., Wu, D., Zhau, H. E., Zayzafoon, M., Weizmann, M. N., Gururajan, M., and Chung, L. W. (2011) *Cancer Res* **71**, 2600-2610

53. Bae, V. L., Jackson-Cook, C. K., Maygarden, S. J., Plymate, S. R., Chen, J., and Ware, J. L. (1998) *Prostate* **34**, 275-282
54. Rojas, A., Liu, G., Coleman, I., Nelson, P. S., Zhang, M., Dash, R., Fisher, P. B., Plymate, S. R., and Wu, J. D. (2011) *Oncogene* **30**, 2345-2355
55. Fu, X., Herrera, H., and Hoffman, R. M. (1992) *Int J Cancer* **52**, 987-990
56. Stephenson, R. A., Dinney, C. P., Gohji, K., Ordonez, N. G., Killion, J. J., and Fidler, I. J. (1992) *J Natl Cancer Inst* **84**, 951-957
57. Thalmann, G. N., Anezinis, P. E., Chang, S. M., Zhau, H. E., Kim, E. E., Hopwood, V. L., Pathak, S., von Eschenbach, A. C., and Chung, L. W. (1994) *Cancer Res* **54**, 2577-2581
58. Smolen, G. A., Zhang, J., Zubrowski, M. J., Edelman, E. J., Luo, B., Yu, M., Ng, L. W., Scherber, C. M., Schott, B. J., Ramaswamy, S., Irimia, D., Root, D. E., and Haber, D. A. (2010) *Genes Dev* **24**, 2654-2665
59. Janda, C. Y., Li, J., Oubridge, C., Hernandez, H., Robinson, C. V., and Nagai, K. (2010) *Nature* **465**, 507-510
60. Figueiredo, C., Wittmann, M., Wang, D., Dressel, R., Seltsam, A., Blasczyk, R., and Eiz-Vesper, B. (2009) *Blood* **113**, 3008-3016
61. Thiery, J. P. (2003) *Curr Opin Cell Biol* **15**, 740-746
62. Polette, M., Gilles, C., Nawrocki-Raby, B., Lohi, J., Hunziker, W., Foidart, J. M., and Birembaut, P. (2005) *Cancer Res* **65**, 7691-7698
63. Chambers, A. F., and Matrisian, L. M. (1997) *J Natl Cancer Inst* **89**, 1260-1270
64. Nistico, P., Bissell, M. J., and Radisky, D. C. (2012) *Cold Spring Harb Perspect Biol* **4**
65. Radisky, D. C., Levy, D. D., Littlepage, L. E., Liu, H., Nelson, C. M., Fata, J. E., Leake, D., Godden, E. L., Albertson, D. G., Nieto, M. A., Werb, Z., and Bissell, M. J. (2005) *Nature* **436**, 123-127
66. Eustace, B. K., Sakurai, T., Stewart, J. K., Yimlamai, D., Unger, C., Zehetmeier, C., Lain, B., Torella, C., Henning, S. W., Beste, G., Scroggins, B. T., Neckers, L., Ilag, L. L., and Jay, D. G. (2004) *Nat Cell Biol* **6**, 507-514
67. Lagarrigue, F., Dupuis-Coronas, S., Ramel, D., Delsol, G., Tronchere, H., Payrastre, B., and Gaits-Iacovoni, F. (2010) *Cancer Res* **70**, 6978-6987
68. Song, X., Wang, X., Zhuo, W., Shi, H., Feng, D., Sun, Y., Liang, Y., Fu, Y., Zhou, D., and Luo, Y. (2010) *J Biol Chem* **285**, 40039-40049
69. Ito, H., Duxbury, M., Benoit, E., Clancy, T. E., Zinner, M. J., Ashley, S. W., and Whang, E. E. (2004) *Cancer Res* **64**, 7439-7446
70. Yoshida, T., Hisamoto, T., Akiba, J., Koga, H., Nakamura, K., Tokunaga, Y., Hanada, S., Kumemura, H., Maeyama, M., Harada, M., Ogata, H., Yano, H., Kojiro, M., Ueno, T., Yoshimura, A., and Sata, M. (2006) *Oncogene* **25**, 6056-6066
71. Hinck, L., Nathke, I. S., Papkoff, J., and Nelson, W. J. (1994) *J Cell Biol* **125**, 1327-1340
72. Liwosz, A., Lei, T., and Kukuruzinska, M. A. (2006) *J Biol Chem* **281**, 23138-23149
73. McCready, J., Sims, J. D., Chan, D., and Jay, D. G. (2010) *BMC Cancer* **10**, 294
74. Batlle, E., Sancho, E., Franci, C., Dominguez, D., Monfar, M., Baulida, J., and Garcia De Herreros, A. (2000) *Nat Cell Biol* **2**, 84-89
75. Cano, A., Perez-Moreno, M. A., Rodrigo, I., Locascio, A., Blanco, M. J., del Barrio, M. G., Portillo, F., and Nieto, M. A. (2000) *Nat Cell Biol* **2**, 76-83
76. Grooteclaes, M. L., and Frisch, S. M. (2000) *Oncogene* **19**, 3823-3828
77. Yang, J., Mani, S. A., Donaher, J. L., Ramaswamy, S., Itzykson, R. A., Come, C., Savagner, P., Gitelman, I., Richardson, A., and Weinberg, R. A. (2004) *Cell* **117**, 927-939
78. Johnson, T. R., Koul, S., Kumar, B., Khandrika, L., Venezia, S., Maroni, P. D., Meacham, R. B., and Koul, H. K. (2010) *Mol Cancer* **9**, 148
79. Jorda, M., Olmeda, D., Vinyals, A., Valero, E., Cubillo, E., Llorens, A., Cano, A., and Fabra, A. (2005) *J Cell Sci* **118**, 3371-3385

80. Sun, L., Diamond, M. E., Ottaviano, A. J., Joseph, M. J., Ananthanarayan, V., and Munshi, H. G. (2008) *Mol Cancer Res* **6**, 10-20
81. Zhao, X. L., Sun, T., Che, N., Sun, D., Zhao, N., Dong, X. Y., Gu, Q., Yao, Z., and Sun, B. C. (2011) *J Cell Mol Med* **15**, 691-700
82. Sims, J. D., McCready, J., and Jay, D. G. (2011) *PLoS One* **6**, e18848
83. Ellenrieder, V., Hendler, S. F., Boeck, W., Seufferlein, T., Menke, A., Ruhland, C., Adler, G., and Gress, T. M. (2001) *Cancer Res* **61**, 4222-4228
84. Vial, E., Sahai, E., and Marshall, C. J. (2003) *Cancer Cell* **4**, 67-79
85. Doehn, U., Hauge, C., Frank, S. R., Jensen, C. J., Duda, K., Nielsen, J. V., Cohen, M. S., Johansen, J. V., Winther, B. R., Lund, L. R., Winther, O., Taunton, J., Hansen, S. H., and Frodin, M. (2009) *Mol Cell* **35**, 511-522
86. Shin, S., Dimitri, C. A., Yoon, S. O., Dowdle, W., and Blenis, J. (2010) *Mol Cell* **38**, 114-127
87. Johnson, J. L., Dwivedi, A., Somerville, M., George, S. J., and Newby, A. C. (2011) *Arterioscler Thromb Vasc Biol* **31**, e35-44
88. Rajasekaran, A. K., and David, J. M. (2012) *Cancer Res* **72**, 2917-2923
89. Hahn-Dantona, E., Ruiz, J. F., Bornstein, P., and Strickland, D. K. (2001) *J Biol Chem* **276**, 15498-15503
90. Mantuano, E., Inoue, G., Li, X., Takahashi, K., Gaultier, A., Gonias, S. L., and Campana, W. M. (2008) *J Neurosci* **28**, 11571-11582
91. Luo, L. Y., Herrera, I., Soosaipillai, A., and Diamandis, E. P. (2002) *Br J Cancer* **87**, 339-343
92. Vidal, C. I., Mintz, P. J., Lu, K., Ellis, L. M., Manenti, L., Giavazzi, R., Gershenson, D. M., Broaddus, R., Liu, J., Arap, W., and Pasqualini, R. (2004) *Oncogene* **23**, 8859-8867
93. Becker, B., Multhoff, G., Farkas, B., Wild, P. J., Landthaler, M., Stolz, W., and Vogt, T. (2004) *Exp Dermatol* **13**, 27-32
94. Tanaka, H., Kono, E., Tran, C. P., Miyazaki, H., Yamashiro, J., Shimomura, T., Fazli, L., Wada, R., Huang, J., Vessella, R. L., An, J., Horvath, S., Gleave, M., Rettig, M. B., Wainberg, Z. A., and Reiter, R. E. (2010) *Nat Med* **16**, 1414-1420

ACKNOWLEDGEMENTS

We thank Joy Ware for the P69 and M12 cells, Chris Lindsey and Craig Beeson for synthesis of DMAG-N-oxide (NPGA), and Enzo Life Sciences for their generous reagent support. Imaging facilities for this research were supported, in part, by Cancer Center Support Grant P30 CA138313 to the Hollings Cancer Center, Medical University of South Carolina. We also thank Philip Howe and Simon Hayward for their critical comments on this manuscript.

FOOTNOTES

This work was primarily supported by NIH grant R01 CA135297 (to J. S. I.). Additional funding sources include NIH T32 training grant CA119945 (to M.W.H.) and
IRACDA training grant K12 GM081265 (to J. E. B.)
[§]These authors contributed equally

[*]To whom correspondence should be addressed:
Department of Cell and Molecular Pharmacology
Medical University of South Carolina
Hollings Cancer Center
86 Jonathan Lucas St
Charleston, SC, 29425
Tel: 843-792-8393
Fax: 843-792-3200
email:isaacsj@musc.edu

Abbreviations: eHsp90, extracellular Hsp90; ERK, extracellular signal-regulated kinase; PCa, prostate cancer; MMP, matrix metalloprotease, NPGA, nonpermeable GA; EMT, epithelial to mesenchymal transition; PSA, prostate specific antigen; MEK, MAPK kinase; FAK, focal adhesion kinase; LRP1, low density lipoprotein related protein; shRNA, short hairpin RNA; fluorescence-activated cell sorting, FACS

FIGURE LEGENDS

FIGURE 1. An eHsp90-LRP1 signaling pathway initiates prostate cancer cell motility. *A*, Representative results from a scratch wound assay with PC3 prostate cancer cells following treatment with NPGA (1 uM) or either of two eHsp90 targeting antibodies (SPA-830, Ab1; SPS-771, Ab2). *B*, Similar assay with DU145 cells transduced with either scrambled (scr) shRNA or shLRP1. *C*, Pharmacologic targeting of eHsp90 with NPGA (1 uM, 16 hr) and effects upon FAK and ERK activity. *D*, Comparison of shLRP1 and NPGA upon FAK and ERK activity. UT refers to untreated vehicle control. Asterisks (*) indicate significance of $p \leq 0.05$.

FIGURE 2. eHsp90 is elevated in more aggressive PCa cell types and is essential for cell motility. *A*, Detection of secreted eHsp90 alpha from the conditioned media of indicated cell pairs was assessed by ELISA. Each cell pair is lineage related, with the more metastatic derivative in black. *B*, Scratch wound assay assessed the effects of either exogenous eHsp90 protein (3 day pre-treatment, 3 ug/ml) upon ARCaPE cell motility, or treatment of ARCaPM cells with NPGA. *C*, Similar treatment of epithelial P69 cells with eHsp90, and NPGA treatment of the metastatic counterpart M12. *D*, Effect of shLRP1 upon eHsp90 mediated cell motility in ARCaPE. UT refers to untreated vehicle control. Asterisks (*) indicate significance of p-value ≤ 0.05.

FIGURE 3. eHsp90 induces molecular and morphological changes consistent with an epithelial to mesenchymal transition. *A*, ARCaPE cells treated for the indicated times with exogenous Hsp90 protein, and immunoblot analysis of epithelial E-cadherin (E-cad) and mesenchymal proteins N-cadherin (N-Cad) and Twist. Phase contrast images of cell morphology. *B*, Effects of NPGA treatment of ARCaPM upon E- and N-cadherin expression and corresponding cell morphology. *C*, Analysis of eHsp90 treatment of P69 non-tumorigenic cells as in A. *D*, Analysis of NPGA treatment of M12 as in B.

FIGURE 4. Modest elevation of eHsp90 is sufficient to suppress E-cadherin function and promote cell motility. *A*, (Upper panel) ELISA analysis of eHsp90 secretion from conditioned media collected from parental ARCaPE cells stably transduced with control (lacZ) or V5 tagged eHsp90 alpha lentivirus. (Lower panel) Immunoblot detection of total (endogenous and exogenous) eHsp90 alpha, or V5 detection of transduced eHsp90 protein. *B*, Immunoblot analysis of cell lysates from ARCaPE-LacZ or ARCaPE-eHsp90 confirmed consistent levels of intracellular eHsp90 alpha (IC Hsp90). Indicated analysis of E- and N- cadherin and ERK activity. *C*, Representative morphology of indicated ARCaPE cells. Analysis of cell motility of ARCaPE-eHsp90 either untreated or treated with NPGA. *D*, Effect of NPGA upon E-cadherin expression in ARCaPE-eHsp90. *E*, Analysis of E-cadherin localization in ARCaPE-LacZ and ARCaPE-eHsp90 untreated cells, or treated for the indicated times with NPGA. *F*, Membrane localization of ZO1 in ARCaPE-LacZ and ARCaPE-eHsp90 untreated cells, or treated with NPGA for 3 days. Asterisks (*) indicate significance of p-value ≤ 0.05. Scale bar is 50 um.

FIGURE 5. eHsp90 modulates the expression of multiple genes associated with EMT activation. *A*, A focused EMT qRT-PCR array was utilized to assess EMT regulated genes modulated by eHsp90 in ARCaPE cells. Samples for array data were derived from two identical biological replicate experiments. *B*, Transcript expression of E-cadherin and the indicated EMT transcriptional effectors from the array were validated by qRT-PCR in untreated (UT) ARCaPE or cells treated with eHsp90 protein for 1, 3, or 5 days (upper panel), whereas a similar analysis was performed for control or ARCaPE-eHsp90 genetically modified cells (lower panel). *C*, Increased expression of proteolytic MMP transcripts was also validated from both protein treated (upper panel) and ARCaPE-eHsp90 modified cells (lower panel). Quantitative PCR

levels were normalized to GAPDH expression. UT refers to untreated vehicle control. Asterisks (*) indicate significance of p-value $\leq$ 0.05.

FIGURE 6. MMP and ERK activity are required for eHsp90 mediated motility and EMT events . *A*, A gelatin zymography assay was utilized to assay MMP-2/9 activity in control or ARCaPE-Hsp90 cells. For indicated inhibitors, cells were treated for 2 days prior to media collection. Cells were treated with ERK inhibitor (UO126, 10 uM), MMP-2/9 inhibitor (SB-3CT, 1 uM), or NPGA (1 uM). B, Transcript expression of E-cadherin was evaluated in ARCaPE-eHsp90 following a 3 day treatment with the following: NPGA (1 uM), pan-MMP inhibitor (GM6001, 1 uM), MMP-2/9 inhibitor (SB-3CT, 1 uM), MMP-3 inhibitor (inhibitor IV, 5 uM) or ERK inhibitor (UO126, 10 uM). *C*, Immunoblot analysis of E-cadherin and ERK proteins in ARCaPE-eHsp90 following the time dependent inhibition of the following: MMP-2/9, MMP-3, or ERK. *D*, The effect of 3 days of MMP and ERK inhibition upon E-cadherin and ZO-1 localization in ARCaPE-LacZ and ARCaPE-eHsp90 was assessed by confocal microscopy. Cells were treated as in *A*, with inclusion of the pan-MMP inhibitor (GM6001, 1 uM) and the MMP-3 inhibitor (inhibitor IV, 5 uM). *E*, Evaluation of MMP and ERK in directing eHsp90 cell motility following a scratch wound assay. Scale bar is 50 um. UT refers to untreated vehicle control. Asterisks (*) indicate significance p-value $\leq$ 0.05.

FIGURE 7. Detection of eHsp90 protein and regulated transcripts in human prostatectomy tumor specimens. *A,* Prostate tissue from 2 patients was FACS sorted for $eHsp90^{low}$ and $eHsp90^{high}$ populations using a PE-conjugated antibody specific for Hsp90 alpha. In each instance, the subpopulation of $eHsp90^{high}$ cells represented approximately 5% of the cell population. Patient 1 was identified as Gleason 3+4 (stage T3aNO), while Patient 2 was Gleason 4+5 (stage T3bNO). *B*, RNA was harvested from these subpopulations and transcripts for MMP-2, MMP-3 and MMP-9 were evaluated via qRT-PCR. *C*, Proposed mechanism for eHsp90 mediated regulation of cell motility and EMT events. Tumor secreted eHsp90 functions in an autocrine manner via its receptor LRP1 to transduce ERK phosphorylation. eHsp90-LRP1-ERK signaling subsequently initiates transcription of several pro-EMT transcription factors (Snail/Zeb/Twist), as well as MMPs. MMP activation serves to reinforce sustained ERK activation and E-cadherin suppression through several potential mechanisms (dotted arrows, see text for details). These concurrent processes deregulate junctional complexes (E-cadherin and ZO-1), resulting in a loss of cell polarity, increased migratory potential, and initiation of a subset of EMT events.

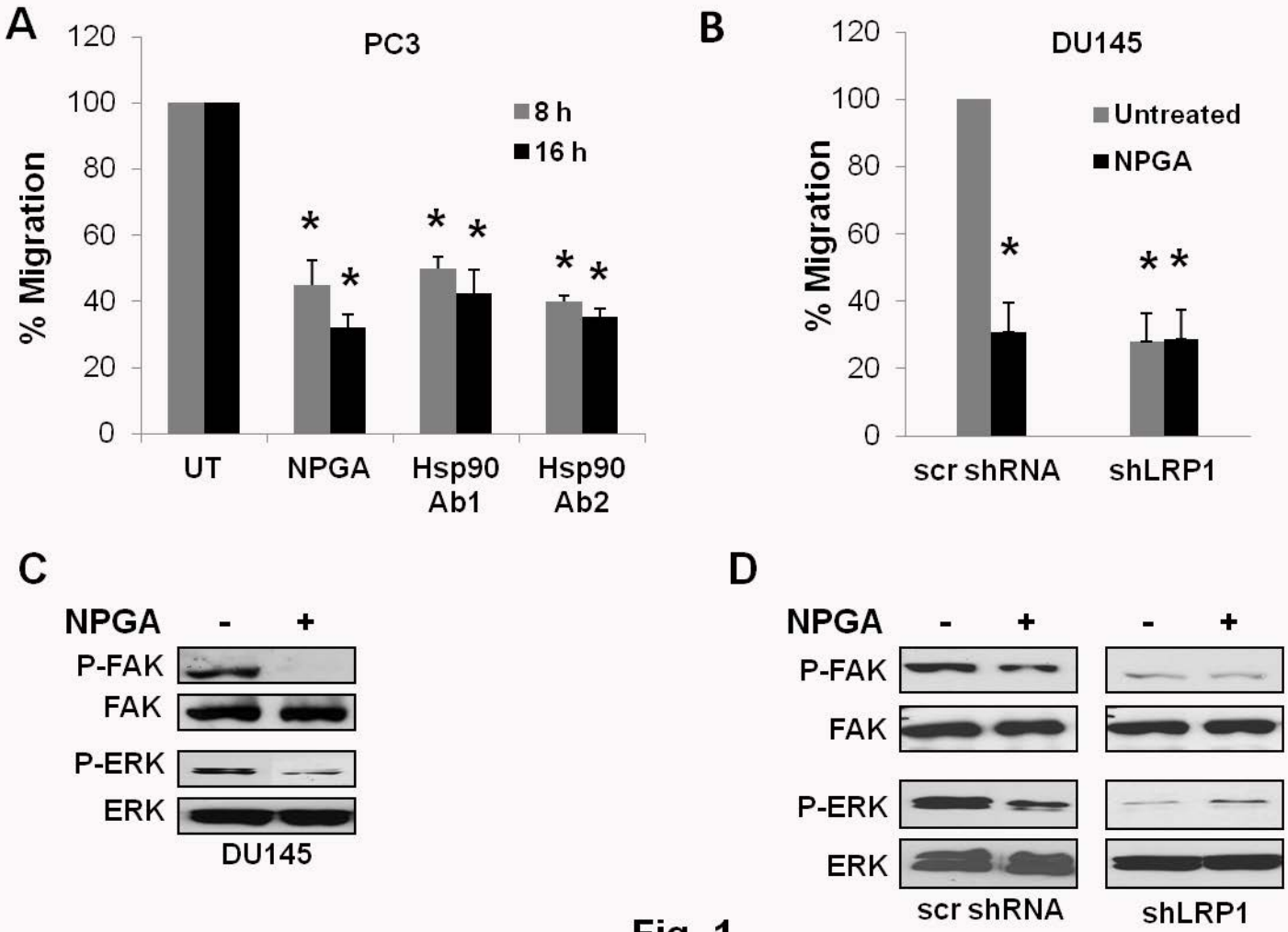

Fig. 1

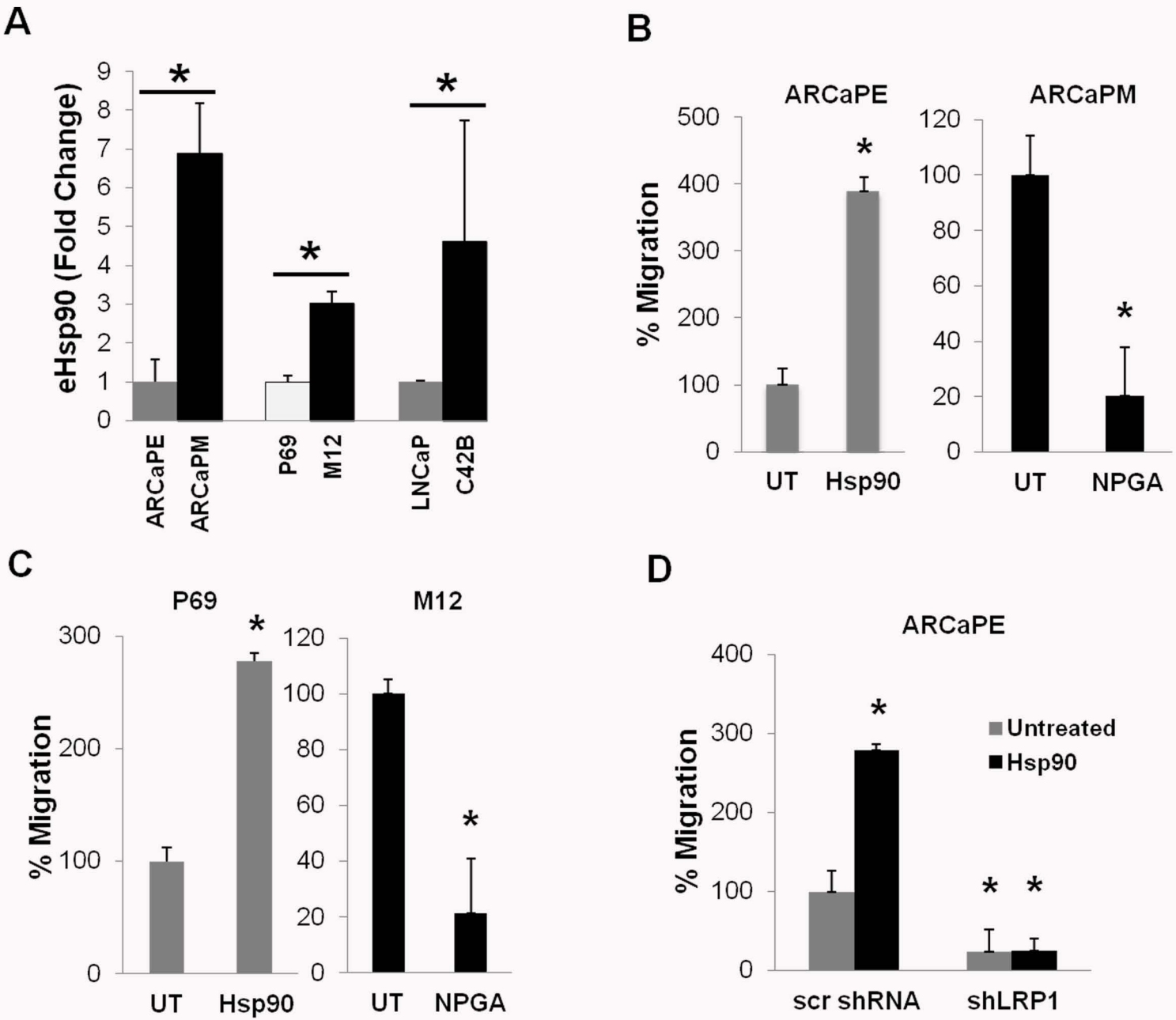

Fig. 2

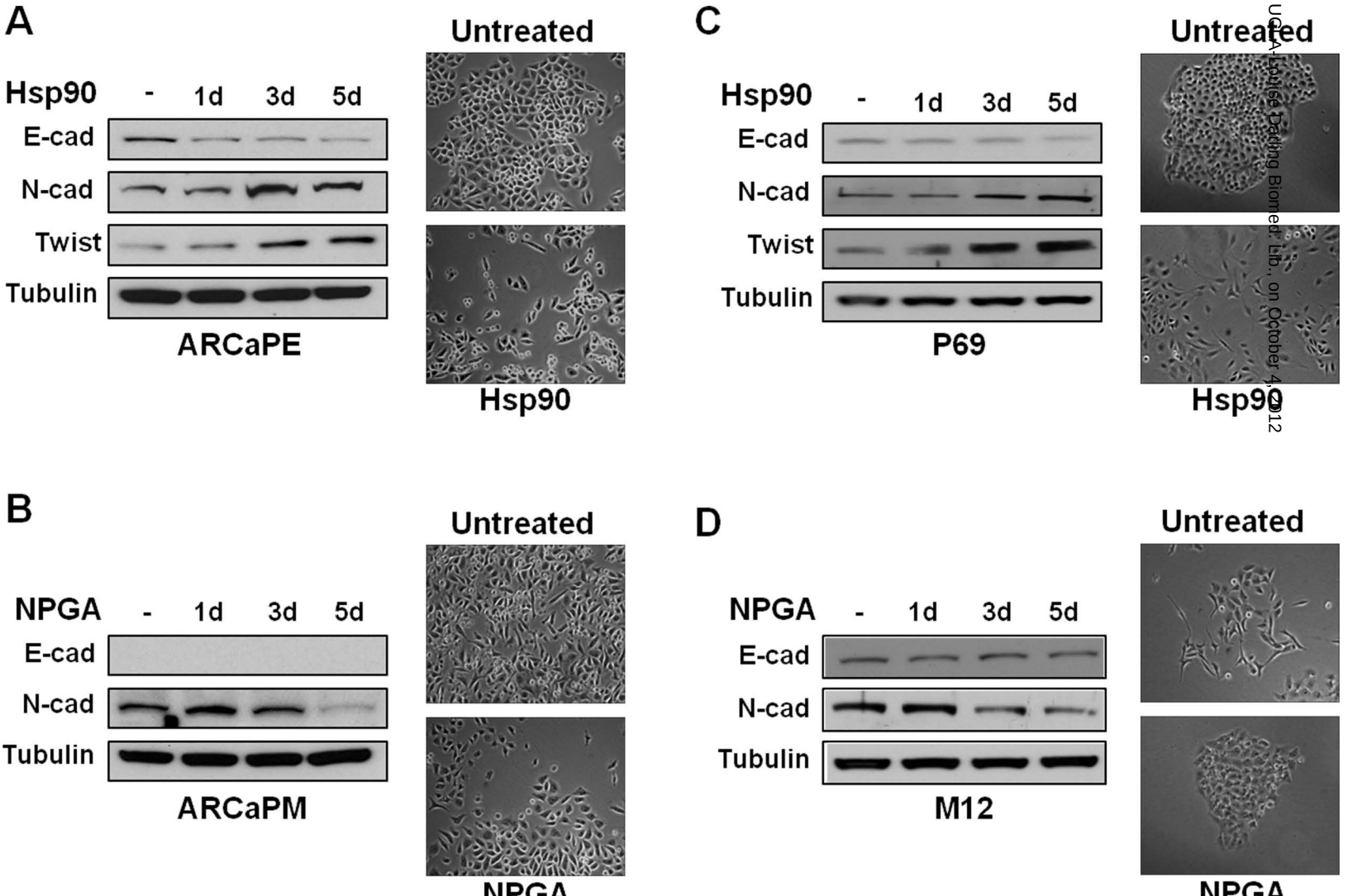

Fig. 3

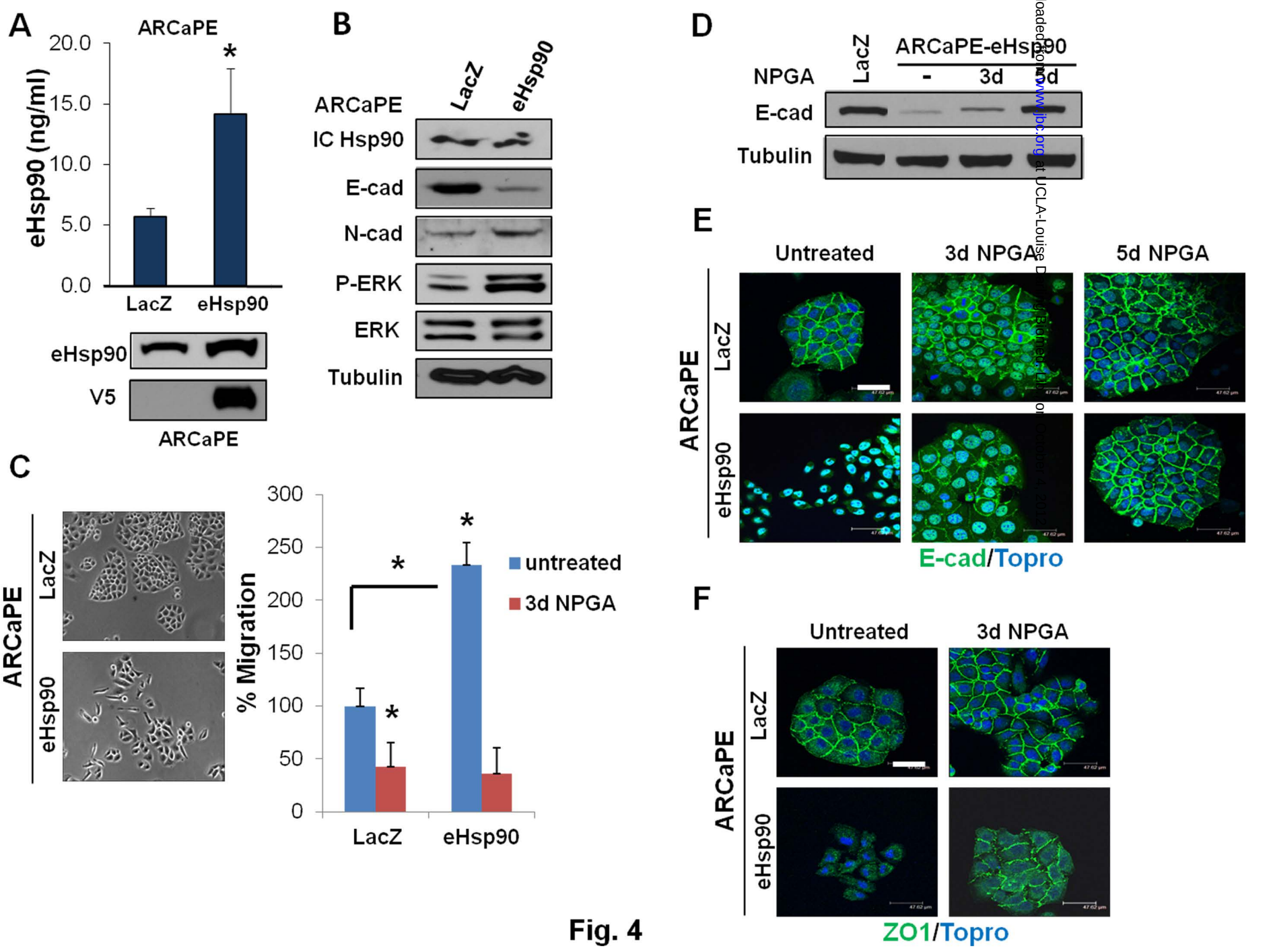

Fig. 4

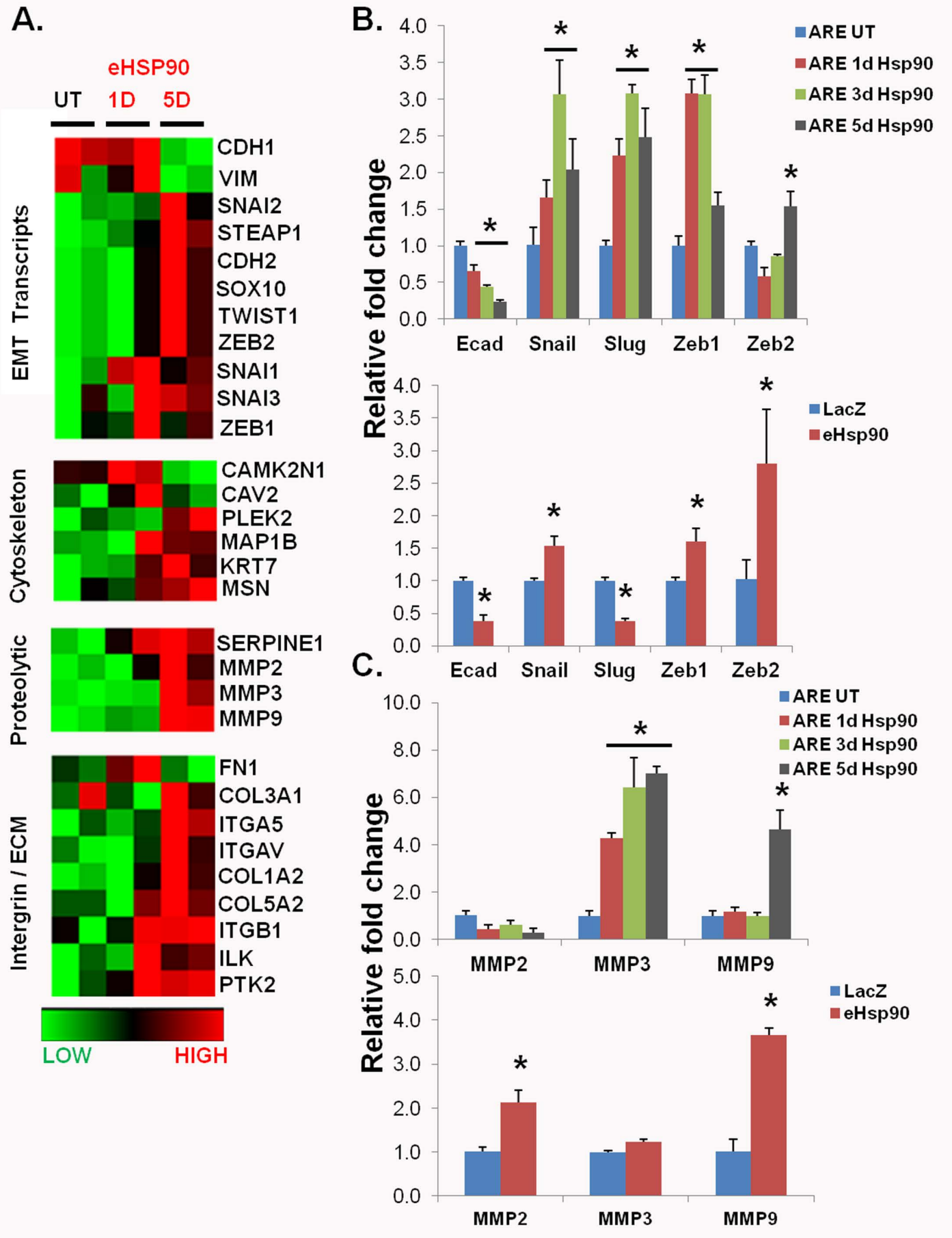
A.
eHSP90
UT
1D
5D
EMT Transcripts
CDH1
VIM
SNAI2
STEAP1
CDH2
SOX10
TWIST1
ZEB2
SNAI1
SNAI3
ZEB1
Cytoskeleton
CAMK2N1
CAV2
PLEK2
MAP1B
KRT7
MSN
Proteolytic
SERPINE1
MMP2
MMP3
MMP9
Intergrin / ECM
FN1
COL3A1
ITGA5
ITGAV
COL1A2
COL5A2
ITGB1
ILK
PTK2
LOW
HIGH
B.
Relative fold change
ARE UT
ARE 1d Hsp90
ARE 3d Hsp90
ARE 5d Hsp90
Ecad
Snail
Slug
Zeb1
Zeb2
LacZ
eHsp90
C.
MMP2
MMP3
MMP9

Fig. 5

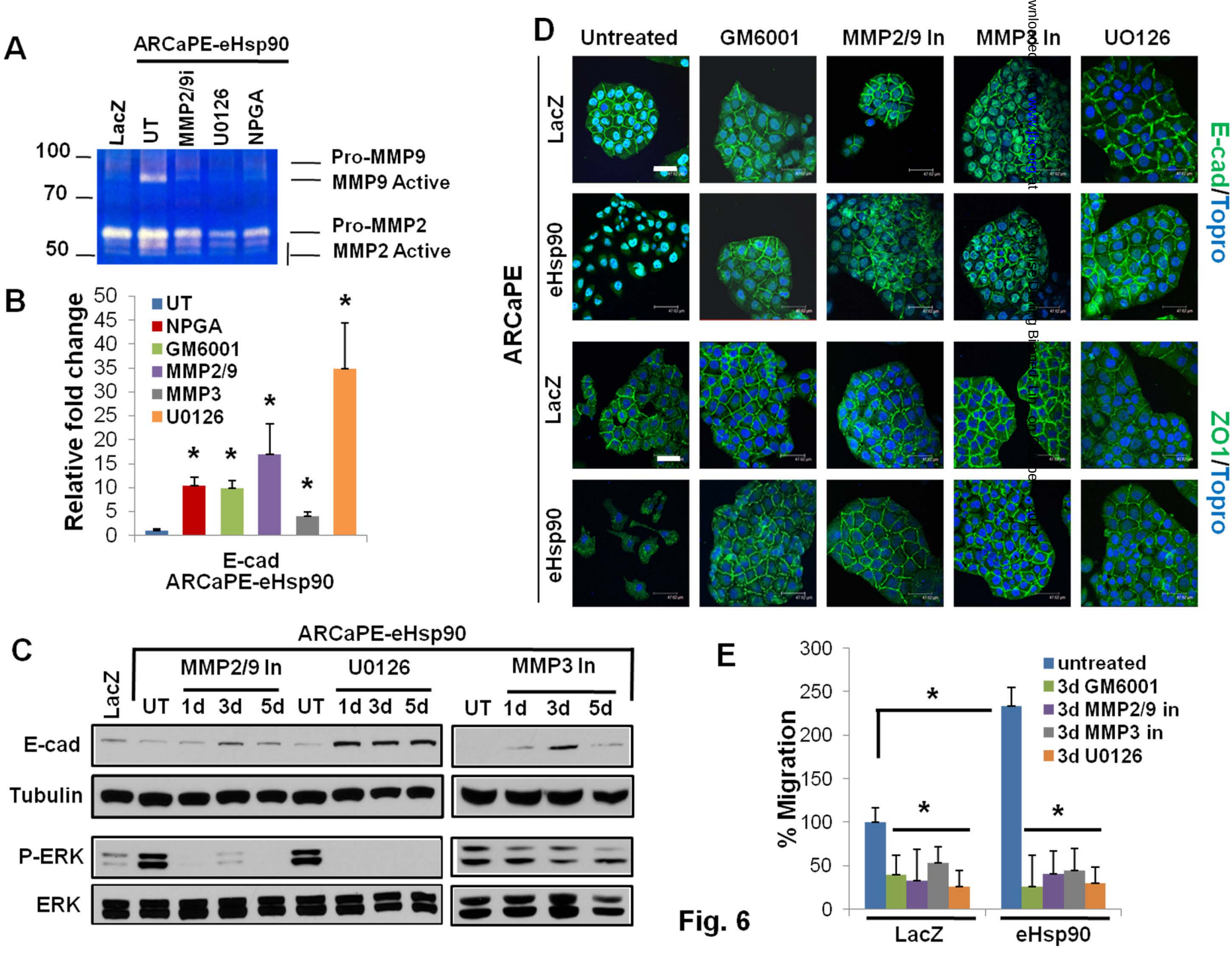
A
ARCaPE-eHsp90
LacZ
UT
MMP2/9i
U0126
NPGA
100
70
50
Pro-MMP9
MMP9 Active
Pro-MMP2
MMP2 Active
B
Relative fold change
UT
NPGA
GM6001
MMP2/9
MMP3
U0126
E-cad
ARCaPE-eHsp90
C
ARCaPE-eHsp90
LacZ
MMP2/9 In
U0126
MMP3 In
UT 1d 3d 5d UT 1d 3d 5d UT 1d 3d 5d
E-cad
Tubulin
P-ERK
ERK
D
Untreated
GM6001
MMP2/9 In
MMP3 In
U0126
ARCaPE
LacZ
eHsp90
LacZ
eHsp90
E-cad/Topro
ZO1/Topro
E
% Migration
untreated
3d GM6001
3d MMP2/9 in
3d MMP3 in
3d U0126
LacZ
eHsp90

Fig. 6

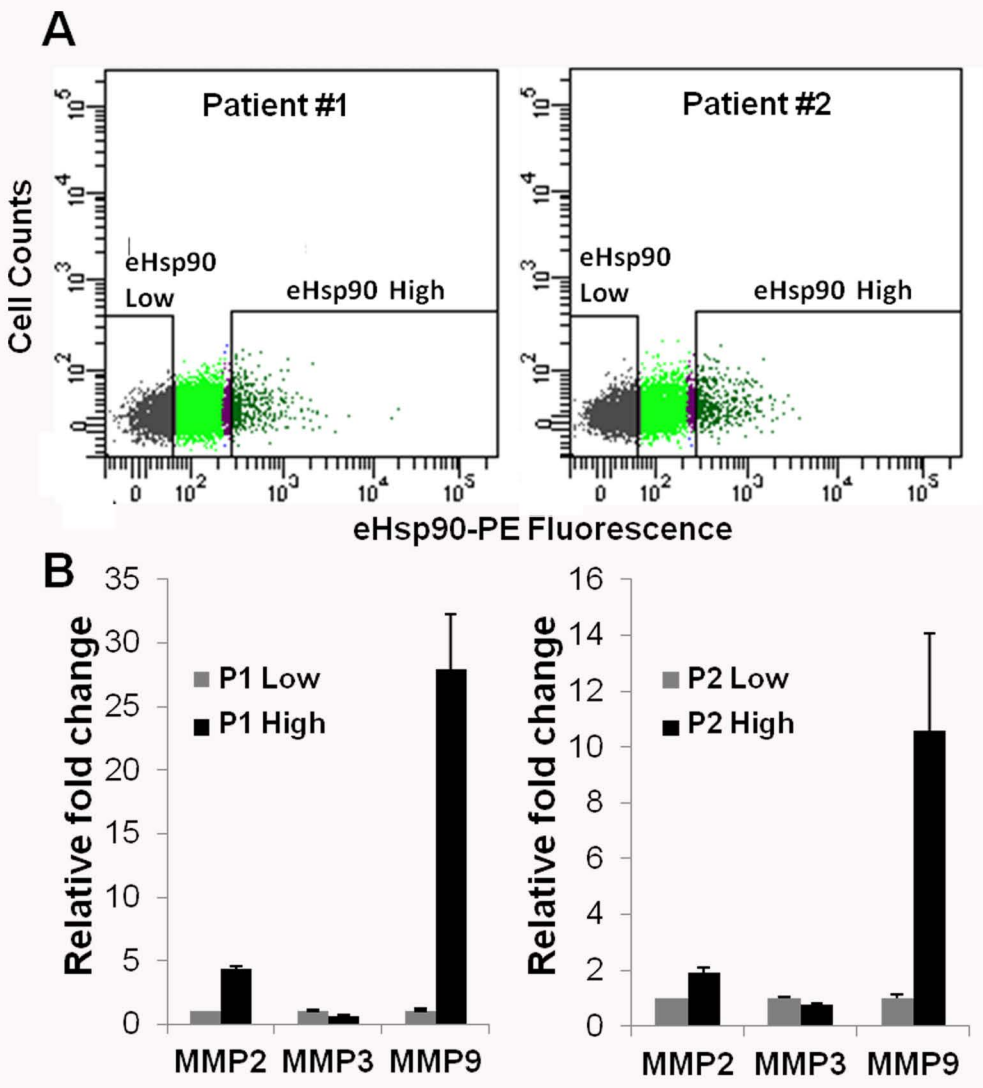

Fig. 7